Politecnico di Torino

POLITECNICO DI TORINO

DIPARTIMENTO DI INGEGNERIA MECCANICA E AEROSPAZIALE

Corso di Laurea Magistrale in Ingegneria Aerospaziale

Tesi di laurea magistrale

CONCEPTUAL DESIGN AND OPERATING COSTS ESTIMATION OF A SUBSONIC AIRLINER POWERED BY LIQUID HYDROGEN

Relatore: Davide Ferretto

Correlatore: Roberta Fusaro

Candidato: Simone Camboni

ANNO ACCADEMICO 2022/2023

1 Introduction

Air pollution represents one of the most significant environmental challenges of our time. Among the many sources of pollution, commercial aviation has garnered increasing attention due to its contribution to the accumulation of greenhouse gases in the atmosphere and its effects on climate change. Commercial aviation is a significant source of atmospheric pollution, contributing both to greenhouse gas emissions and air pollution. Its impact on the greenhouse effect and climate change is more significant than direct emission statistics suggest, due to the high altitudes at which emissions occur. However, significant efforts are underway to reduce the environmental impact of commercial aviation through the adoption of more efficient technologies, sustainable biofuels, and carbon dioxide emission charges [1].

1.1 Aircraft and High-Level Requirements

The commercial aviation industry is constantly evolving, driven by technological innovation and the growing demand for more efficient and environmentally friendly transportation solutions. In this context, the design and development of next-generation aircraft are a current focus, with the goal of reducing environmental impact and improving efficiency while continuing to ensure passenger comfort and safety. In this thesis project, a preliminary study of such a new generation of commercial aircraft will be carried out, designed to meet a set of high-level requirements. This aircraft will utilize cryogenic hydrogen as its energy source and will feature a classic configuration with a narrow-body fuselage, twin engines, and the ability to transport passengers on medium-haul routes.

The next-generation aircraft will adopt a classic configuration for passenger transport consisting a circular cross-section fuselage, low-mounted wings positioned just behind the center of gravity, and a classic three-element tail with one vertical and two horizontal stabilizer. This arrangement has been extensively tested over decades and has undergone continuous improvements to optimize aerodynamics, efficiency, and safety. The aircraft will be equipped with a twin-engine configuration, which has proven to be the right compromise between reliability and efficiency in the vast majority of current aircraft. The engines will be conventional high-bypass turbofans modified for operating with liquid hydrogen.

The aircraft under consideration must be sized to accommodate approximately 150 passengers. This capacity has been selected to meet the needs of medium-haul routes, striking a balance between operational efficiency and internal volumes. Indeed, the fuselage must be appropriately designed to accommodate not only a spacious and comfortable cabin but also the bulky hydrogen tanks. The aircraft must be capable of operating on routes with a distance of approximately 3000 kilometers up to a maximum of 4000 kilometers flying cruise at mach 0,82 making it ideal for regional and medium-haul connections. This autonomy, while theoretically lower than many current competitors, allows it to cover a wide range of destinations without the need for intermediate stops.

1.2 Commercial Aviation and Pollution

The commercial aviation industry is one of the most fuel-intensive economic sectors, primarily relying on fossil fuels, notably kerosene. This has led to significant emissions of greenhouse gases, including carbon dioxide (CO_2) and nitrogen oxide (NOx). CO_2 is the primary greenhouse gas responsible for the greenhouse effect, while NOx contributes to the formation of tropospheric ozone, a potent greenhouse gas [2]. The commercial aviation industry significantly contributes to the accumulation of atmospheric CO_2. In 2019, Global CO_2 emissions from commercial aviation reached approximately 1000 million tonnes, representing about 2-3% of total global CO2 emissions from human activities [3,4]. However, its impact on climate change is greater than one might expect. This is because CO_2 emissions from aircraft occur at higher altitudes, where they have a much more potent warming effect compared to the same emissions at ground level. It is estimated that the actual contribution of aviation to the greenhouse effect is at least double its direct CO_2 emissions [5]. In addition to greenhouse gas emissions, the commercial aviation industry also emits a range of air pollutants, including NOx, carbon monoxide (CO), fine particulate matter, and other chemical compounds. These pollutants can have direct effects on air quality and human health [6].

Effectively addressing the atmospheric pollution generated by commercial aviation requires international collaboration and joint commitment to develop and implement sustainable solutions. Balancing the need for efficient air transport with growing environmental concerns requires a balanced, evidence-based approach. In the context of combating atmospheric pollution generated by commercial aviation, hydrogen emerges as a promising alternative to fossil fuels.

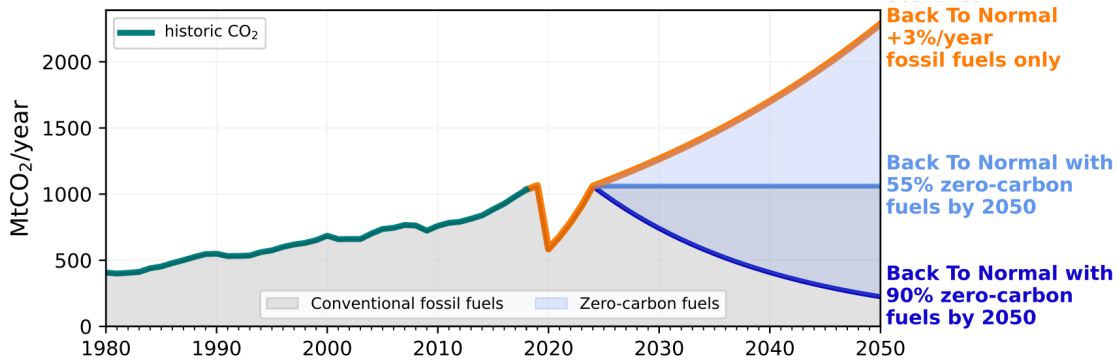

Figure 1.1: CO2 aviation emissions following the 3% annual air traffic growth with increasing use of zero-carbon fuels [1]

1.3 Hydrogen

The use of hydrogen as a fuel for aircraft could significantly contribute to reducing greenhouse gas emissions and atmospheric pollution [7]. Hydrogen burned in aircraft engines would primarily produce water vapor as a byproduct: there are no direct emissions of CO_2 when hydrogen is used as a fuel. Additionally, hydrogen has a very high energy density, meaning it can provide the necessary power without an excessive fuel load, reducing the weight of aircraft and further enhancing efficiency. Airports could be equipped with hydrogen refueling stations, enabling refueling of aircraft.

However, the introduction of hydrogen into the aviation industry is not without significant challenges. Hydrogen production requires considerable energy, and to reduce global emissions it is necessary to produce hydrogen using renewable energy sources or low-carbon emission processes. Hydrogen is highly flammable and requires specialized storage and transportation infrastructure to ensure safety. The transition to hydrogen will require significant investments in research, development, and infrastructure, which could pose an economic challenge.

It is essential that efforts to develop and implement hydrogen-based technologies are carried out responsibly, considering environmental, social, and economic aspects. It is worth emphasizing that the adoption of hydrogen in aviation should go hand in hand with the adoption of appropriate government policies and incentives to promote the transition to a more sustainable industry by introducing the use of renewable energies throughout the production chain.

1.3.1 Production

Hydrogen can be produced in various ways, and its "color" refers to the origin and production methods, as well as the associated greenhouse gas emissions for each technology. Production costs of hydrogen vary significantly depending on the type of technology used for its production. Here is an overview of the production methods for different types of hydrogen. [8,9]

Grey Hydrogen

Grey hydrogen is primarily produced from fossil hydrocarbon sources, such as natural gas or coal, through a process called methane steam reforming. During this process, carbon is separated from hydrogen, producing hydrogen and carbon dioxide as a byproduct. Grey hydrogen is highly polluting because its production involves significant CO_2 emissions that contribute to climate change. However, it is currently the most widely used method as grey hydrogen is often considered the most cost-effective type to produce initially: the methane reforming process is well-established and requires existing infrastructure. Production costs of grey hydrogen are generally competitive compared to other fuels.

Blue Hydrogen

Blue hydrogen is similar to grey hydrogen: in fact it is produced from fossil hydrocarbon sources, but CO_2 emissions are captured and stored (CCS, Carbon Capture and Storage) instead of being released into the atmosphere. This technology can partially mitigate the climate impact of grey hydrogen. Although blue hydrogen reduces CO_2 emissions compared to grey hydrogen, the carbon capture and storage process may result in some CO_2 losses and require suitable infrastructure for safe storage. Blue hydrogen implies higher costs compared to grey hydrogen due to the infrastructure needed for capturing, transporting, and storing the carbon emitted during production. Investments required to reduce carbon emissions make blue hydrogen less polluting than grey hydrogen. However, environmental costs depend on the efficiency of the CCS process and emission management.

Green Hydrogen

Green hydrogen is produced using water electrolysis, powered by renewable energy sources such as solar, wind, or nuclear (depending on the definition of "sustainable energy" used). During this process, water (H_2O) is split into hydrogen (H_2) and oxygen (O_2) using renewable electrical energy. Green hydrogen is considered the cleanest type of hydrogen as it does not produce direct CO_2 emissions during production. However, its environmental impact depends on the sustainability of the energy used for electrolysis. If the energy comes from renewable sources, green hydrogen has a low ecological footprint. Green hydrogen is often considered the most expensive type to produce due to the renewable energy used for water electrolysis. Investments in renewable energy production facilities can represent significant upfront costs. Despite higher production costs, green hydrogen is the most environmentally sustainable option even if environmental costs are linked to the sustainability of the renewable energy used.

Green hydrogen, despite higher initial costs, is considered the only viable solution for a future low-carbon economy and addressing issues related to climate change. With the evolution of technologies and increased large-scale production, it is expected that green hydrogen costs will gradually decrease, making these options more competitive. The adoption of green hydrogen is considered one of the most sustainable solutions to promote a transition to a low-carbon economy. For these reasons, green hydrogen will be the only option considered in the continuation of this work.

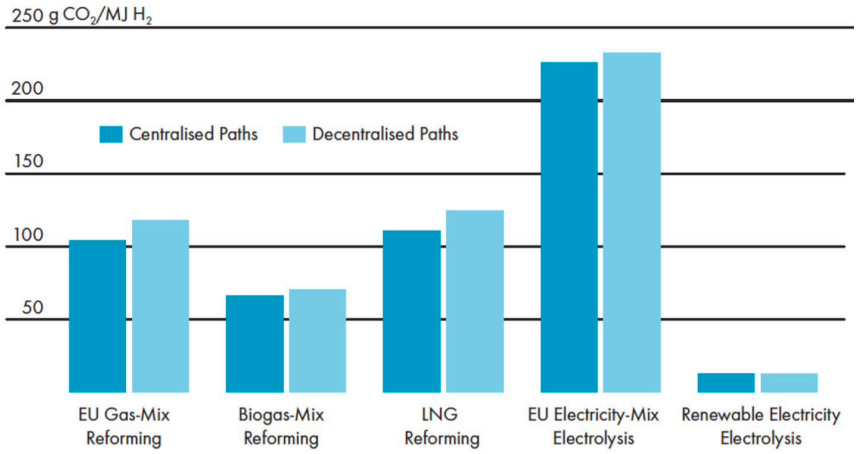

Figure 1.2: Environmental impact of LH_2 production [18]

1.3.2 Costs

Hydrogen production costs can vary depending on the geographical region, energy policies, and specific technologies used. The future cost trend of green hydrogen is of great interest, as interest in this technology is expected to increase in the near future. However, accurately predicting the evolution of green hydrogen costs is difficult and depends on several factors. The cost of green hydrogen is closely linked to the development of hydrogen production and renewable energy generation technologies. Technological innovation can lead to more efficient and cost-effective processes, contributing to cost reduction.

Since green hydrogen is produced using electrolysis powered by renewable energy, the costs of renewable energy itself play a key role in influencing hydrogen costs. Lowering the costs of solar and wind energy

makes green hydrogen more competitive. In this context, nuclear power, considered a sustainable energy source by the EU, can also play an equally important role [10]. Furthermore, in the future with the expansion of large-scale green hydrogen production, economies of scale can be achieved, reducing unit production costs. Investments in larger infrastructure and production capacity can contribute to making green hydrogen more cost-effective. Indeed, the cost of green hydrogen will be influenced by the dynamics of supply and demand. Increased demand could stimulate investments and large-scale production, helping to reduce costs. For all these reasons, the cost of green hydrogen is expected to decrease over the years. According to most current research, the pump price in 2035 is estimated to be significantly lower than today and it will continue to decrease in price until 2050. Liquid Hydrogen (LH_2) price projected to drop by a factor of 4 from today to roughly the same cost per unit energy as for kerosene by 2050 [11].

The current situation is quite limited, with few production facilities capable of meeting a still-limited demand for green hydrogen. Additionally, hydrogen storage would require specialized infrastructure optimized to operate with this new technology. As a result, the current cost is very high when compared to traditional fuels. Assuming significant industrial investments to optimize production, costs can be reduced to around 5-7 $/kg depending on the technology used and the desired product [12]. Furthermore, currently the transport chain would not be ready to effectively distribute the produced hydrogen. Estimating a cost per kilogram of liquid hydrogen at 5,38 $, this would increase to 14,24 $ at the pump when considering transportation and storage [13]. Of course current conditions do not allow for widespread use. However the increasing number of research and investments is changing estimates downward. Current models suggest that by 2035, the cost per kilogram of hydrogen at the pump could drop well below 4 $ [14]. Within these estimates, many factors come into play, including geographical location: the direct correlation with the availability of low-cost renewable energy makes some regions more favorable than others. For example, Brazil manages to obtain 65% of its national electricity from hydropower due to its geographical layout. This allows for lower costs of electricity from renewable sources which in turn affects potential green hydrogen production. This enables significant progress for the region. It is estimated that hydrogen could be obtained at a cost of 3,1 USD/kg in 2030 and 1,8 USD/kg in 2050, including liquefaction costs (which are far from negligible) [15]. In even

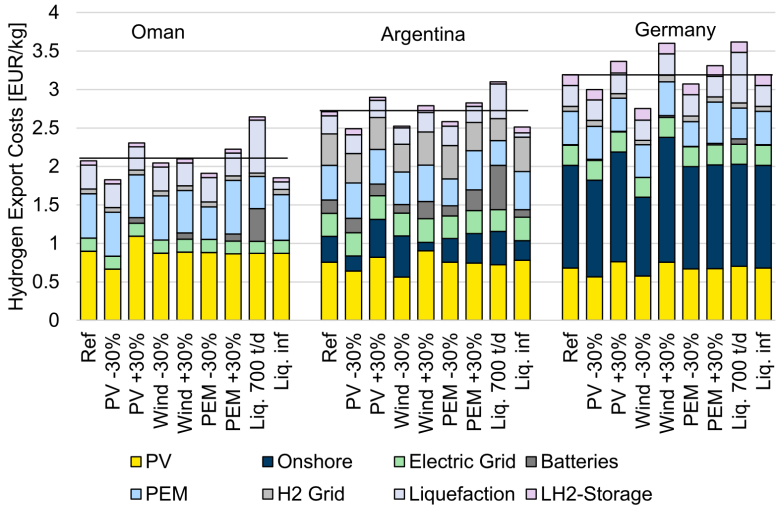

Figure 1.3: Cost analysis for different countries exemplarily for 10% of the country-wise maximum export in 2050 [19]

more optimal regions, a 62% cost reduction is estimated by 2030, reaching costs in the range of 1,5 $/kg [16]. Many other less optimistic estimates suggest costs around 3,5 € per kg in 2030, especially for production in European Union countries [17]. Even for 2050 estimates are uncertain: in general, it can be said that the cost of hydrogen can go below 2 €/kg [18], but at the same time, the variables can prevent cost reduction keeping it well above the competition depending on the production country and the amount of hydrogen produced [19].

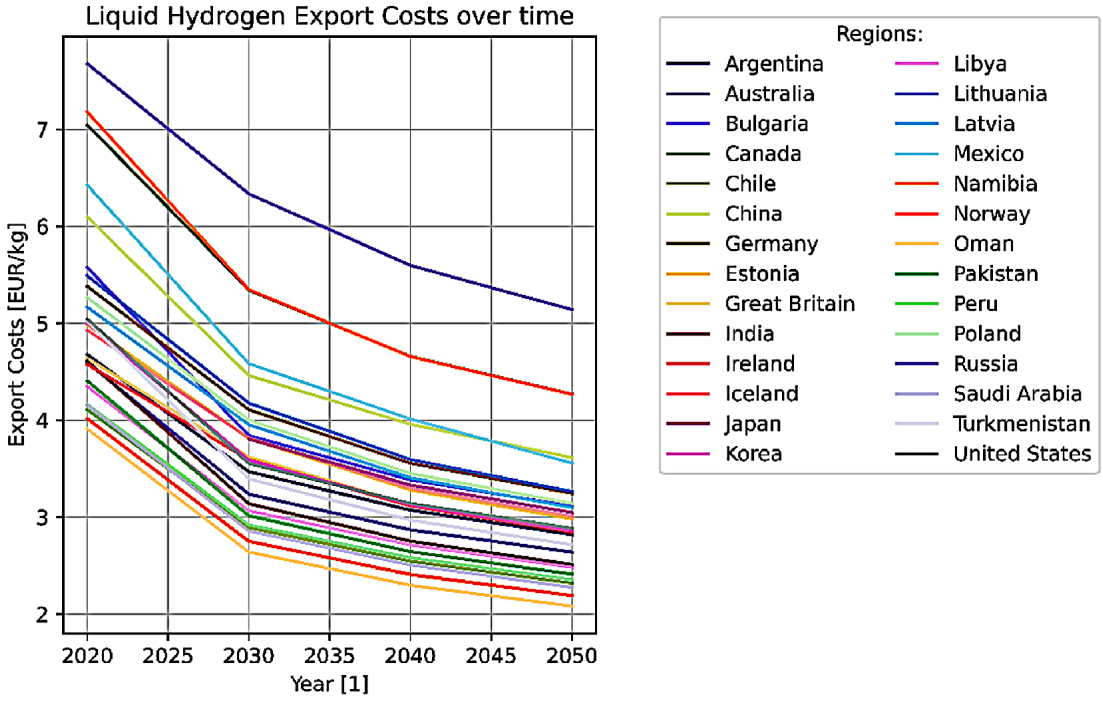

Figure 1.4: Liquid hydrogen cost development from 2020 to 2050 at 20% of the maximum export. [19]

Another parameter to consider is government policies and economic incentives, which can have a significant impact on green hydrogen costs. Financial support, tax incentives, and environmental regulations can help reduce costs for investors and industry operators.

1.3.3 Hydrogen for Aviation

Overall, the use of green hydrogen as a fuel for commercial aviation presents an interesting prospect for reducing the environmental impact of the aviation industry [20]. It will require close collaboration between industry, governments, and international organizations to overcome the technical, infrastructural, and regulatory challenges to make this vision a reality by 2035. However, while there are still technological and infrastructural challenges to overcome, many airlines and industry organizations are exploring this possibility [21,22]. Of course, adequate infrastructure will be needed to produce, transport, store, and refuel green hydrogen at airports worldwide. This infrastructure requires significant investments and international coordination. To complicate matters, it should be noted that simply updating existing refueling infrastructure will not be sufficient: an entirely new distribution chain will need to be built. This parameter is also linked to the safety of new technologies, which will need to ensure the proper security measures [23]. Aviation regulatory authorities will need to develop standards and regulations for the safe and reliable use of liquid

hydrogen as a fuel for commercial aircraft. Safety certifications and operational procedures will need to be established. Due to these difficulties, the adoption of green hydrogen in commercial aviation may occur gradually, starting with smaller aircraft or regional flights before expanding to long-haul aircraft. This would allow for the gradual addressing of challenges, requiring smaller investments and smaller infrastructure and, most importantly, accumulating experience before a full transition, given that the conversion of long-haul airplanes presents even greater challenges.

Current aircraft use combustion engines that require significant adaptations to run on hydrogen as a fuel. Hydrogen engine technologies are still under development and will need to ensure safety, efficiency, and the high performance required by the commercial aviation sector. Moreover, using hydrogen as a fuel for a commercial airliner presents additional significant challenges, many of which are related to the physical and chemical characteristics of hydrogen compared to traditional fuels such as kerosene [24,25]. Hydrogen has a much lower volumetric density than kerosene, which means that much more space is required to store it onboard the aircraft. This necessitates a redesign of the aircraft and the provision of appropriate storage structures. Currently, fuel is stored onboard aircraft within tanks integrated into the wings, essentially using the spaces between structural elements. Hydrogen tanks, on the other hand, will need to be separate from the aircraft's structure and, being much bulkier, will need to be accommodated in the fuselage transforming the layout of interior spaces [26].

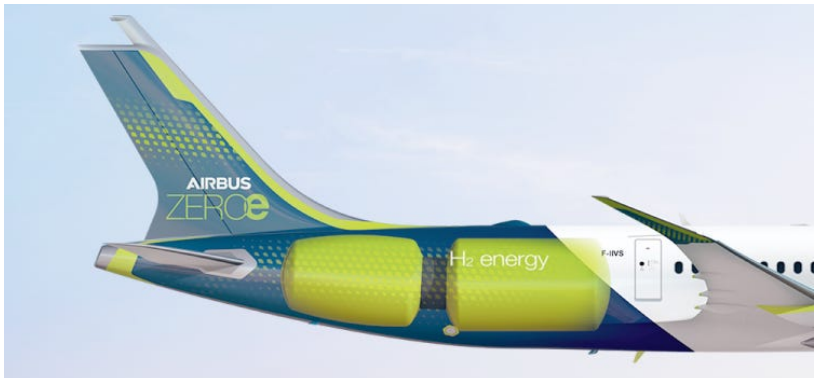

Figure 1.5: Airbus Zeroe turbofan - positioning hydrogen tank in fuselage [21]

1.3.4 Tanks

The only way to carry hydrogen onboard an aircraft is in the form of cryogenic liquid hydrogen (LH_2). Liquid hydrogen has a density of 70,9 g/L, which requires much less volume for the same quantity of gaseous hydrogen (H_2). This allows for a significant reduction in fuel volume but presents other complexities. To store cryogenic hydrogen, it is essential to maintain an extremely low temperature and pressure hundreds of times greater than atmospheric pressure.

Pressurized cryogenic hydrogen tanks are devices designed to allow the safe and efficient transport and storage of large quantities of hydrogen. Hydrogen becomes a liquid when cooled to a temperature of approximately -253°C (20°K). At these extremely low temperatures, hydrogen has a much higher energy density compared to its gaseous state, making it more suitable for long-term transport and storage. To keep it in liquid form, hydrogen must be subjected to high pressures to mitigate boiling. The pressure in cryogenic

hydrogen tanks can vary but is generally in the range of 200-350 bar. Cryogenic tanks are designed with advanced insulating materials to keep temperatures inside the tank low and prevent heat entering from the outside. These materials often include layers of foam, aerogel, or low thermal conductivity insulating materials. Additionally, there are often vacuum layers and chambers between the inner and outer tank walls to further enhance thermal insulation. For these reasons, cryogenic tanks can become quite bulky and heavy, posing a challenge for integration into aircraft [27].

The volumetric and gravimetric efficiency of pressurized cryogenic hydrogen tanks are performance assessments of these tanks in terms of the quantity of hydrogen they can store in relation to the tank's volume and weight. These parameters are essential for determining the suitability of tanks for use in aviation. Volumetric efficiency measures the amount of hydrogen that can be stored inside the tank relative to the total tank volume. Since liquid hydrogen has a very low volumetric density, cryogenic tanks must be designed efficiently to minimize the space inside that is not occupied by fuel. Volumetric efficiency is often expressed in liters (or cubic meters) of liquid hydrogen per liter (or cubic meter) of tank volume and is usually measured as a percentage. In the past, volumetric efficiencies were around 70% [28]. However, thanks to research in the field, technologies have improved and currently tanks with vacuum insulation can achieve volumetric efficiencies of 85,5% [29,30]. A cryogenic tank with an 85% volumetric efficiency can contain 85 liters of liquid hydrogen in a 100-liter tank.

On the other hand, gravimetric efficiency measures the amount of hydrogen that can be stored inside the tank relative to its total weight. To be sufficiently robust and insulating for efficient hydrogen storage, tanks reach considerable weights, especially when compared to the weight of the hydrogen they contain due to its low density. Gravimetric efficiency is expressed in kilograms of liquid hydrogen per kilogram of tank weight and is also measured as a percentage. This parameter depends on various factors, including the tank's size. Space rocket tanks have a single chamber that holds an enormous amount of hydrogen, allowing them to achieve gravimetric efficiencies where the tank structure's mass is only 15% of the hydrogen mass [31]. However, aircraft tanks, in addition to being smaller, can be even more complex. This is because they must be able to maintain internal temperature for a longer time, and safety must be much higher. For these reasons, the gravimetric efficiencies of transport tanks are extremely low. Current efficiencies are around 20-35%, meaning they transport between 0,2 kg and 0,35 kg of hydrogen per kg of total mass (tank + fuel) [11,32]. Modern technologies promise to reach 50%, and future estimates suggest that new tank generations will be able to achieve efficiencies beyond 70% [33,34]. However, most research states that 50% is a reasonably reliable value to which efficiency can tend in the near future [33,35,36].

The performance of a cryogenic tank depends on various factors including tank design, materials used, thermal insulation technology, and storage pressure. Many of these elements are still under study, and the technologies that will be used in future hydrogen aircraft may not yet be known. For these reasons, the tanks onboard the treated aircraft will be approximated as cylinders connected by hemispheres characterized by a gravimetric efficiency of 0,855 and a volumetric efficiency of 0,5.

2. Conceptual design

Sizing an aircraft is the most crucial calculation in the design process. Sizing literally determines the dimensions of the aircraft, specifically the weight at which the aircraft must be designed so that it can perform its intended mission by carrying the desired payload. An aircraft that is too small simply cannot carry enough fuel to fulfill its task. This chapter will explain the workflow that led to the realization of the conceptual design of the airplane in question. In order to obtain a realistic result, it is essential to base the workflow on a reliable source. In this thesis project, the work was carried out using the method outlined in the book "Aircraft Design: A Conceptual Approach" by Daniel P. Raymer [37]. As will be observed in this chapter, this method is capable of providing a preliminary estimate of what the aircraft could be, providing values for fundamental quantities with a high degree of accuracy. This sizing method is more accurate when used for missions that do not involve combat or payload drops, making it an excellent candidate for this work. Although it is simplified, this method incorporates all the essential features of more sophisticated sizing methods.
The workflow used, like others in this field, is highly iterative. Each phase often depends on the previous one and estimates of values that can be obtained in the next phase, so many attempts were made before reaching convergence. In this chapter, the final results are reported directly for the sake of brevity.

2.1 Statistic analysis

To ensure an optimal result, it is of fundamental importance to have reliable data as a starting point for the calculations. In this case, a reference point was found by basing the project on the existing aircraft A320 Neo. Indeed, despite the freedom in configuring the aircraft under consideration, having a real starting point can be very useful for estimating some values relevant to the overall project. Although the A320 will be used to obtain many of the required data, a quick statistical study has still been conducted. This has the advantage of providing the designer with an overview of current competitors and, above all, provides a reliable benchmark for both the data that need to be hypothesized and for quantities that are calculated at the end of further procedures. Keeping in mind the high-level requirements outlined in paragraph 1.1, a statistical analysis was carried out to identify current aircraft that are: passenger transport aircraft, twin-engine, narrow-body, capable of carrying up to 250 passengers, and characterized by an operational range of less than 7000 km. For each of the identified aircraft, the following parameters were analyzed:

- Maximum Takeoff Weight - MTOW
- Dimensions (length - L, wingspan - W, wing surface - WS)
- Max payload - MP
- Maximum thrust - T
- Empty Weight - EW
- Empty Mass Fraction - EMF
- Aspect Ratio - AR

The analysis of the statistical population is reported in the table 2.1. [38-59]

Aircraft	MTOW [t]	L [m]	W [m]	WS [m²]	MP [t]	Cruise [Mach]	Range [km]	T [kN]	EW [t]	EMF	Pax	AR
Douglas DC-9 -30	49,0	36,40	28,4	93,0	14,5	0,84	2800	125,5	25,8	0,53	127	8,67
McDonnell Douglas MD-82	67,8	45,10	32,8	112,0	17,4	0,76	3800	186,0	37,9	0,56	172	9,61
McDonnell Douglas MD-83/88	75,6	45,10	32,8	112,0	16,6	0,76	4600	192,0	38,7	0,51	172	9,61
McDonnell Douglas MD-87	63,8	39,70	32,8	112,0	18,2	0,76	4400	189,0	35,3	0,55	172	9,61
Airbus A318	68,0	31,44	34,1	122,6	13,3	0,78	5750	212,0	39,5	0,58	131	9,48
Airbus A319 NEO	75,0	33,84	35,8	122,6	14,0	0,78	6950	214,0	40,8	0,54	160	10,45
Airbus A320 NEO	78,0	37,57	35,8	122,6	16,6	0,78	6500	241,2	42,6	0,55	194	10,45
Airbus A321 NEO	93,5	44,51	35,8	122,6	21,2	0,78	7400	294,6	48,5	0,52	244	10,45
Boeing 737-300	63,3	33,40	28,9	105,4	15,0	0,74	2900	194,0	32,8	0,52	149	7,92
Boeing 737 MAX 7	80,3	35,60	35,9	127,0	14,0	0,80	7000	260,0	62,9	0,78	172	10,15
Boeing 737 MAX 8	82,2	39,50	35,9	127,0	20,9	0,80	6500	260,0	66,0	0,80	210	10,15
Boeing 737 MAX 9	88,3	42,20	35,9	127,0	22,6	0,80	6500	260,0	71,0	0,80	220	10,15
Antonov An-148	43,7	29,13	28,9	87,3	12,1	0,77	3600	134,0	22,5	0,51	92	9,57
Comac C919-All ECO	78,9	38,90	35,8	129,2	15,0	0,78	5555	137,9	42,1	0,53	168	9,92
Comac ARJ21	43,5	33,46	27,3	79,9	8,9	0,78	3700	151,2	25,0	0,57	105	9,32
Fokker F100	45,8	35,53	28,1	93,5	11,2	0,77	3170	123,2	24,5	0,54	122	8,43
Embraer ERJ 145	22,0	29,87	20,0	51,2	5,8	0,78	2871	66,0	12,0	0,55	50	7,84
Embraer 195	52,3	38,65	28,7	92,5	13,7	0,80	4260	164,6	42,6	0,81	122	8,92

Table 2.1: Statistic population

2.2 Raymer method

The Raymer method is highly useful for calculating a preliminary estimate of the maximum takeoff weight and the required amount of fuel. The design takeoff weight can be broken down into crew weight, payload weight (or passenger weight), fuel weight, and the remaining weight (or "empty" weight). The empty weight includes the structure, engines, landing gear, fixed equipment, avionics, and anything else not considered part of the crew, payload, or fuel.

$$W_{TO} = W_{crew} + W_{payload} + W_{empty} + W_{fuel}$$

The crew and payload weights are known since they are specified in the design requirements. Raymer suggests to consider an average weight of 100 kg per passenger, including the weight of carried baggage. For the crew, a weight of 85 kg per crew member is considered. Additionally, regulations require one flight attendant for every 50 passengers, so the crew consists of one captain, one first officer, and 3 flight attendants. Taking these factors into account, we have:

$$W_{crew} = 425 \text{ kg} \qquad\qquad W_{payload} = 15000 \text{ kg}$$

The only unknowns are the fuel weight and the empty weight. However, both depend on the total weight of the aircraft. For this reason, both the fuel weight and the empty weight can be expressed as fractions of the total takeoff weight, i.e. W_f/W_{TO} and W_e/W_{TO}. Therefore, we have the equation:

$$W_{TO} = W_{crew} + W_{payload} + \left(\frac{W_f}{W_{TO}}\right) \cdot W_{TO} + \left(\frac{W_e}{W_{TO}}\right) \cdot W_{TO}$$

This equation can be solved for W_{TO} as follows:

$$W_{TO} = \frac{W_{crew} + W_{payload}}{1 - \left(\frac{W_f}{W_{TO}}\right) - \left(\frac{W_e}{W_{TO}}\right)}$$

Now W_{TO} can be determined if we can estimate W_f/W_{TO} and W_e/W_{TO}.

2.3 Fuel fraction

Estimating the necessary fuel to execute the mission is a crucial step. Simple statistical methods won't suffice: we must consider the aircraft through its required mission. The quantity of fuel needed is primarily influenced by the particular mission, the aerodynamic characteristics of the aircraft, and the fuel consumption of the engine. Additionally, the aircraft's weight during the mission impacts the level of resistance it encounters, thereby establishing a correlation between fuel consumption and the aircraft's weight. For analysis purposes, various mission segments, or "phases," are considered: takeoff, climb, cruise, descent, and landing. At the same time, the aircraft's weight at each part of the mission can be numbered. So, W_0 represents the initial weight (takeoff weight), W_1 would be the weight at the end of the first mission segment, W_2 would be the weight at the end of the climb, etc until the end of the entire mission. During each mission

segment, the aircraft loses weight by burning fuel. The weight of the aircraft at the end of a mission segment divided by its weight at the beginning of that segment is called the "mission segment weight fraction". For any mission segment, the mission segment weight fraction can be expressed as W_i/W_{i-1}. If these weight fractions can be estimated for all mission phases, they can be multiplied together to find the ratio of the aircraft's weight at the end of the entire mission W_n to the initial weight W_0. This can then be used to calculate the total required fuel fraction. The mission segment weight fractions for the cruise segment can be calculated using the Breguet range equation:

$$R = \frac{V}{SFC}\frac{L}{D} \cdot ln(\frac{W_{i-1}}{W_i})$$

Where:

- R = range [km]
- SFC = specific fuel consumption [kg/s daN]
- V = velocity [km/s]
- L/D = lift-to-drag ratio
- Wi = weight at the beginning of the mission segment i
- D = duration of the phase [s]

By manipulating Breguet's formula, we obtain the equations used to calculate mission segment weight fractions:

$$\frac{W_{i-1}}{W_i} = e^{\frac{-R \cdot SFC}{V \cdot L/D}} \qquad \frac{W_{i-1}}{W_i} = e^{\frac{-D \cdot SFC}{L/D}}$$

The first equation will be used in the phases where the travel range is known (such as cruising), while the second will be useful in the phases where the duration is known (such as waiting). The weight fractions for warm-up, takeoff, and landing can potentially be estimated from tabulated values based on historical and statistical analyses. However, these values can vary slightly depending on the type of aircraft. It should also be noted that the aircraft under study will adopt different technologies from conventional ones, significantly altering the distribution of weight between fuel and structure. For this reason, the estimated average values cannot be considered reliable even for initial sizing. Therefore, it was chosen to estimate the weight fractions for all mission phases using the Breguet equation. The fuel fraction can be estimated based on the specific mission using approximations of fuel consumption and aerodynamics. In the following paragraphs, all assumptions will be analyzed by examining fuel consumption estimates and aerodynamic quantities. Finally, the mission profile to which the model will be applied will be described.

2.3.1 Specific Fuel Consumption

To calculate the onboard fuel mass for a given mission, it is crucial to estimate the engine's efficiency accurately. Specific Fuel Consumption (SFC) serves as a critical metric in this regard, representing the engine's efficiency in converting fuel into thrust or power. This is calculated as the rate of fuel consumption divided by the resulting thrust or power output.

When it comes to aviation engines, particularly jet engines, SFC is typically measured in terms of fuel mass flow per unit of time (usually hours) and force or thrust. It plays a pivotal role in determining the aircraft's fuel efficiency and range. Lower SFC values indicate that an engine can produce a given amount of thrust while burning less fuel, which is a hallmark of a more efficient engine. However, the specific fuel consumption of a hydrogen-powered turbofan engine differs significantly from that of a conventional aviation engine that relies on traditional fossil fuels like kerosene [29]. This divergence arises from the unique properties of hydrogen as a fuel source. Hydrogen, as a fuel, possesses some remarkable characteristics that exert a profound influence on SFC. Most notably, it boasts a substantially higher calorific value compared to kerosene. This means that a given quantity of hydrogen contains considerably more energy per unit of mass than an equivalent quantity of kerosene. Consequently, hydrogen-powered turbofan engines can attain significantly higher energy efficiency i.e. lower SFC, as they can produce the same level of thrust or power while consuming less fuel mass [60,30].

For traditional kerosene-powered turbofan engines, typical SFC values can vary, generally falling in the range of approximately 0,5 to 0,7 pounds of fuel (Jet-A or JP-8) per hour per pound of thrust (lb/hr/lbf) or about 12 to 17 grams of fuel per second per Newton of thrust (g/s/N) [61-63]. However, actual values can vary based on engine design and operating conditions. It's essential to note that SFC values can also exhibit variations during different phases of flight. This consideration highlights the importance of accurately estimating SFC values for various mission segments.

Regarding hydrogen-powered turbofan engines, it's crucial to acknowledge that this technology is still in the research and development phase, and commercial hydrogen-powered turbofan engines are not yet available. Consequently, there is a scarcity of readily available typical SFC values to compare, making the estimation of this parameter a rather intricate task. Nonetheless, extensive research has been conducted in this field over the years. For instance, NASA has shown significant interest by conducting studies and conceptual designs of hydrogen-powered aircraft, especially in the past, with a focus on fuel subsystems. NASA's Study of fuel systems for LH2-fueled subsonic transport aircraft focuses in this area, exploring ways to adapt and optimize turbofan engines for hydrogen as a fuel source [64]. They have explored various enhancements, including compressor air pre/intercoolers, regenerative fuel heating, and the refinement of bypass ratios and fan pressure ratios. As a result of these efforts, NASA estimated that these modified engines could achieve specific fuel consumption values of approximately 0,1045 kg/hr/daN at sea level under standard conditions [65]. However, as aircraft typically operate at various altitudes, it's important to consider that fuel consumption during cruise phases tends to be higher than at sea level due to the reduced air density and other factors. Therefore, in the specific context of this project, the estimations provided by NASA were adjusted to

account for the cruise phase. For instance, when flying at Mach 0,85 at 35000 feet, their research estimated specific fuel consumption values of approximately 0,2054 kg/hr/daN [65].

Recent advancements in materials and technologies have further contributed to the refinement of these estimates. As a result, more recent researches have indicated that hydrogen-powered engines can achieve even more impressive efficiency. For instance, some studies suggest specific fuel consumption values as low as 0,1701 kg/hr/daN for the cruise phase [66]. However, more structured works similar to this thesis project, study the presence of both conventional and unconventional engines on future hydrogen-powered aircraft. Recent works estimate that it is possible to achieve SFC values of 5,755 kg/s/MN during cruise at 11000m while flying at Mach 0,8 with a conventional engine adapted for hydrogen [67]. This value is much closer to what NASA estimated decades earlier compared to the more optimistic ones. In this project, a conservative approach was taken: it's been chosen a slightly higher specific fuel consumption compared to values of more recent research, based on older but more comprehensive studies that show results that align with a greater number of findings. In this case, the following values were used:

$$SFC_{Take-Off} = 3{,}33 \cdot 10^{-5}\ \text{kg/s/daN} \qquad SFC_{Cruise} = 5{,}83 \cdot 10^{-5}\ \text{kg/s/daN}$$

These values aim to provide a reasonable estimation of specific fuel consumption for hydrogen-powered turbofan engines, taking into account the available research and historical data while acknowledging the dynamic nature of this field.

2.3.2 Aerodynamic characteristics

The Lift-to-Drag ratio represents the overall aerodynamic efficiency of the aircraft and is the final unknown in the equations for endurance and loiter. Aerodynamic efficiency is the aircraft's ability to minimize aerodynamic drag during flight, thereby reducing fuel consumption and maximizing endurance, while simultaneously reducing polluting emissions. Unlike the parameters estimated earlier, L/D heavily depends on the aircraft's configuration. At subsonic speeds, L/D is primarily influenced by two design aspects: the wing aspect ratio and the wetted area of the aircraft. Achieving optimal aerodynamic efficiency involves various factors, including the aircraft's external geometry, wing layout, control surfaces, and aerodynamic details such as wing profiles. In the context of level flight, the lift generated by the aircraft is a known quantity and is equal to the aircraft's weight. Consequently, L/D depends solely on drag, which is aerodynamic resistance. At subsonic speeds, drag consists of two components. Induced drag is the drag caused by lift generation and is mainly a function of wing aspect ratio (AR): a crucial determinant for optimal lift generation. On the other hand, parasitic drag is the portion of drag that is not directly related to lift and is primarily due to viscous resistance, directly proportional to the total exterior surface area of the aircraft exposed to the airflow, a metric commonly referred to as the wetted area. Historically, wing aspect ratio has been used as a primary indicator of wing efficiency. This parameter mathematically equates to the square of the wingspan divided by the wing reference area, representing the ratio of wingspan (width) to mean chord (depth) of the wings. A high aspect ratio is related to elongated, slender wings, while a low aspect ratio suggests the presence of shorter, wider wings. The choice of aspect ratio profoundly influences

the aircraft's performance. High aspect ratios are characteristic of jetliner designs, typically in commercial aviation where long-haul flights are the norm. This configuration yields superior aerodynamic efficiency.

$$AR = \frac{Wingspan^2}{S_{ref}}$$

However, L/D ratio is influenced by both induced and parasitic drag. While induced drag's main determinant is the wing aspect ratio, parasitic drag depends on the total wetted area of the aircraft, a value that takes into account not only the wing area but the entirety of the aircraft's exterior surface exposed to the surrounding air. For convenience, engineers have introduced a novel parameter: the wetted area ratio S_{wet}/S_{ref}. In a classic configuration, the wing surface is usually considered as the reference surface. The wetted area ratio can be used, alongside the aspect ratio, for a preliminary estimation of L/D at subsonic speeds. For what has been said so far, it is useful to consider a new parameter: the wetted aspect ratio, defined as the square of the wingspan divided by the total wetted area of the aircraft. Although resembling the aspect ratio, the wetted aspect ratio considers the collective surface area exposed to airflow, rather than just the wing reference area.

$$A_{wetted} = \frac{Wingspan^2}{S_{wetted}} = \frac{AR}{S_{wet}/S_{ref}}$$

Remarkably, historical and statistical data has been analyzed, revealing distinct trends in aircraft performance relative to this parameter. The data, spanning various aircraft categories, has been invaluable in not only providing initial estimates of L/D but also in corroborating results derived from detailed calculations.

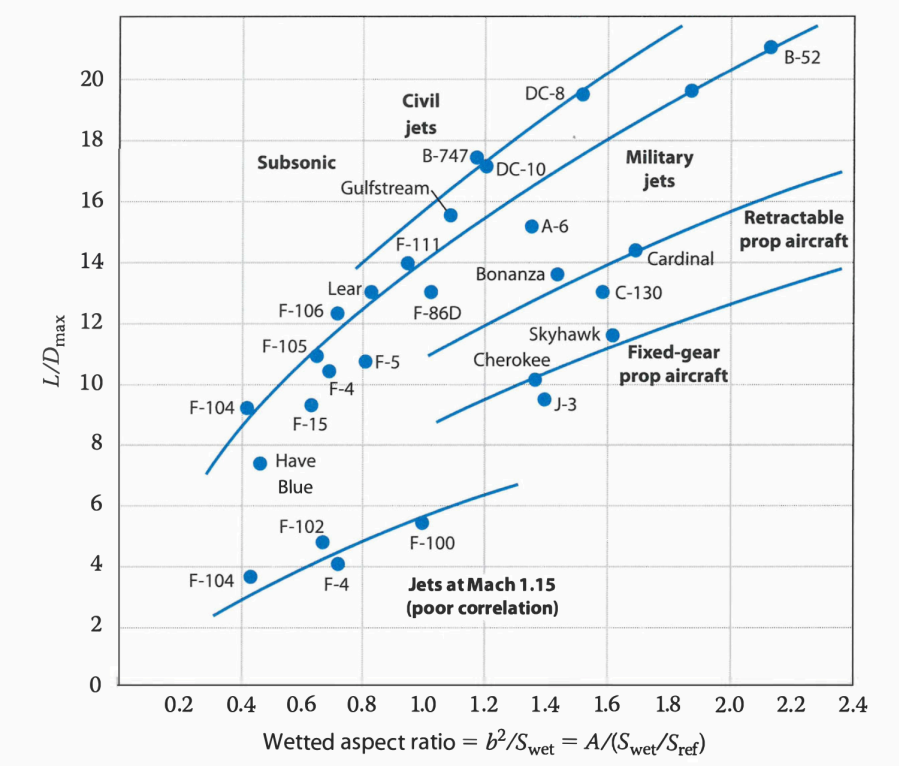

Figure 2.1: Maximum lift-to-drag ratio trends [37]

Furthermore, considering relating L/D to the square root of the wetted aspect ratio gives particularly valuable results because it produces remarkably linear data. The linearity of the data allows the derivation of practical equations to predict the maximum L/D: a very useful tool as it allows an extremely fast estimation.

$$\left(\frac{L}{D}\right)_{max} = K_{LD}\sqrt{A_{wetted}} = K_{LD}\sqrt{\frac{AR}{S_{wet}/S_{ref}}}$$

Where K_{LD} is a factor that varies according to the category of aircraft and is 15,5 for civil jets.

The challenging task at this point remains to estimate the wetted aspect ratio before the layout of the configuration design is done. This necessitates the imposition of some geometric parameters on the aircraft. To avoid design complications, a classic narrow-body configuration has been maintained, characterized by low-wing placement and high-bypass-ratio turbofan engines mounted under the wings, one engine per wing. In this preliminary phase, we assumed the use of conventional engines converted to run on liquid hydrogen. The technical aspects related to adapting these engines and the technologies used have been neglected as they represent a level of detail beyond the preliminary design and are not part of this thesis project.

The A320 Neo aircraft features an ellipsoidal cross-section fuselage with external dimensions ranging from 3,95 m to 4,10 m. However, for the sake of simplicity in our initial calculations, a circular cross-section fuselage with a diameter of 4 m has been considered. Continuing with the definition of the aircraft's external geometry, the dimensions of its main components have been assigned to provide an initial estimate of their surfaces. To calculate the lift-to-drag ratio, it's crucial to estimate the total wetted area of the aircraft's surface. As a starting point, let's assume that the wing configuration of the aircraft mimics that of the A320 Neo, characterized by a wingspan of 34,1 m and a wing area of 122,6 m². Even when it comes to the control surfaces the dimensions derived from the existing aircraft are used, ensuring a degree of realism in estimations. Specifically, for the tail components a horizontal stabilizer with an area of 27 m² and a vertical tailplane with an area of 43 m² are considered [68]. The engine dimensions are also based on those of the 2 CFM International LEAP-1A engines installed on A320 family aircraft. These engines are approximated as cylinders with a diameter of 2,5 m and a length of 5 m [69]. Moving on to the fuselage, its length mirrors that of the A320 at least at this stage, measuring 37,6 meters. For the diameter, the previously estimated value of 4 meters is maintained. With these dimensions in hand, it's now possible to calculate the total wetted surface area of the aircraft, approximable as follow:

$$S_{wet} = S_{ref} \cdot 2 + S_{H_{tail}} \cdot 2 + S_{V_{tail}} \cdot 2 + \pi \cdot D_{iameter_{fuselage}} \cdot L_{ength_{fuselage}} + S_{engine} \cdot 2 = 935{,}86\, m^2$$

This calculation allows for the determination of the Wetted Area Ratio as the ratio between the wetted surface area and the reference surface area of the aircraft. Consequently:

$$Wetted\ Area\ Ratio = \frac{S_{wet}}{S_{ref}} = 7{,}63$$

Now it's possible to calculate the aspect ratio. Initially, the simple formula is used:

$$Aspect\ Ratio = \frac{Wingspan^2}{S_{ref}}$$

However, assuming that the aircraft is equipped with winglets designed to optimize aerodynamic efficiency, it is better to correct the calculation taking these into account. In particular, a more accurate estimation of the aspect ratio can be obtained as follows:

$$Aspect\,Ratio = \left(\frac{Wingspan^2}{S_{ref}}\right) + 1{,}9 \cdot \frac{h}{Wingspan}$$

Where h represents the height of the winglets, which in our scenario is assumed to be equal to that of the A320 Neo measuring 2,43 m. As a result, adjusted aspect ratio is:

$$Aspect\,Ratio = 9{,}62$$

Now, with all the necessary data available, it is possible to calculate the maximum aerodynamic efficiency of the aircraft:

$$E_{Max} = 15{,}5 \cdot \sqrt{\frac{Aspect\,Ratio}{Wetted\,Area\,Ratio}} = 17{,}4$$

Aircraft experience varying levels of resistance as they change altitude and velocity. At any given altitude, there exists an optimal velocity at which the aircraft attains its maximum Lift-to-Drag ratio. To enhance the efficiency of cruise or loiter phases, the aircraft should ideally operate at the velocity that produces the maximum L/D. For jet aircraft, the most efficient loiter speed precisely corresponds to the velocity at which the maximum L/D is achieved. In essence, during loitering jet aircraft should maintain the velocity at which L/D is at its peak. However, for efficient cruise jet aircraft typically operate at a slightly higher speed, resulting in an L/D of 86,6% of the maximum L/D. Therefore, as a first approximation, cruise efficiency is calculated as 86,6% of the maximum efficiency, resulting in:

$$E_{Cruise} = E_{Max} \cdot 0{,}866 = 15$$

More advanced versions of the A320 can achieve efficiencies slightly above 16 during the cruise phase, indicating that our calculations, based on conservative values, provide a realistic foundation for initial aerodynamic assessments [70].

2.3.3 Mission profile

Once the fuel consumption by the engines and the aerodynamic characteristics have been determined, the other fundamental variable to consider is the mission profile.

The aircraft is sized to provide a specific required cruise range. The "Simple Cruise" mission is used for many transport and general aviation projects. However, for safety reasons, it would be prudent to carry extra fuel in case the destination airport is closed or there are other landing issues. For this reason an overflight phase is added, usually lasting 20-30 minutes (at 10000 feet). Additional range could be included: according to commercial IFR rules, fuel is required to fly to an alternate airport after overflight and attempting to land at the intended destination. For these reasons, the mission profile considered takes into account a 30-minute hold near the destination airport, sufficiently large to provide some safety margin in case of emergencies. Furthermore, to make the mission profile more accurate and consider all real possibilities, a diversion

following a touch and go with subsequent go-around and climb has also been assumed, with an estimated diversion phase of around 500 km; finally the ultimate landing can happen. Now, let's proceed with the detailed description of the various phases.

2.3.3.1 Take off

To define the takeoff phase, it is necessary to estimate the required distance and the aircraft's velocity. Regarding the takeoff distance, the value of 1951 m, the same as that of an A320, has been assumed [71]. To what concern the velocity, a consideration needs to be made. During takeoff, there are usually three characteristic speeds:

- V1 or decision speed: Once V1 is reached, the takeoff cannot be aborted even in the event of problems because beyond V1 it is impossible to avoid crossing the end of the runway, even by braking with maximum intensity.
- Vr or rotation speed: The pilot acts on the elevator, raising the nose of the aircraft and lifting the wheels off the ground.
- V2 or takeoff safety speed: The pilot can continue the maneuver without risk even in the event of an engine failure.

In the case of an A320, under nominal conditions the safety speed is 268 km/h and has also been selected for the aircraft under study [71]. For simplicity, it has been decided not to study the progressive speed along the runway but to base it on an average speed equal to half of V2. This rough estimate is only used to calculate the time spent during takeoff using the following formula, which turns out to be quite realistic.

$$Duration_{TO} = \frac{Distance_{TO}}{V2} \cdot 2 = 52\,s$$

It is also estimated that during takeoff, the aerodynamic configuration of the aircraft is such that the lift-to-drag ratio assumes the maximum efficiency value, E_{Max}. At this point, recalling what was mentioned in paragraph §2.3, it is possible to estimate the fraction of the aircraft's weight lost due to the fuel consumed during takeoff:

$$w1w0 = e^{\left(-\frac{Duration_{TO} \cdot SFC_{takeoff}}{E_{Max}}\right)} = 0{,}9999$$

2.3.3.2 Climb

After completing the takeoff phase, the climb phase begins. The climb phase could be envisioned as a straight line on the altitude/distance graph; however, it is decided to refine this method. In reality, no aircraft follows this profile during the climb: instead it is divided into several sub-phases with different climb rates and speeds. To obtain an accurate result, the climb phase of an Airbus A320 Neo was analyzed considering all the various segments that, in this case, are 4. To study the climb and descent phases, the data available by Eurocontrol were of great help [71]. Indeed, values for the rate of climb (ROC), speed, and flight level (FL)

of each sub-phase were obtained, from which it was possible to estimate the duration of the studied section using the formula:

$$Duration_{Climb_i} = \frac{(FL_i - FL_{i-1}) \cdot 100}{ROC_i} \cdot 60$$

In this case as well, the next step involves calculating the remaining mass fraction at the end of the climb phase. Given the discretization reported, it is necessary to perform the calculation for each of the sub-phases and multiply the values only at the end to obtain the final result. However, some considerations need to be made. The climb phase (as well as the descent phase) extends from sea level to the cruise altitude, and several parameters change during this phase. One of these is the specific fuel consumption (SFC), but only the values during takeoff and cruise are known. For this reason, it was decided to use an SFC equal to that during takeoff for the first climb phase. This phase occurs at low altitudes, and thus the error incurred is acceptable. For all the other phases, the cruise SFC value was considered. This may be plausible for the final stages of the climb, while for the middle stages it may introduce an error that, however, helps create a conservative margin. The equations mentioned earlier were used in the different climb phases to calculate the values shown in the following table.

	Vertical range	ROC [ft/min]	Duration [s]	SFC [kg/s/daN]	E	Velocity [km/h]	$w2w1_i$
Climb phase 1	From SL To FL50	2200	136	SFC_{TO}	E_{Max}	324	0,9997
Climb phase 2	From FL50 To FL150	2000	300	SFC_{Cruise}	E_{cruise}	537	0,9988
Climb phase 3	From FL150 To FL240	1500	360	SFC_{Cruise}	E_{cruise}	537	0,9986
Climb phase 4	From FL240 To FLcruise	1000	360	SFC_{Cruise}	E_{cruise}	897	0,9986

Table 2.2: mission segment weight fraction of the climb phase

At this point, all that remains is to calculate the percentage of total mass lost due to the fuel consumed during the climb phase:

$$w2w1 = w2w1_1 \cdot w2w1_2 \cdot w2w1_3 \cdot w2w1_4 = 0{,}9958$$

2.3.3.3 Cruise

At the altitude of 30000 feet, the cruise phase begins. It should be noted that the distance covered during the cruise phase can be significantly different from that of the entire mission profile, as the distances covered during climb and descent are not negligible. For this reason, the distance covered during the cruise was set at 2400 km. By choosing this value, the aircraft will achieve a range of approximately 3000 km, which is in line with an mission imposed. However, the range requirement dictates that the aircraft should be able to extend well beyond this to about 4000 km. For this reason, it is appropriate to estimate the volume of fuel

that can be carried based on this design point, as it turns out to be the most challenging one. Consequently, the calculation is repeated by setting a range of 3400 km to satisfy the 4000 km requirement. High level requirements dictate a speed of mach 0,82 which corresponds to 897 km/h at 30000 ft. Knowing the distance covered and the flight speed, it is immediate to calculate the mass fraction consumed in the nominal mission using the formula:

$$w3w2 = e^{\left(-\frac{Range \cdot SFC_{cruise}}{V_{cruise} \cdot E_{cruise}}\right)} = 0{,}9634$$

Repeating the calculation considering the extended range:

$$w3w2_{RangeMax} = e^{\left(-\frac{Range_{max} \cdot SFC_{cruise}}{V_{cruise} \cdot E_{cruise}}\right)} = 0{,}9485$$

2.3.3.4 Descent

After completing the cruise phase, the descent begins. The same principles applied during the climb phase also apply here. In fact, the descent phase has been divided into several sub-phases, each with different parameters, to obtain a more precise estimate. In particular, in the first descent phase, there are two segments that bring the aircraft to the holding altitude at 10000 feet. Similarly, knowing the starting and ending altitudes of each sub-phase and the rate of descent, it is possible to calculate the duration:

$$Duration_{Des_i} = \frac{(FL_i - FL_{i+1}) \cdot 100}{ROD_i} \cdot 60$$

And subsequently, the mass fraction:

$$w4w3_i = e^{\left(-\frac{Duration_{Des_i} \cdot SFC_{cruise}}{E_{Cruise}}\right)}$$

The calculated data is summarized in the following table.

	Vertical range	ROD [ft/min]	Duration [s]	SFC [kg/s/daN]	E	Velocity [km/h]	$w4w3_i$
Descent phase 1	From FLcruise To FL240	1000	360	SFC_{Cruise}	E_{cruise}	897	0,9995
Descent phase2	From FL240 To FL100	3000	280	SFC_{Cruise}	E_{cruise}	537	0,9995

Table 2.3: mission segment weight fraction of the descent phase

Regarding the holding phase, a duration of 30 minutes was predetermined. Consequently, it is straightforward to calculate the mass fraction:

$$w4w3_3 = e^{\left(-\frac{Duration_{holding} \cdot SFC_{cruise}}{E_{Max}}\right)} = 0{,}9940$$

Finally consider the approach phase which, being a proper descent, uses the equations previously mentioned for the initial descent phases:

$$Duration_{Approach} = \frac{FL100 \cdot 100}{ROD_A} \cdot 60 \qquad w4w3_4 = e^{\left(-\frac{Duration_A \cdot SFC_{takeoff}}{E_{Max}}\right)} = 0{,}9992$$

We can summarize the results of the descent phase into a single coefficient:

$$w4w3 = w4w3_1 \cdot w4w3_2 \cdot w4w3_3 \cdot w4w3_4 = 0{,}9922$$

2.3.3.5 Landing

The landing phase is very brief, but to avoid excessive approximations it is calculated within the mission profile. In particular, to estimate the duration it is sufficient to estimate the landing speed and distance. Both were set based on the values of the A320 Neo, resulting in a landing speed of 250 km/h and a landing distance of 1650 m [71]. At this point, it is easy to calculate the duration of the landing phase, which is then used in the calculation of the mass fraction consumed:

$$w5w4 = e^{\left(-\frac{Duration_{Landing} \cdot SFC_{takeoff}}{E_{Max}}\right)} = 0{,}9999$$

At this point, the standard mission profile can be considered complete. However, to avoid the risk of estimating a too limited quantity of onboard fuel that could jeopardize safety in case of unexpected events, the need for a go-around with subsequent additional fuel consumption is hypothesized. Therefore, the phase just described is not considered the final landing but only an attempted landing, followed by a go-around and diversion.

2.3.3.6 Diversion

The diversion has a profile similar to the one just described for the standard mission. The takeoff phase is incorporated into the attempted landing, followed by the climb phase. This phase is calculated using the same method mentioned during the climb phase in section §2.3.3.2 using the same equations and parameters, with the only difference being that the final climb phase will now take the aircraft to the diversion altitude of 25000 ft. Similarly, the percentage of remaining mass at the end of each climb segment was calculated, and everything was combined into a single factor that considers the entire climb phase. The cruise phase during diversion, at a speed of 870 km/h, was estimated to be 200 km and the calculations performed are the same as those mentioned in section 2.3.3.3 for the cruise phase. The range during cruise is less than expected, but when added to the climb and descent phases, it ensures a diversion of about 500 km. For the descent phase at the end of the diversion, the same calculations as those performed in section 2.3.3.4 for the nominal descent are applied. The only difference is that in this case the first descent phase does not start at the cruise altitude but at the diversion altitude. Also, the holding phase, present in this case as in the case of regular descent, was estimated to last only 5 minutes. The coefficients of the various segments are combined into a single value as before. Finally, the (final) landing is nothing more than a repetition of what has already been calculated in section 2.3.3.5, with a landing speed estimated to be half that one considered before as this time the aircraft will stop completely . The found values and the data used to calculate them are presented in the following table.

	Vertical range	ROC/ROD [ft/min]	Duration [s]	SFC [kg/s/daN]	E	Velocity [km/h]	$w_i w_{i-1}$
Climb phase 1	From SL To FL50	2200	136	SFC_{TO}	E_{Max}	324	0,9997
Climb phase 2	From FL50 To FL150	2000	300	SFC_{Cruise}	E_{cruise}	537	0,9988
Climb phase 3	From FL150 To FL240	1500	360	SFC_{Cruise}	E_{cruise}	537	0,9986
Climb phase 4	From FL240 To FL250	1000	60	SFC_{Cruise}	E_{cruise}	870	0,9998
Total climb							0,9970
Diversion	FL250	0		SFC_{Cruise}	E_{cruise}	870	0,9972
Descent phase1	From FL250 To FL240	1000	60	SFC_{Cruise}	E_{cruise}	870	0,9995
Descent phase2	From FL240 To FL100	3000	280	SFC_{Cruise}	E_{cruise}	537	0,9995
Holding	FL100	0	300	SFC_{Cruise}	E_{Max}	537	0,9990
Approach	From FL100 To SL	1500	400	SFC_{TO}	E_{Max}	426	0,9992
Total descent							0,9972
Landing	SL	0	48	SFC_{TO}	E_{Max}	125	0,9999

Table 2.4: mission segment weight fraction of the diversion phases

2.3.3.7 Mission profile chart

Thanks to the work done in the previous sections, the mission profile has been defined. To get an overview, it may be useful to visualize the various segments on a graph that relates altitude and distance to have a two-dimensional representation of the aircraft's behavior. However, to do this it is necessary to first obtain the data. As for the altitudes they have already been used in the calculations and are therefore available. For the distances on the other hand, it is necessary to calculate the distance covered for each flight phase. As for

takeoff and landing, this is immediate since these values were assigned beforehand as well as for the cruise and diversion phases. Regarding the climb, descent and holding phases (both nominal and during diversion), the distance can be easily calculated by multiplying the duration (calculated previously) by the respective speed maintained in that specific phase. For precision, it should be noted that in the final climb phase and the first descent phase a speed equal to the cruise speed was imposed. During the holding phase it was chosen to estimate the speed as the same as in the previous phase, while during the approach the speed was approximated as the average between the initial approach speed equal to 463 km/h and the minimum control speed equal to 389 km/h [71]. The calculated distances and the data used are reported in the following table.

	Distance [km]	Total distance (range) [km]	Total distance (range max) [km]
Take off	1,951	2	2
Climb	200	202	202
Cruise	2400	2602	
Cruise max	3400		3602
Descent	131	2733	3733
Holding	269	3000	4000
Approach	47	3047	4047
Landing	1,65	3049	4049
Diversion	476	3527	4527

Table 2.5: distances of mission profile

As can be seen from the data presented, both a mission of approximately 3000 km and one capable of covering a distance of 4000 km have been studied. In both cases, a possible attempted landing with diversion has been considered, bringing the total distance covered to 3500 km and 4500 km respectively. The latter will be the hypothesized project point to estimate the amount of fuel to be carried on board and subsequently the fuselage volumes, as it turns out to be the most critical. At this point, it is possible to represent the profile of the standard 3000 km mission.

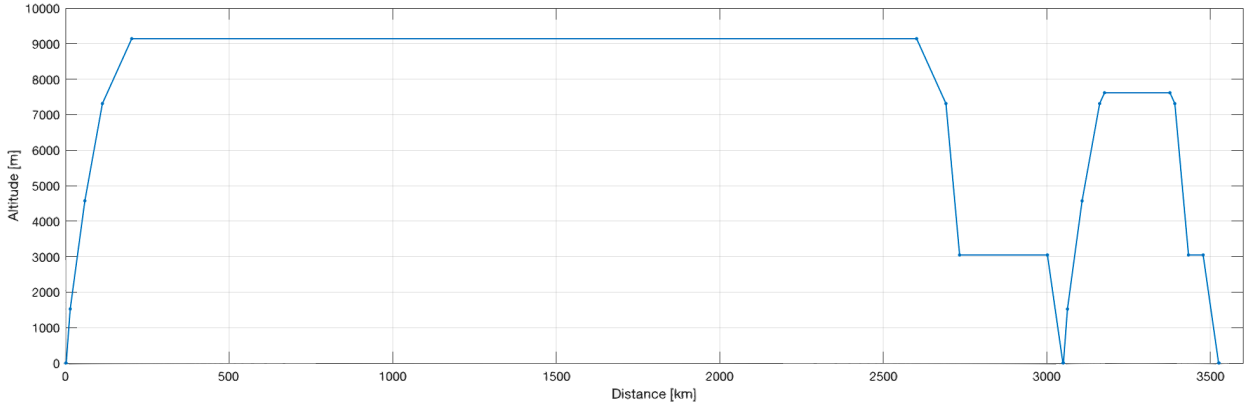

Figure 2.2: Mission profile

2.3.4 Fuel Fraction estimation

The calculations performed so far have allowed to estimate for each mission phase the remaining weight fraction resulting from the fact that a portion of fuel is consumed during that phase, thus causing a change in the total mass of the aircraft. To calculate the coefficient that takes into account the entire mission, it is sufficient to multiply the individual coefficients together, obtaining:

- For the 3500 km profile:

$$w9w0 = w1w0 \cdot w2w1 \cdot w3w2 \cdot w4w3 \cdot w5w4 \cdot w6w5 \cdot w7w6 \cdot w8w7 \cdot w9w8 = 0{,}9434$$

- For the 4500 km profile:

$$w9w0_{RangeMax} = w1w0 \cdot w2w1 \cdot w3w2_{RangeMax} \cdot w4w3 \cdot w5w4 \cdot w6w5 \cdot w7w6 \cdot w8w7 \cdot w9w8 = 0{,}9288$$

In addition, it could be useful to estimate this parameter for a standard 3000 km route without diversion since it is assumed to be the actual operational mission:

$$w5w0 = w1w0 \cdot w2w1 \cdot w3w2 \cdot w4w3 \cdot w5w4 = 0{,}9517$$

In fact, assuming that the aircraft does not always travel to the limits of its operational range and assuming the absence of issues requiring diversion from the destination airport, this situation is considered a good benchmark for what could be the average mission the aircraft will operate on. With the remaining mass fraction available, it is immediate to calculate the consumed mass as $1 - w_n w_0$. This, representing the fraction of mass consumed during the flight, approximates perfectly the fuel burned relative to the total mass of the aircraft. However it is appropriate to correct this value by a factor of 1,087 which takes into account the fact that only a portion of the aircraft's fuel is available for the mission ("mission fuel") [65]. The other fuel includes "reserve fuel" as required by civil or military design specifications (primarily to allow for engine performance degradation) and also includes "trapped fuel," which is fuel that cannot be pumped out of the tanks. For the three cases:

$$wfw0 = 1{,}087 \cdot (1 - w9w0) \qquad 3500\text{km}$$

$$wfw0_{RangeMax} = 1{,}087 \cdot (1 - w9w0_{RangeMax}) \qquad 4500\text{km}$$

$$wfw0_{actual} = 1{,}087 \cdot (1 - w5w0) \qquad 3000\text{km}$$

Usually, commercial aircraft are not designed to fly at the limits of their operational range with maximum embarkable payload. Instead, there is a tradeoff between fuel capacity and payload to avoid exceeding the Maximum Takeoff Weight (MTOW). For this reason, the calculation made considering the 3400 km cruise will be useful only to estimate the tank volume but not to calculate the mass of fuel loaded if considering the mission with 150 passengers. This aspect will be clearer in section §2.8 when defining the payload-range diagram.

2.4 Empty Mass Fraction estimation

After the aircraft will be fully designed, the actual Empty Weight (EW) is calculated by estimating and summing the weights of all the aircraft's components. For now, it can be estimated as a fraction of the maximum takeoff weight with simpler methods using the Empty Mass Fraction EMF. The fraction of empty weight statistically varies from about 0,3 to 0,7 and decreases as the total weight of the aircraft increases. However, as can be seen in Table 2.1, the values of EMF are approximately 0,5 for most of the statistical population analyzed which is plausible considering that all the analyzed aircraft fall into the same category. Indeed, the type of aircraft has a strong effect. The fraction of empty weight must be statistically estimated for preliminary calculations. Simple equations that use only one independent variable W_{TO} can be applied to predict the fraction of empty weight, calibrated using data from recent airplanes similar to the new airplane under design. However, this methodology seemed too simplified and was discarded, also considering the fact that a revolutionary aircraft is being worked on that cannot be compared to any other currently available. Another approach is to develop statistical equations using additional independent variables, based on wing aspect ratio, thrust-to-weight ratio, wing loading, maximum speed, and, of course, gross takeoff weight W_{TO}. These additional variables result in a better statistical fit, reducing the standard deviation by about half compared to the simplified equations. For this reason, the empty mass fraction is estimated as:

$$EMF = \left(0.32 + 0.66 \cdot M_{TO}^{-0.13} \cdot AR^{0.3} \cdot \frac{T}{M_{TO}}^{0.06} \cdot \frac{M_{TO}}{S_{ref}}^{-0.05} \cdot Mach_{max}^{0.05} \right) \cdot K$$

Where T is the thrust (assumed in this phase equal to 241 kN, i.e. the thrust installed on board an A320) and K is a correction factor.

It should be noted that EMF strongly depends on the type of aircraft, and since this is a hydrogen-powered aircraft that introduces different technologies from those used on standard aircraft, EMF must be corrected. Hydrogen-powered aircraft must carry hydrogen tanks, which are often lightweight but may require a specific structure and architecture to ensure safety and structural integrity. The design of these tanks and their integration into the aircraft influence the empty weight. In particular, hydrogen is much less dense than traditional fuel, so it is lighter for the same volume. Therefore, by including the payload and fuel on board of the empty aircraft, the maximum takeoff weight obtained will be much lower than that calculable in a similar case with a traditional aircraft. Due to this reduced discrepancy between M_{TO} and EW, the empty mass fraction in hydrogen-powered aircraft is larger. Furthermore, traditional aircraft have integrated tanks, which means that fuel is loaded into the wings between ribs, making the tank's weight practically negligible compared to the structure's weight. Regarding hydrogen, a dedicated non-integrated tank must be considered, resulting in additional mass. As mentioned in section §1.3.4, the gravimetric efficiency of the tank (0,5) must be taken into account and EMF is corrected by a factor $0,5 \cdot wfw0$.

$$EMF_{correct} = EMF + 0,5 \cdot wfw0_{RangeMax}$$

Furthermore, it must be remembered that in traditional commercial aircraft the presence of fuel inside the wings relieves the wing load by adding a weight which counteracts the lift acting on the wings. In hydrogen

aircraft this phenomenon will not be present due to the absence of fuel in that area and therefore the wing structure may have to be strengthened. For this reason, a 15% additional weight was assumed, taken into consideration by the factor $K = 1{,}15$.

Since the tank must be able to contain the fuel needed for the most demanding mission, this correction must be made using $wfw0_{RangeMax}$. However as mentioned earlier, even though the presence of a tank capable of holding such an amount of hydrogen must be taken into account, it should be remembered that by carrying the maximum payload it will not be possible to carry all the fuel. For this reason, it is necessary to set a design point, which in this case has been chosen to be the standard 3000 km mission with possible diversion. Because of this, the fraction $wfw0$ is used when calculating the maximum takeoff weight, but $wfw0_{RangeMax}$ is used as a correction factor for EMF.

2.5 Take-Off weight calculation

Using the fuel fraction found and the statistical equation for empty weight, the gross takeoff weight can be determined iteratively from:

$$W_{TO} = \frac{W_{crew} + W_{payload}}{1 - \left(\frac{W_f}{W_{TO}}\right) - \left(EMF_{correct}\right)}$$

This is done by estimating the gross takeoff weight, calculating the statistical empty weight fraction, and then recalculating the gross takeoff weight. If the result does not match the estimated value, the estimate is changed as the next attempt. The equation was solved iteratively in the Matlab environment with an initial M_{TO} of 20000 kg and a step of 100 kg to estimate the new attempt, resulting in:

$$M_{TO} = 61485 \text{ kg}$$

Once the maximum takeoff mass has been calculated, it is immediate to calculate the various quantities of fuel needed by multiplying the fuel factors $wfw0$ by the value of M_{TO}. Regarding the fuel to be loaded to complete the 3000 km mission, also covering the potential diversion, is achieved:

$$FuelMass = wfw0 \cdot M_{TO} = 3784 \text{ kg}$$

If the extended mission of 4500 km with reduced payload were considered, it would be necessary to load:

$$FuelMass_{RangeMax} = wfw0_{RangeMax} \cdot M_{TO} = 4756 \text{ kg}$$

Additionally, it is seemed useful to calculate the fuel consumed in the standard 3000 km mission without requiring a diversion:

$$FuelMass_{actual} = wfw0_{actual} \cdot M_{TO} = 3230 \text{ kg}$$

With the final maximum takeoff mass available, it is also possible to calculate EMF:

$$EMF = 0{,}6492$$

Taking into account the correction due to the presence of the LH2 tank:

$$EMF_{correct} = 0{,}6878$$

In this way, another very important parameter can be calculated: the empty weight. The empty weight of an aircraft represents the total weight of the aircraft when it is completely devoid of fuel, passengers, cargo, and other loads but is equipped with all other systems, components, and accessories necessary for flight and basic operations.

$$EW = 42230\,\text{kg}$$

Observing Table 2.1, it can be noted that EW is in line with the empty weight values of aircraft in its category, especially the A320 family of aircraft. This is true despite a very different M_{TO}, which confirms the accuracy of the EMF calculation and the truthfulness of the corrected EMF value. In fact, since fuel is not counted in EW, it is correct to assume that EW is in line with the values of traditional aircraft despite the different technology (except for the correction K estimating the wing stiffening). This may not be true for hydrogen fuel cell powered aircraft.

2.6 Internal volumes arrangement

The fundamental masses of the aircraft have all been calculated. To proceed with the project, it is now necessary to move on to volumes, particularly in organizing the internal volumes of the aircraft: it is crucial to estimate the size of the tanks and therefore the fuel volume. As previously explained, tank design is based on the design point that requires the highest quantity of fuel, namely a total travel distance of 4500 km. It has been calculated that in this case, a total of 4756 kg of fuel is required, which corresponds to 67 m^3 of LH2. Now the volumetric efficiency of the liquid hydrogen tanks comes into play, which is an important parameter that measures how much liquid hydrogen can be stored in a given tank volume. This efficiency is influenced by various factors, including storage temperature, pressure, and the density of liquid hydrogen. Recalling what was mentioned in section §1.3.4, an efficiency value of 0,855 has been assumed. Therefore, to contain 4756 kg of fuel, tanks occupying a volume of 77 m^3 will be required. To study the internal geometry of the fuselage, the A320 Neo aircraft has been observed. However, it is necessary to consider the fact that a rearrangement of the internal volumes is required due to the presence of the fuselage tanks which will occupy a significant space as will be seen later. In particular, considering that the density of liquid hydrogen is significantly lower than that of Jet 1-A, it is evident that it will be necessary to occupy the entire section of the fuselage to accommodate a large tank that will contain a relatively low weight. To ensure the static stability of the aircraft, it is natural to place this tank at the tail to have the payload in the front of the fuselage and shift the center of gravity forward. However, during landing with empty tanks, the stability margin of the aircraft could be too large, making it less maneuverable. To solve this problem, it was observed the technique installed on the Concorde which, for different reasons, was able to shift its center of gravity through the airframe thanks to the fuel [72]. Exploiting the freedom of configuration, it is therefore considered to house part of the fuel in forward tanks allowing the transfer of some fuel from the rear to the front of the fuselage and vice versa when the tanks are not full, thus providing some control over the center of gravity's position. Summing up, the fuselage must have the typical dimensions of a narrow-body aircraft

and accommodate the payload, landing gear bays, and the tanks positioned differentially. As can be seen in Airbus' official documents [68], the A320 aircraft can be configured in two different layouts. Both feature the classic arrangement of modern narrow-body aircraft with 6 seats per row divided by a central aisle. However, the first configuration is characterized by narrower seats to provide a wider central aisle, while the second configuration offers greater comfort to passengers but a narrow aisle. Considering that the examined aircraft will have a range of approximately 3000 km and will be used for relatively short routes, it is possible to create a hybrid configuration with compact seats and a narrow central aisle to reduce space occupancy. In this way, it is possible to raise the cabin floor to recover valuable space under it which can be used for forward tanks. The fuselage is about 15 cm thick with an internal diameter of 3,7 m. 50 cm wide seats each combined with a 48 cm wide center aisle reduce lateral encumbrance, allowing the floor to be positioned 20 cm higher at 1,63 m from the lower fuselage inner wall.

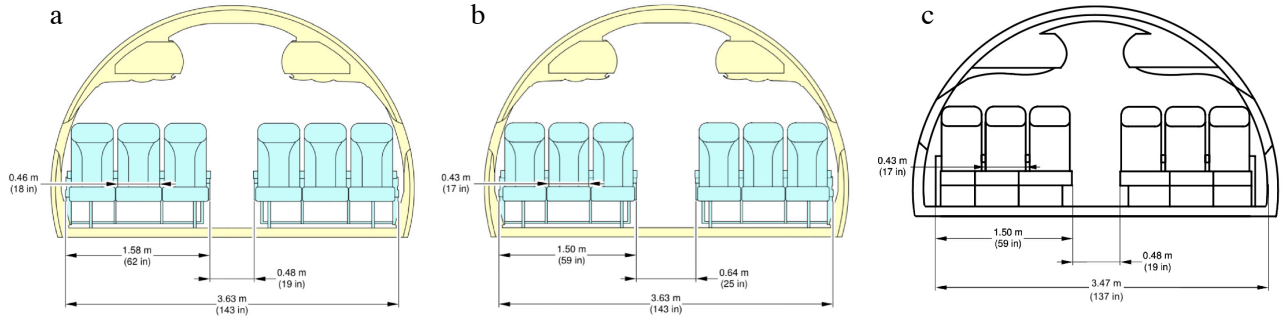

Figure 2.3: Passenger cabin of the (a) A320 with larger seat (b) A320 with smaller seat (c) aircraft examined

With the passenger cabin section now available, it is time to study the geometry of the tanks. The liquid hydrogen tanks will be subjected to high pressures, so the chosen configuration must minimizes stress as much as possible. This configuration consists of a cylinder with its two ends joined to two hemispheres. Consequently, the rear tank, which will occupy the entire section of the fuselage, only has its length as unknown variable, which will be calculated once the stowable fuel in the front tanks will be estimated. For the forward tanks, it is evident that it is not possible to occupy all the available space under the cabin using integrated tanks. Therefore, it is necessary to determine the arrangement that optimizes the available space. Additionally, due to the low volumetric efficiency of liquid hydrogen tanks and considering the technical challenges posed by pressure, it is advisable to avoid tanks that are too elongated with a small radius. For these reasons, despite tanks with a smaller cross-section would be a better choice for space optimization, it was decided to consider a maximum of 3 tanks below the passenger cabin. To choose the best configuration, the cabin section was studied, assuming the presence of cylindrical tanks positioned longitudinally under the passenger cabin floor. Assuming a single tank (red case in Figure 2.4), the limiting dimension is the distance between the passenger cabin floor and the inner fuselage wall, estimated at 1,63 m. In this configuration, a tank with a diameter of 1,6 m, featuring a frontal area of 2,01 m^2, can be accommodated. If two tanks are attempted, the dimensions must be reduced to avoid interference with the fuselage's lower part. Specifically, the tanks with a larger radius that can fit within the available space have a diameter of 1,35 m and a frontal

area of 1,43 m² each, resulting in a total frontal area of 2,86 m². Finally, by studying the positioning of three tanks, it becomes evident that they would need to be significantly smaller to fit laterally within the available space. In this configuration, each tank would have a diameter of only 1 m and an area of 0,79 m², providing a total frontal area of 2,35 m². Analyzing these three configurations, it becomes clear that the best solution is to opt for two tanks as they offer the largest frontal surface area and, therefore, can contain a larger volume while maintaining the same length.

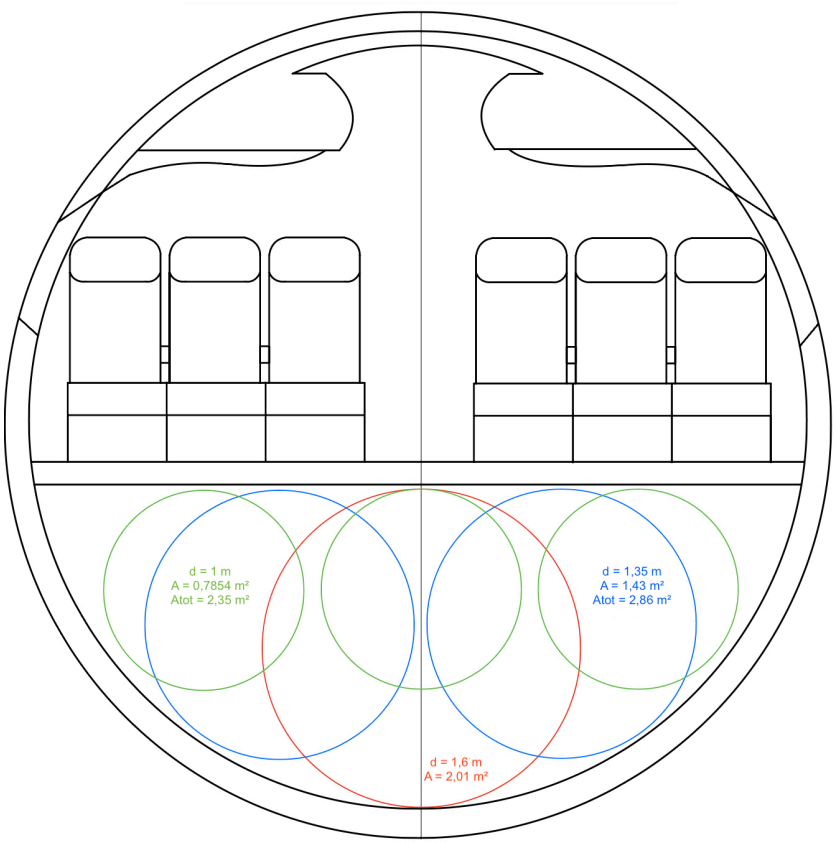

Figure 2.4: forward tanks arrangement

Having defined the cross-section of the fuselage, it is now time to study its longitudinal section. As a commercial transport aircraft, the primary focus is on the passenger cabin. The aircraft must be capable of carrying 150 passengers in rows of 6 seats each, requiring the cabin to accommodate 15 rows of seats. For optimization purposes, a seat spacing of 75 cm between seats is chosen allowing the seats to require 18,75 m within the cabin. Given the need for additional space for lavatories, galleys, and flight attendant seats, a length of 21 m is assigned to the cabin. Continuing with the payload analysis, the cargo bay is now examined. For simplicity, it is assumed that baggage is loaded on board using LD3-45 ULD containers, the same ones used on the A320 Neo [73]. Each container has a depth of 153,4 cm and can hold approximately 35 large bags. Assuming the presence of 5 containers with a total length of 7,67 m, a length of 8 m is destined to the cargo hold. The height of the containers allows them to be placed below the passenger cabin, as is the case with most aircraft. The main landing gear bays also need to find space under the cabin. The main landing gear has a significant footprint even though the retraction is transversal. The nose landing gear,

on the other hand, retracts longitudinally occupying a larger length, however it retracts forward occupying the space below the cockpit. Therefore, 4 m are assigned to the main landing gear bay, and 1 m is allocated to the portion of the nose landing gear bay that occupies the space beneath the passenger cabin. Following a brief calculation, it is clear that 8 m remain available in the lower part of the fuselage for the forward tanks, but the position of the main landing gear is not free and must be studied to ensure correct rotation during takeoff, avoiding a tailstrike. As a result of various geometric iterations, it is found that the main landing gear bay cannot be positioned directly beneath the rear end of the cabin but must be located slightly forward, approximately 1 m. The remaining 7 m can be used to accommodate the forward tanks that, to provide a margin, will be 6,5 m long. To achieve this geometry, each tank consists of cylinders 5,15 m long, closed with two hemispheres with a diameter equal to the diameter of the cylinders of 1,35 m. Remembering that two identical tanks are positioned, this composition guarantees a total volume of 17 m^3. From previous calculations, it is known that the tanks require a total volume equal to 77 m^3. Therefore, the main tank must be 60 m^3 big. Considering that the fuselage has a inner diameter of 3,7 m and that the tank will not be integrated into the aircraft's structure, a tank with a diameter of 3,6 m is considered. To contain the required volume, a cylinder with a length of 3,5 m joined to two hemispheres (similarly to the forward ones), for a total length of 7,1 m is judged suitable. In fact the main tank as described occupies a volume of 60 m^3. At this point, the central section of the fuselage trunk has been defined, capable of meeting all requirements. It will contain:

- A passenger cabin accommodating 150 passengers plus flight attendants.
- The main landing gear bay.
- A portion of the nose landing gear bay.
- A cargo hold capable of accommodating a sufficient number of bags.
- Forward tanks with a total volume of 17 m^3.
- The main tank with a volume of 60 m^3.

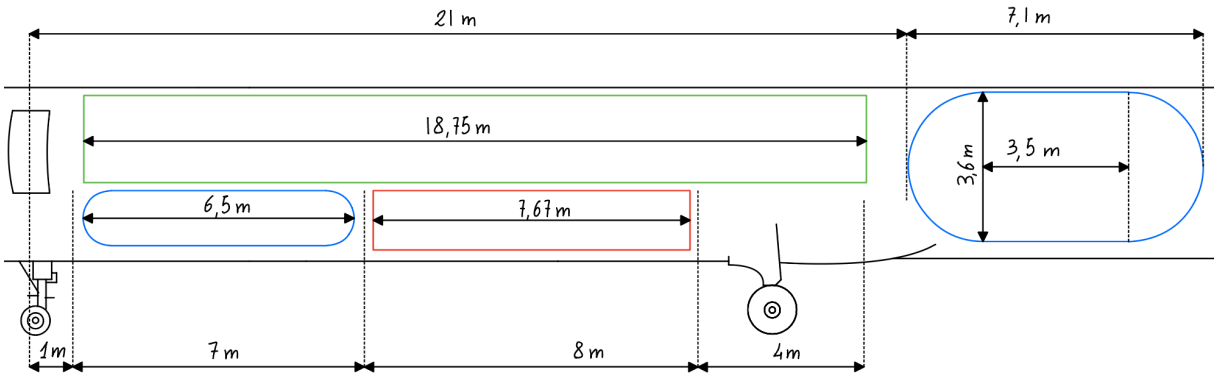

Figure 2.5: internal arrangments

2.7 External dimensions

Once the internal constraints have been defined, it is possible to determine the external geometry of the aircraft. Since this is a preliminary design of an aircraft similar to the Airbus A320 Neo, the aircraft itself will be used as an example. Upon observing the A320 Neo, it can be noted that it features a nose section approximately 5 m long which houses the cockpit and, below it, the front landing gear bay [68]. On the other hand, the rear section of the aircraft, the tail, is approximately 9,3 meters long, accommodating the APU. In a first approximation, the nose and tail cones of the aircraft under design are considered to be simple copies of those of the current A320 Neo. Furthermore, the shapes and roundness of the forms are also identical to those of the reference aircraft, thereby avoiding unpleasant errors and significantly reducing the geometric design workload. The resulting aircraft has an external length of 42,5 meters. Certainly, a more detailed revision would be necessary in the future, but it is not part of this thesis project.

An important aspect to consider when working with passenger aircraft is emergency exits. Indeed, these are crucial and are governed by specific regulations. A reliable source in this field is the document "*DOT - EMERGENCY PROVISIONS"* compiled by the Federal Aviation Administration, as it addresses Emergency exits in section §25.807 [74]. Of particular interest for this document are sub-sections:

- 25.807 (a) Type.
    - (1) "*Type I. This type is a floor-level exit with a rectangular opening of not less than 24 inches wide by 48 inches high*".
    - (3) "*Type III. This type is a rectangular opening of not less than 20 inches wide by 36 inches high". "If the exit is located over the wing, the step-down outside the airplane may not exceed 27 inches*".
- 25.807 (f) Location.
    - (3) "*If more than one floor-level exit per side is prescribed … at least one floor-level exit must be located in each side near each end of the cabin".*
    - (4) "*For an airplane that is required to have more than one passenger emergency exit for each side of the fuselage, no passenger emergency exit shall be more than 60 feet from any adjacent passenger emergency exit*".
- 25.807 (g) Type and number required. "*The maximum number of passenger seats permitted for each exit of a specific type installed in each side of the fuselage is as follows: Type A - 110, Type B - 75, Type C - 55, Type I - 45, Type II - 40, Type III - 35, Type IV - 9*".
    - (6) "*For a passenger seating configuration of more than 110 seats, the emergency exits on each side of the fuselage must include at least two Type I or larger exits*".

The aircraft under examination will be equipped with 4 Type I exits, one in the forward area and one in the rear area on each side of the fuselage. These exits would already meet the requirements. However, in the event of a water landing, the two rear exits would not be usable, which is why it was decided to add two Type III exits at wing level, one on each side. This configuration ensures that the aircraft is equipped with:

- Emergency exits on each side of the fuselage that include at least two Type I or larger exits.

- At least one floor-level exit located in each side near each end of the cabin.
- 4 Type I exits and 2 Type III exits capable of evacuating up to 250 passengers in case of land emergencies or 160 passengers in water emergencies.
- Exits spaced no more than 60 feet apart, taking into account that the cabin's full length is 21 meters and considering the presence of an additional Type III emergency exit at approximately 2/3 of the cabin's length.

In summary, the aircraft studied so far carries 150 passengers over a distance of 3000 km or a lower payload for up to 4000 km. It is characterized by a maximum takeoff weight of 61485 kg, has a wingspan of 34,1 m, and a circular fuselage with a 4 m diameter, with a total length of 42,5 m. Observing the data presented in the statistical population in table 2.1, it can be noted that the obtained aircraft has external dimensions and geometries similar to those of an A321 Neo, while the maximum takeoff weight is closer to that of an A318 within the same family of aircraft. This outcome was expected due to the characteristics of liquid hydrogen technology, which has a significantly lower density compared to traditional fuels, and this characteristic has an impact on the entire aircraft.

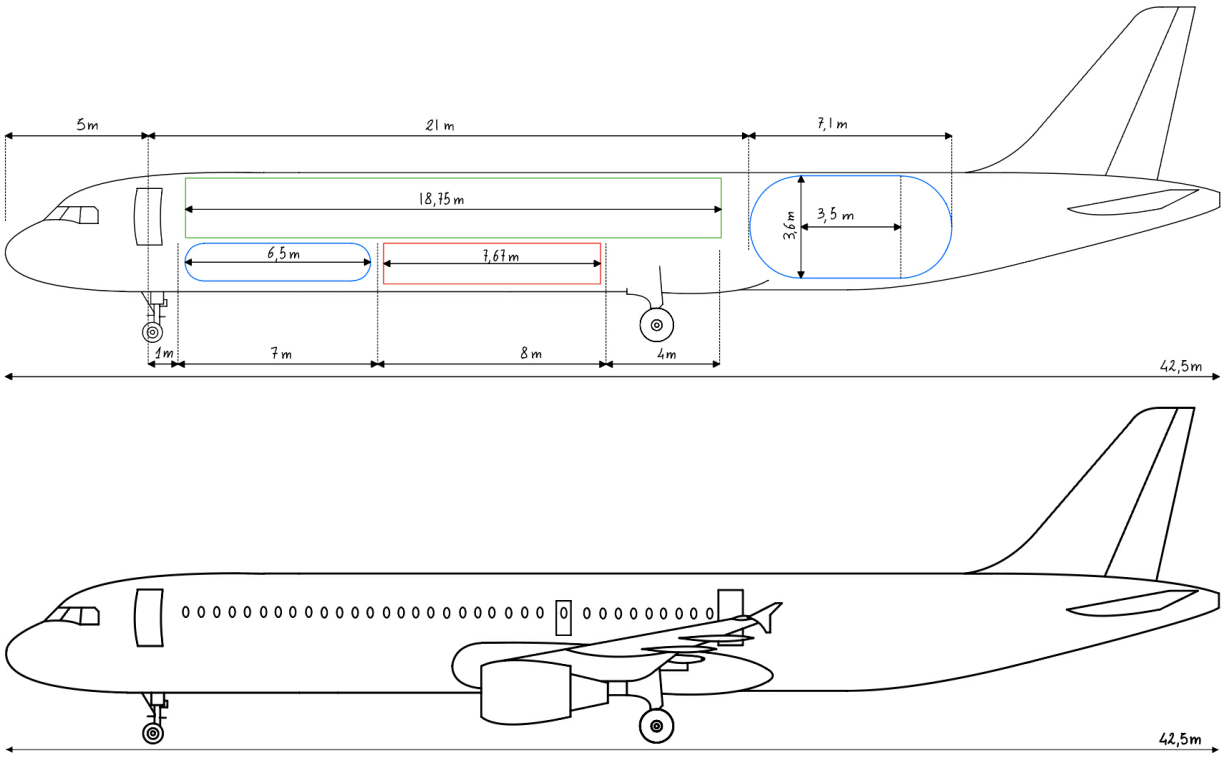

Figure 2.6: external dimensions

2.8 Payload-Range diagram

The Payload-Range diagram is a fundamental tool in the field of aeronautical and aerospace engineering, as well as in the commercial airline sector. The Payload-Range diagram provides a clear and intuitive graphical representation of the relationship between the payload (the amount of cargo or passengers an aircraft can carry) and the maximum distance the aircraft can cover with that specific payload. In other words, the diagram relates the quantity of payload an aircraft can carry to the maximum distance it can travel based on that payload configuration. This instrument plays a crucial role in evaluating the operational capabilities of a commercial airplane.

The Payload-Range diagram is typically presented as a two-dimensional graph with the y-axis representing the payload (usually expressed in weight or as a percentage of the maximum capacity) and the x-axis representing the maximum distance the aircraft can cover with that specific payload. The graph may show a series of curves or lines representing different operational conditions or load configurations, as well as different airplane to compare them. Calculating the Payload-Range diagram requires a set of parameters and technical data related to the aircraft in question. The key factors to consider include the payload, the range and the fuel consumption.

The payload can vary significantly between different commercial aircraft. In the case of the studied aircraft, even though it draws inspiration from the Airbus A320 Neo, it can carry only 150 passengers resulting in a payload mass estimated at 15000 kg. This value is the one used for the creation of this graph. It is worth noting that while the actual weight of passengers may vary from one flight to another, the payload-range diagram must be applicable to the general case: therefore estimated passengers mass values provided by Raymer based on aviation regulations are used.

The fuel consumption represents the amount of fuel required to cover a specific distance. It is influenced by various factors, including engine type, cruising speed, and atmospheric conditions. However, similar to the payload, fuel consumption can also vary from one flight to another due to factors like air traffic control holding patterns, wind effects, deviations from the flight path to avoid adverse weather. Despite that the payload-range diagram is a graph plotted a priori for a specific aircraft and it must be applicable to various scenarios. For this reason in this case, the quantity of fuel calculated in previous sections to cover the entire mission profile, including fuel consumed during potential holding or diversion phases, is used. These contingencies are considered unforeseen and cannot be included in route planning. The calculated fuel is related to a simplified mission profile that does not account for diversions.

The range is the maximum distance that the aircraft can cover with a specific amount of fuel. It is a critical parameter that significantly influences aircraft design and operation. As seen in section §2.3.3.3, a mission characterized by a cruise phase in which a certain distance is covered can connect two airports that are further apart than the cruise distance (approximately 600 km more). This will be the value used to generate the graph, assuming that the attempted landing of the complete profile is the final landing at the destination airport. However, as previously mentioned, even though this nominal range value is used, the estimated fuel required to complete the mission will also take into account the fuel needed for a potential diversion, which

is not included in the operational range. The payload-range diagram is not simply a fuel consumption index but a tool used by airlines to plan their routes. Taking for example the mission characterized by a cruise of 2400 km, it has been shown in section §2.3.3.3 that it achieves a distance of 3000 km under nominal conditions. In emergencies or unexpected events, this range can be extended to 3500 km if a diversion is considered. The fuel required to cover the entire mission, including the 500 km diversion, has been estimated to be a total of 3784 kg. However, the point calculated on the payload-range diagram will consider this quantity of fuel required to cover a range of 3000 km, as an emergency diversion cannot be included in the operational mission planning.

2.8.1 Payload-range diagram building

The graph is made with points and lines, the main components of the graph are:

- Point 1: *R*ange = 0; $M_{pay} = M_{pay_{MAX}}$

  This is a purely theoretical point representing the fully loaded aircraft traveling zero distance. The payload is at its maximum since the fuel tanks are empty and consequently it is far from the maximum takeoff weight. This point has no practical utility but serves as the starting point for the graph. From this point, one can move to the right: fuel can be added as needed to reach any range in this area, but the payload cannot increase further since it is already at the certified or physical maximum possible for the aircraft. M_{TO} increases from point 1 to point 2.

- Point 2: *R*ange = $Range(M_{pay_{MAX}})$; $M_{pay} = M_{pay_{MAX}}$; $M_{TO} = M_{TO_{MAX}}$

  There is still space in the fuel tanks to add more fuel, but at point 2, the maximum take-off weight of the aircraft has been reached. In order to fly further, some payload must be offloaded to allow more fuel to be loaded. $M_{TO_{MAX}}$ is reached and kept constant from point 2 to point 3.

- Point 3: *R*ange = $Range(M_{fuel_{MAX}})$; $M_{pay} = M_{pay_{MAX}} - (M_{fuel_3} - M_{fuel_2})$; $M_{TO} = M_{TO_{MAX}}$

  The aircraft fuel tanks are full, so the only way to fly further is to reduce the total weight of the aircraft by reducing the payload even more. Due to the reduced total aircraft weight, the aircraft is then able to fly further, even with the same amount of fuel. M_{TO} decreases from point 3 to point 4.

- Point 4: *R*ange = $Range(M_{fuel_{MAX}}, M_{pay_0}) = Range_{MAX}$; $M_{pay} = 0$

  This is the point where the curve reaches the maximum possible distance for a given aircraft. The tanks are full, and the total weight of the aircraft has been reduced acting on the payload weight until it is $M_{pay} = 0$.

  In point 4, all the weight added to the empty weight is due to fuel, representing the maximum distance that the aircraft can theoretically cover without carrying payload.

- Payload-Range Curves

  In the diagram, there are not only the four points described above, but also the lines that connect them. These lines indicate that, although the graph is calculated discretely, it represents continuous solutions not

only between one point and another but throughout the area under the graph. Consequently, any point below the segments can be possible points of use.

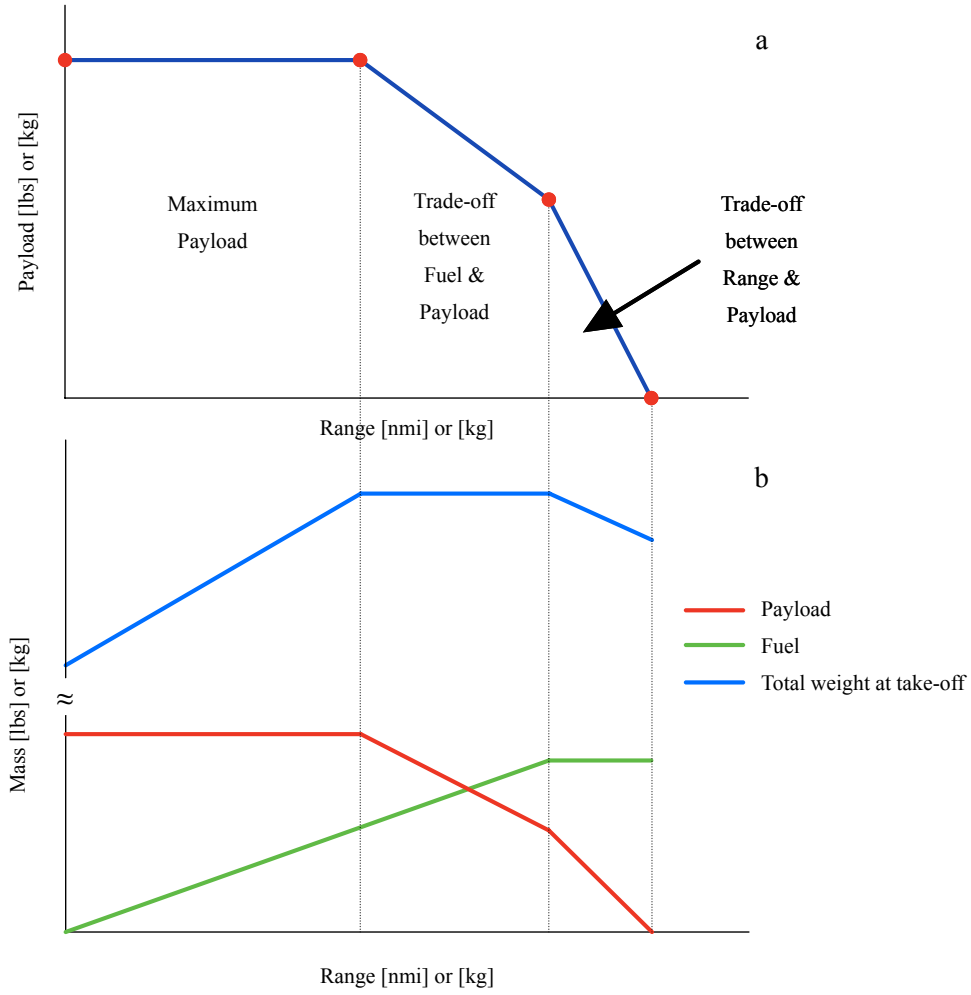

Figure 2.7: examples of (a) payload-range diagram
(b) combined payload-range-fuel diagram

Following what has just been explained, it is easy to construct the payload-range diagram of the aircraft under examination. Point 1 is characterized by a maximum payload of 15000 kg with a range null and as previously explained it has no operational utility, it merely represents the starting point for constructing Point 2. By keeping the payload constant, it is possible to increase the onboard fuel, thereby ensuring an increasingly greater range. The maximum mandatory fuel limit is reached when the total mass of the aircraft reaches (M_{TO} = 61485 kg) which corresponds to 3784 kg of fuel that allows covering a range of 3000 km. To construct Point 3, it is assumed that the LH2 tank is completely filled, therefore embarking 4756 kg of fuel. This enables a distance of 4000 km to be covered, but if this amount of fuel were loaded on board when the aircraft is fully loaded, it would result in a takeoff weight of 62457 kg: greater than the maximum allowable. It is clear, therefore, that 972 kg of payload must be removed to construct Point 3: to cover this distance, it will be possible to load only M_{pay} = 14012 kg, resulting in 140 passengers. Finally, to calculate Point 4, it is

assumed that the payload is zero. To calculate the achievable range in this configuration, the equations used to calculate the takeoff mass are reversed. It is immediately evident that the takeoff mass in this case is

$$M_{TO}(M_{pay} = 0) = M_{TO} - M_{pay_{RangeMAX}} = 47472 \text{ kg}$$

from which it is possible to calculate the $w_f w_0$ ratio. At this point, it is assumed that the weight ratios of the various phases of the mission profile remain unchanged, except for the one characterizing the cruise phase.

$$wfw0_{M_{pay}=0} = \frac{M_{Fuel_{RangeMax}}}{M_{TO_{M_{pay}=0}}} \qquad w_3w_{2_{M_{pay}=0}} = \frac{1 - \frac{wfw0_{M_{pay}=0}}{1.087}}{w2w0 \cdot w9w3}$$

Adopting these assumptions, it is possible to apply the Breguet formula to calculate the range.

$$Range_{M_{pay}=0} = -\frac{V_{cruise} \cdot E_{cruise} \cdot \log\left(w_3w_{2_{M_{pay}=0}}\right)}{SFC_{cruise}} = 4872 \text{ km}$$

As has been fully explained previously, the distance to be traveled in the event of a diversion, equal to 476 km, must be subtracted from this range. Consequently, the range that can be covered with a null payload to be inserted into the diagram is equal to:

$$Range_{M_{pay}=0} = 4396 \text{ km}$$

At this point, the payload-range diagram with its four points is available, as shown in Figure 2.8.

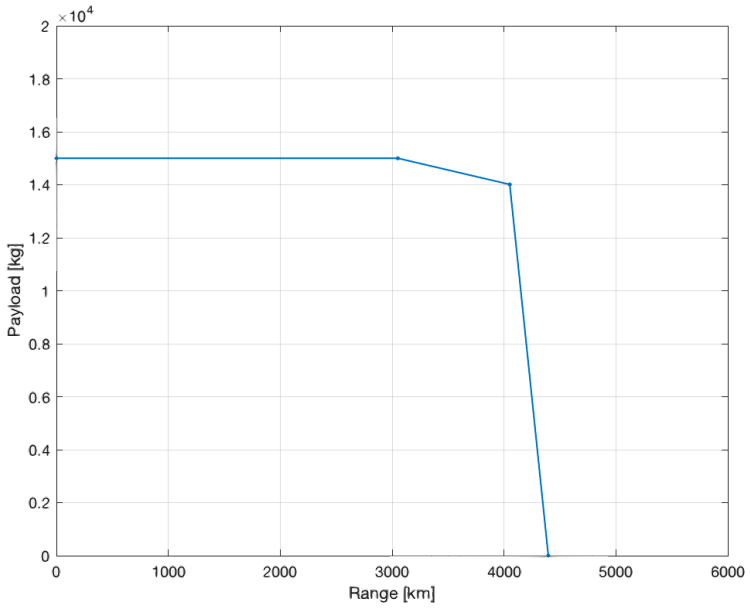

Figure 2.8: Payload-Range diagram

2.8.3 Utility and highlights

The Payload-Range diagram is of utmost importance for several aspects not only in the design phase, but also in the commercial aviation industry. It represents a real tool that can be used for:

- Cost Reduction in Development: designing and developing a new aircraft is expensive and time-consuming. An accurate and comprehensive Payload-Range diagram enables engineers to avoid costly mistakes and design decisions. This can lead to a reduction in development costs and greater efficiency in the design process. Each iteration during the design of an aircraft takes time and money, so it is necessary to minimize them whenever possible. With this tool, the risk of advancing a project that may not meet market demands is mitigated.
- Aeronautical Design: it helps aeronautical engineers optimize aircraft design, allowing them to balance payload and range based on specific customer and market needs. In particular, in the case at hand, examining the payload-range diagram clarifies that the aircraft is capable of carrying the required payload of 150 passengers for a distance of 3000 km, with the possibility of extending the operational range up to a maximum of 4000 km while still carrying a useful payload, respecting high level requests.
- Competition Assessment: in the aviation industry, competition is fierce. Airlines are constantly looking for aircraft that offer the best cost-effectiveness. An accurate Payload-Range diagram allows engineers to compare the performance of a new aircraft model with those already on the market. This helps determine whether the new aircraft will have a competitive advantage in terms of payload capacity and range compared to competitors. The payload-range diagram can be seen as the best advertisement for a particular aircraft, showing potential buyers the clear and simple relationship between fuel consumption, passengers carried, and distance traveled.
- Operational Flexibility: a well-understood Payload-Range diagram enables engineers to design more flexible aircraft. Airlines use the Payload-Range diagram to plan routes and determine maximum payload capacity based on the distances to be covered. This helps maximize operational efficiency and profit. These aircraft can adapt to a variety of operational scenarios, allowing airlines to use them more flexibly. For example, an aircraft with good long-range payload capacity can be used on intercontinental routes or shorter routes with a heavier payload. This is exactly what happens with current aircraft. It is rare for an aircraft to operate at the limits of its operational range, especially when fully loaded; it is much more likely that the actual mission for which an aircraft is used falls within the center of its payload-range diagram, at any point within the area defined by the curves connecting the characteristic points. Therefore, a well-designed aircraft with a convenient diagram can be an advantage for the airline, offering a range of operational possibilities.
- Profit Maximization: the Payload-Range diagram helps airlines maximize the profitability of their flights. Airlines can determine the maximum load they can carry on a given route to achieve maximum profit, taking into account fuel costs and other operational expenses. This analysis can help set ticket prices and plan sales strategies. Usually, the payload-range diagram is read thinking about a single mission. However, it should be remembered that in most cases, especially for low-cost airlines, an aircraft performs more than

one mission before refueling. Considering that this type of airline operates a large number of narrow-body aircraft on medium to short-haul routes, even if the aircraft under study may not be attractive to low-cost carriers, it is still an aspect to consider.

- Operational Efficiency: airlines must efficiently manage their aircraft fleet to maximize profits. The Payload-Range diagram helps determine which aircraft is best suited for a given route and specific cargo, minimizing empty or underutilized flights. This leads to greater operational efficiency and cost reduction. Especially if the airline has a large fleet, sometimes it is necessary to operate flights to move aircraft from one airport to another. These flights, if operated with light loads compared to the aircraft's capacity, can be unproductive or even costly for the airline. This aspect should also be considered when choosing which aircraft to purchase.
- Fleet Management: the Payload-Range diagram is also useful for fleet management. Airlines can assess whether they need to acquire new aircraft with specific payload and range capabilities to meet passenger or cargo demand. This analysis helps make strategic decisions regarding fleet expansion or reduction. Since airlines do not frequently update their fleets, selling old aircraft and purchasing new ones, having payload-range diagrams for each aircraft in the fleet allows the airline to move different aircraft on different routes, maximizing the overall fleet performance.
- Environmental Sustainability: in an era where environmental sustainability is a critical factor, the Payload-Range diagram can help airlines choose fuel-efficient aircraft and reduce greenhouse gas emissions. This can be an important selling point to attract environmentally conscious passengers.

Observing the obtained Payload-Range diagram, the significantly reduced range compared to the category average stands out. This reduction is a result of design constraints: the aircraft has already reached dimensions similar to those of an Airbus A321 Neo, the largest aircraft in the A320 family. Consequently, it would be challenging to add more fuel while maintaining the typical external dimensions of the category. A reduced maximum range could potentially have a negative impact on the competitiveness of the aircraft; otherwise it could conversely become one of its strengths. Based on Table 2.1, it is evident that if we look at the aircraft in the A320 family for example, they all have very extensive ranges that are almost never fully utilized. Apart a few exceptions, these narrow-body aircraft are used on domestic routes or routes with significantly shorter ranges than their maximum. This involves that the aircraft is oversized in terms of weight, wing area, and engine power to perform these missions. This results in high and unnecessary emissions and contributes to global warming. An aircraft with a more limited Payload-Range diagram (as the one under study) which operates at the limits of its diagram is characterized by significantly greater efficiency compared to traditional aircraft that operate on missions in the center of their diagram. This is because it does not carry unnecessary weight but is always utilized to its maximum potential, demonstrating by the low takeoff weight obtained in section §2.5. Furthermore, as can be observed in Figure 2.9, this issue is not marginal but affects the vast majority of missions in which this category of aircraft is used [75]. The diagrams presented show that this problem is systematic: one solution could be to revise the top-level aeronautical requirements that the next generation of aircraft should consider to minimize their impact on

global warming, making them more similar to those of this thesis. The Payload-Range diagram is an essential tool for understanding the operational performance of an aircraft based on payload and maximum range. It is used in aeronautical design, airline operational planning, business decisions, and cost management to ensure that aircraft are used efficiently and profitably in a variety of operational scenarios.

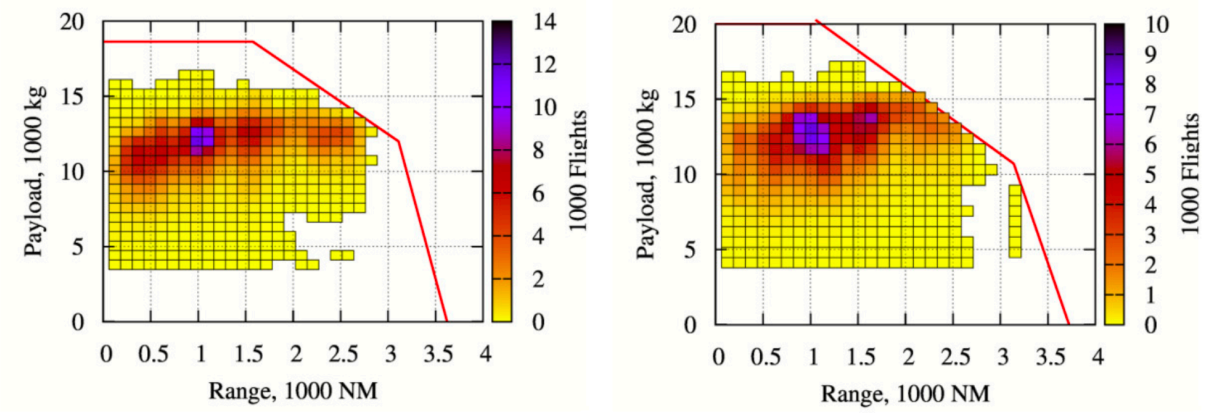

Figure 2.9: annual number of flights and payload-range diagram of an A320-200 (left) and a B737-800 (right) [75].

2.9 Matching chart

In the initial phase of the preliminary design of the aircraft, the most influential parameter M_{TO} is determined. The crucial second step is the estimation of the wing area (S_{ref}) and engine thrust (T). In the 1980s, NASA introduced a simple way to represent propulsion system requirements corresponding to the vehicle configuration within the so-called Matching Chart. The matching chart is a fundamental design tool in the aviation industry. This graphical tool represents a sort of performance map of an aircraft and enables engineers to assess and optimize the Thrust-to-Weight ratio (T/W) and Wing Loading (W/S) at a critical stage of the design process.

- Thrust-to-Weight Ratio (T/W): this parameter measures the aircraft's ability to generate thrust in relation to its weight. A high T/W value indicates that the aircraft can accelerate rapidly, perform agile maneuvers, and have better climb capability.
- Wing Loading (W/S): this parameter represents the ratio between the total weight of the aircraft (including payload, fuel, and aircraft structure) and the wing area. In other words, it indicates how much mass is supported by one unit of wing area. Lower wing loading is often desirable to enable takeoffs and landings on shorter runways and improve cruise performance.

The chart allows for the identification of a feasible design space and the definition of a design point that describes the optimal configuration of the vehicle in terms of maximum thrust, maximum takeoff weight, and wing area while meeting all high-level requirements. It should be noted that this methodology, after being introduced by NASA, has been widely analyzed and further improved by various authors, including Roskam and Raymer. The Matching Chart theory is currently widely used and implemented in various conceptual

design tools. Unlike the procedure considered for estimating M_{TO}, in this case the methodology requires a more detailed investigation of the aircraft's performance requirements and employs flight mechanics theories. It should be emphasized that the matching chart can accommodate different requirements, provided that the chosen ones can faithfully represent the characteristics of the aircraft. In this project, the matching chart has been developed considering the following performance requirements for the aircraft:

- Stall Speed
- Maximum Speed
- Rate of Climb
- Takeoff Distance
- Ceiling Altitude
- Instantaneous Turn
- Sustained Turn
- Second Segment
- Cruise Endurance

In the Matching Chart the requirements are represented by various curves or lines derived from mathematical equations that express the requirements for different phases of the mission in terms of T/W as a function of W/S. A procedure can be followed:

1. Derive equations for each performance requirement, attempting to express them as functions of T/W and W/S.
2. Rewrite the equations in the form $\frac{T}{W} = f\left(Req, \frac{W}{S}\right)$ and generate the graph of the obtained relationships. To facilitate comparison, it is necessary to graphically represent the curves on a single chart with wing loading as the horizontal axis and thrust-to-weight ratio as the vertical axis. Additionally, the equations may refer to requirements evaluated in different flight phases with different environmental conditions. For this reason, the equations need to be corrected using a factor that scales them to sea level conditions to ensure a fair comparison. This can be achieved using the ratio between air density at the considered altitude and the density at sea level, denoted as $\sigma = \frac{\rho}{\rho_0}$.
3. Once the chart is created, it is necessary to identify the acceptable region. Each curve defines the boundary between a feasibility zone and a zone to be discarded. The intersection of all feasibility areas represents the region where the design point should be located.
4. Identify the optimal design point within the acceptable region. Even though any point within the identified region represents a possible design point, it is necessary to find the optimum point, one that minimizes thrust and maximizes wing loading. The engine must generate sufficient thrust to satisfy all requirements. Therefore at the boundary of the acceptable region, among all the requirements curves, the one with the most stringent T/W value should be considered. To ensure that the wing provides sufficient lift in all flight conditions, the designer must consider the lowest estimated wing loading among all the

requirement curves and thus the highest value of S that will delineate the feasibility area. This ensures the least powerful engine and the smallest possible wings to meet all requirements of the mission.

Once the point is fixed, the evaluation of T and S is needed: setting W equal to M_{TO}, it is sufficient to multiply the takeoff weight by the thrust-to-weight ratio to find the necessary thrust that the engines must deliver. Conversely, dividing M_{TO} by wing loading will yield the wing area needed to ensure the required lift. The calculation of various requirements can now proceed.

2.9.0.1 Parasite Drag coefficient

First of all, the calculation of the zero-lift drag coefficient CD_o is carried out. This is not actually a requirement that is part of the matching chart but is a parameter necessary for writing the equations of some of the requirements. CD_o represents the aerodynamic drag generated by the shape of the aircraft and its surface when the aircraft is flying in zero-lift conditions. It is a measure of the aerodynamic efficiency of the aircraft and is one of the key parameters used in aircraft design. A low CD_o is desirable because it contributes to improving the aircraft's performance, particularly in terms of fuel efficiency and range. Parasite drag is influenced by various factors, including the aircraft's shape, wing and body surface, as well as surface finish (how smooth or clean the aircraft's profile is). Since it is a parameter that depends on a multitude of factors, different methods for its estimation have been followed.

The zero-lift drag coefficient can be estimated based on a few parameters that have been fixed at this stage of the conceptual design, such as the aspect ratio and the maximum efficiency of the aircraft [76]. In particular, to calculate CD_o, it's possibile to write:

$$CD_{0_1} = \frac{\pi \cdot A \cdot e}{4 \cdot E_{Max}^2} = 0{,}02$$

Where the Oswald efficiency factor (e) is set to 0.8, as suggested by most authors in the preliminary phase.

Raymer states that a well-designed subsonic aircraft will have zero-lift drag primarily due to skin friction plus a small pressure drag. The latter is a reasonably significant percentage of skin friction drag and this leads to the concept of the equivalent skin friction coefficient C_{fe}, which includes both skin friction and pressure separation drag. C_{fe} is multiplied by the ratio of the aircraft's wetted area to the reference area to obtain an initial estimate of parasite drag [37]. The equivalent skin friction coefficient is estimated for the civil transport to be 0,0026 resulting in:

$$CD_{0_2} = C_{fe}\frac{S_{wet}}{S_{ref}} = 0{,}0198$$

A similar method is used by another authoritative author, Roskam, who suggests that the zero-lift drag coefficient can be expressed as:

$$CD_{0_3} = \frac{f}{S}$$

Where f is the equivalent parasite area and S is the wing area [77]. It is possible to relate the equivalent parasite area to the wetted area S_{wet} using statistical relationships that, in the case of the examined aircraft, produce a value of equivalent parasite area equal to:

$$f = 0.0035 \cdot S_{wet} = 3{,}28$$

Therefore, the coefficient of zero-lift aerodynamic drag is calculated as:

$$CD_{0_3} = 0{,}0267$$

The methods converge towards similar values. $CD_0 = 0{,}02$ is chosen, as it has been frequently found as a preliminary estimate in various literature works: this will be used in the following calculations.

2.9.1 Stall Speed Vs

All fixed-wing aircraft must have a minimum speed to remain in flight, so there is a limit to the minimum allowed speed, defined as the stall speed. To ensure balance, it is necessary that at any flight speed, the lift generated by the wings equals the total weight of the aircraft ($L = W$). As the aircraft's speed decreases, approaching the stall, the wings produce less lift, so the aircraft's lift coefficient must increase approaching CL_{max} (maximum lift coefficient). When the aircraft moves at the minimum speed, which is Vs, the aerodynamic wing configuration must be capable of generating the maximum possible lift. To set the minimum speed of the examined aircraft, one suggestion could be to establish this requirement based on the required approach speed, duly considering safety factors that account for gusts or wind shear. ICAO mandates that the final approach speed during landing must be at least 1,2 times the stall speed [78]. Therefore, given that the airspeed at the runway threshold for an A320 Neo is 135 knots [71], it is required that the stall speed of the aircraft should be

$$Vs = \frac{135}{1{,}2} = 112{,}5 \text{ knots}$$

To have all the necessary parameters, it is also necessary to estimate the maximum lift coefficient (CL_{MAX}). Estimating CL_{MAX} is challenging without knowing the precise wing geometry. Generally, for wings without flaps $1.2 \leq CL_{max} \leq 1.5$ while for wings with flaps $1.5 \leq CL_{MAX} \leq 4$. To obtain more accurate estimates, knowledge of the wing profile is required. However, selecting the wing's aerodynamic profile and performing the necessary calculations to estimate CL require a higher level of detail and are not part of this thesis project. Fortunately, this problem has been overcome thanks to Raymer, who provides an empirical relationship to estimate CL_α: the lift coefficient function of angle of attack (α).

$$CL_\alpha = \frac{2\pi A}{2 + \sqrt{4 + \frac{A^2\beta^2}{\eta^2}\left(1 + \frac{tan^2\Lambda_{max_t}}{\beta^2}\right)}} \frac{S_{exposed}}{S_{ref}} F$$

Where:

- Λ_{max_t} is the sweep of the wing at the chord location where the airfoil is thickest, assumed to be 25° in analogy with the A320 aircraft.

- $\eta = \frac{Cl_a}{2\pi\beta}$. If the airfoil lift-curve slope as a function of Mach number is not known, the airfoil efficiency η can be approximated as about 0,95.
- $\beta^2 = 1 - M^2$
- $S_{exposed}$ is the exposed wing planform, which is the wing reference area minus the part of the wing covered by the fuselage.
- $F = 1{,}07(1 + d/b)$ is the fuselage lift factor that accounts for the fact that the fuselage of diameter d creates some lift due to the "spill-over" of lift from the wing. In this case, the product $(S_{exposed}/S_{ref})F$ is greater than one, implying that the fuselage produces more lift than the portion of the wing it covers (this happens sometimes in the calculations). This is unlikely and should probably be suppressed by setting this product to a value slightly less than 1 (say 0,98) as also reported by Raymer.
- The wing aspect ratio A in this equation is the geometric aspect ratio of the complete reference planform, calculated in paragraph §2.3.2.

Inserting all the data into the equation yields the angular coefficient of the cl-α curve:

$$CL_\alpha = 6{,}1 \left[\frac{1}{rad}\right]$$

At this point, it is sufficient to multiply this value by a certain angle of attack α to obtain the estimate of the coefficient. In this case the CL_{max} is of interest, so α is estimated to be 14°: a value in line with the maximum angle of attack for most aircraft in the category. Remembering that the coefficient CL_α considers the angle a in radians, we obtain:

$$CL_{max} = CL_\alpha \cdot 14^o \cdot \frac{\pi}{180^o} = 1{,}485$$

This is the estimated value of the maximum lift coefficient that can be generated by the wings at an angle of attack of 14° without the use of high-lift devices. It is well-known that the aerodynamic wing configuration can be modified by using devices capable of altering the lift and drag coefficients, such as flaps and slats. Estimating the effect these devices could have on the lift coefficient without knowing their geometric characteristics is tough. Many relations in the literature estimate that such mechanisms can double the wing's lift coefficient, so this assumption has been taken into account:

$$CL_{MAX} = CL_{max} \cdot 2 = 2{,}97$$

This is the maximum lift coefficient that characterizes the aircraft when all high-lift devices are extended and the aircraft travels at the maximum angle of attack. The obtained value is in line with the typical maximum lift coefficient of an aircraft of the same category, so it is considered reliable and will be used for subsequent calculations [77,79].

Now, all the elements are available to write the equation of the stall speed that will be used in the matching chart:

$$\frac{W}{S} = \frac{1}{2}\frac{V_s^2 \rho_o CL_{MAX}}{g}$$

2.9.2 Cruise endurance

The cruise requirement is a fundamental element in the performance of a commercial aircraft and is based on the typical equilibrium condition of the cruise phase when the aircraft is in horizontal flight at a constant speed and altitude. During cruise conditions, it must be verified that T=D, meaning there must be a balance between the thrust (T) generated by the aircraft's engines and the aerodynamic drag (D) encountered by the aircraft. This balance allows for maintaining a constant speed during the cruise without accelerating or decelerating. At the same time, L=W must be true: the equilibrium between the lift generated by the wings and the weight of the aircraft is crucial to maintain level flight at a given altitude. To meet the cruise requirement, the aircraft must be designed so that, at a specific cruise speed, it can generate thrust equal to aerodynamic drag and lift equal to weight. This implies that the aircraft must have the appropriate aerodynamic configuration and engine power to achieve and maintain these equilibrium conditions. The cruise requirement is crucial for long-range flight operations and represents one of the most efficient flight phases, where the aircraft aims to maximize fuel efficiency for covering long distances. For this reason, during the cruise phase, the goal is to minimize drag to maximize flight endurance. Since drag is directly proportional to the coefficient of drag (CD) and velocity (V), it is necessary to fly at a speed that corresponds to the minimum endurance coefficient of drag ($CD_{endurance}$). In the theory of the polar drag, this coefficient of drag value is 4/3 CD_o and is the value considered for the cruise phase. Furthermore, it is essential to bear in mind that during this phase, the engines must be operated well below their maximum capacity. Aircraft engines deteriorate rapidly when run at their maximum performance levels. Therefore, the Takeoff/Go-Around (TO/GA) mode is now only employed when necessary during takeoff and it would be inconceivable to operate the engines at their maximum throughout the entire cruise phase. Consequently, throttle settings (Π) need to be considered. In this case, a conservative estimate has been applied with the throttle set at 60% during the cruise phase. Now, all the elements are in place to formulate the equation:

$$\frac{T}{W} = \frac{1}{2}\rho V_{cr}^2 \cdot \frac{\frac{4}{3}CD_o}{\Pi \frac{W}{S} g}$$

If cruise speed increases, looking at two curves at the same time, it can be said that wing loading increases and T/W increases. Thus more powerful engine are requested and smaller S. If air density increases, the cruise is performed at a lower altitude, T/W increases, keeping the same W/S, thus the same wing geometry; conversely, keeping the T/W constant, W/S increases, thus implying a smaller wing. If drag coefficient increases, T/W increases keeping W/S constant. Conversely, the opposite applies.

2.9.3 Maximum Operating Speed Vmo

High-altitude aircraft have a maximum speed limit (Vmo). This limit is determined by the structural resistance of the aircraft and the ability of the stabilizers and control surfaces to handle aerodynamic forces. Exceeding Vmo can lead to severe structural damage. At high altitudes, it is conventional to refer to Mach number instead of velocity. Typical Mach values are around 0.75 – 0.85 and need to be converted to V values at the corresponding altitude. For commercial transport aircraft, the maximum operational speed is typically reached during cruise conditions. However, for the present case, a margin of maneuverability has been retained by imposing a maximum speed of Mmo=0,85, slightly higher than the nominal cruise speed of M=0,82. The estimated Mach value translates to Vmo = 930 km/h at the altitude of 4000 ft. To ensure the longitudinal balance of the aircraft, the following equilibrium equations can be written:

$$L = W \qquad D = T$$

Using the usual relationships from flight mechanics, it is possible to write:

$$\frac{T}{W} = \frac{\rho V_{mo}^2 C_{Do}}{2\left(\frac{W}{S}\right) g} + \frac{2K}{\rho V_{mo}^2}\left(\frac{W}{S}\right) g$$

2.9.4 Takeoff Distance l_{TO}

Usually takeoff requirements are defined in terms of the minimum ground run since every airport has a limited runway length. l_{TO} can be specified as an operational requirement but represents only a ground run. Since takeoff distance is strongly influenced by the takeoff mass, in this case the value typical of an A320 has not been observed but rather that of an aircraft with a comparable mass. The A318 has a takeoff run of 1400 m: considering that the examined aircraft is lighter than an A318, l_{TO} is set to 1300 m [80]. A linear dependence exists between W/S and T/W.

$$\frac{T}{W} = \frac{W/S}{l_{T0} C L_{TO} \rho}$$

CL_{TO} can be estimated based on CL_{MAX}. During takeoff, the lift coefficient is less than the maximum because not all high-lift surfaces are deployed. For this reason $CL_{TO} = 1{,}83$ was assumed.

ρ may differ from the sea-level density because the airport may be located at a higher altitude. In fact, aircraft of this category, being widely used worldwide, may need to take off from a variety of airports. One of the airports with a higher altitude where the A320 regularly operates is Ouito-Marisca Sucre International airport (UIO) in Ecuador at an altitude of 2800 m. The density ρ has been calculated at this altitude to provide a stringent yet plausible value.

If σ decreases, i.e. the airport altitude increases, T/W increases because with the same S a lower amount of lift is generated. If CL_{TO} increases T/W decreases, keeping W/S constant, meaning that a less powerful engine is requested. Conversely if we want to keep the same engine a smaller wing surface can be designed.

2.9.5 Instantaneous Turn and Sustained Turn

Instantaneous Turn and Sustained Turn are two fundamental concepts in an aircraft's performance during turning maneuvers. They refer to an aircraft's ability to perform turns under different conditions and reflect its agility and maneuverability.

Instantaneous turn refers to an aircraft's capability to execute a rapid and abrupt turn. This type of turn is often used in emergency situations where it is necessary to avoid a sudden obstacle or threat. During an instantaneous turn, the aircraft's speed can decrease significantly, which could lead in extreme cases, to a stall. Therefore, it is more likely to occur at low speeds and close to the ground. For these reasons, a speed equal to the speed at the runway threshold $V_{at} = 135$ knots and a high angle of attack are considered. This generates a very high lift coefficient, estimated as the maximum angle of attack without high-lift devices: $CL_{max} = 1{,}485$. Observing the accelerations that aircraft in this category experience during normal flight operations, it is noticed that they are always close to one. Considering an emergency scenario for the instantaneous turn, requiring the pilot to act abruptly on the flight controls, a load factor $n_{turn} = 2{,}5$ is estimated. At this point, all the parameters are available to write the mathematical for the instantaneous turn:

$$\frac{W}{S} = \frac{1}{2}\rho_0 V_{turn}^2 \frac{CL_{turn}}{n_{turn}}$$

Sustained turn refers to an aircraft's ability to maintain a constant and continuous turn for an extended period without significant loss of speed. The sustained turn is less aggressive than the instantaneous turn but requires efficient distribution of wing loading and power management to avoid loss of speed. This type of turn is often used in situations where it is necessary to follow a constant curved path, such as during a turn in the approach to landing or during a maneuver required by air traffic control. For these reasons, a speed equal to the climb-out speed of 175 knots is assumed, as maneuvers during climb or landing are more likely. As for the load factor, it would have been sufficient to consider a value slightly above one, as mentioned earlier. However, to be conservative a value of $n_{turn} = 2$ has been chosen. Unlike the instantaneous turn, the sustained turn does not depend on CL, so it can be written as:

$$\frac{T}{W} = \frac{\frac{1}{2}\rho V_{turn}^2 C_{Do}}{W/S} + \frac{W}{S}\frac{n_{turn}^2}{\frac{1}{2}\rho_0 V_{turn}^2 \pi A e}$$

At first glance, it may seem sufficient to consider only the instantaneous turn as it appears to be the more stringent one. However, the main difference between these two types of turns is the speed at which they can be executed and the level of acceleration they can generate. Instantaneous turn is faster but less sustainable, while sustained turn is better suited for maintaining a constant turn over time and at higher speeds. Furthermore, from the written equations it is immediate to note that the instantaneous turn imposes a constraint only in terms of wing loading, while the sustained turn relates the two variables. Since they have different natures, it is necessary to consider both to obtain two independent curves on the matching chart.

2.9.6 Second Segment

The second segment is an essential requirement established by regulations for aircraft falling under the CS 25 category, which is the certification specification issued by EASA (European Union Aviation Safety Agency) that deals with airworthiness standards for civil airplanes. This specific requirement pertains to the situation in which an engine failure occurs during the takeoff phase, known as "One Engine Inoperative" (OEI). Its importance lies in ensuring the safety and success of flight operations in critical scenarios. In this context, the requirement demands the definition of a minimum climb gradient (referred to as "G" and measured in percentage) that the aircraft must be able to maintain immediately after an engine failure during takeoff. This implies that, regardless of the aircraft's weight, it must be able to gain a certain vertical altitude concerning the horizontal distance traveled after an engine failure. An important feature of this requirement is that the required climb gradient is specified based on the number of engines available on the aircraft. This is because CS 25 considers scenarios in which even two-engine aircraft (like the one under examination) must be capable of maintaining an adequate level of safety and performance in the event of an engine failure during takeoff. In particular, Section 25.121.b of the Certification Specifications for Large Aeroplanes by EASA states that "*The steady gradient of climb may not be less than 2,4% for two-engined aeroplanes*," so this is the imposed gradient [81].

To satisfy this requirement, the aircraft must be designed to ensure that, under takeoff conditions, it can generate the necessary thrust and lift to maintain the specified climb gradient after an engine failure. The aerodynamic characteristics of the aircraft used to calculate this minimum climb gradient are considered under takeoff conditions, and the efficiency is assumed to be that of the takeoff, which is set as the average between maximum efficiency and cruise efficiency.

$$\frac{T}{W} = \frac{N_{engines}}{N_{engines} - 1}\left(\frac{1}{E_{TO}} + G_{2nd}\right)$$

If the drag increases, higher T/W are requested i.e. more powerful engines. If the lift coefficient increases, T/W can be reduced and smaller and lighter engines might be selected.

2.9.7 Rate of Climb ROC

The maximum rate of climb is an essential parameter, particularly for air traffic management. Especially near airports where many aircraft have to share the same routes, the aircraft's climb capability is crucial for quickly freeing up airspace. Typically measured in feet per minute, it assumes relatively high values (a few tens of thousands of feet per minute). Furthermore as seen in previous section, this value strongly depends on altitude. Starting from the rates of climb defined in section §2.3.3.2, begin generating the curves. Different climb phases require slightly different thrust values, so it would be sufficient to plot only the most stringent one on the graph. However, for completeness it was chosen to generate an independent curve for each climb phase. Additionally, it should be noted that the different equations for the various climb phases must also take into account altitude using the parameter σ. Five different curves will be provided: in addition to the four climb phases described in section §2.3.3.2, an additional equation representing a hypothetical zero-

altitude climb characterized by an ROC 300 ft/min greater than that of the first climb phase will be added to provide a more restrictive parameter, allowing the aircraft to climb more rapidly than expected in emergencies. The maximum climb speed must consider the speed for minimum drag, i.e., maximum aerodynamic efficiency, so all the curves will be plotted for E_{MAX}. Furthermore, for the same reasons already explained in section §2.9.2, it must be taken into account that the engines cannot be pushed at their maximum in this case too. For this reason a throttle of 80% was considered.

$$\frac{T}{W} = \frac{ROC}{\Pi\sqrt{\frac{2g}{\rho\sqrt{\frac{C_{D0}}{K}}}\left(\frac{W}{S}\right)}} + \frac{1}{\left(\frac{L}{D}\right)_{\max}}$$

2.9.8 Absolute Ceiling h_c

The ceiling is defined as the highest altitude at which an aircraft can safely maintain leveled flight. The absolute ceiling is the altitude at which the ROC is zero, so it is easy to derive the characteristic equation from that used in the climb phase of the previous section:

$$\frac{T}{W} = \frac{ROC}{\sqrt{\frac{2g}{\rho\sqrt{\frac{C_{D0}}{K}}}\left(\frac{W}{S}\right)}} + \frac{1}{\left(\frac{L}{D}\right)_{\max}} \quad \Rightarrow \quad \frac{T}{W} = \frac{1}{\sigma\left(\frac{L}{D}\right)_{\max}}$$

2.9.9 Matching chart plot

Now that all the curves related to the various requirements are available, it is possible to generate the matching chart, shown in the Figure 2.10.

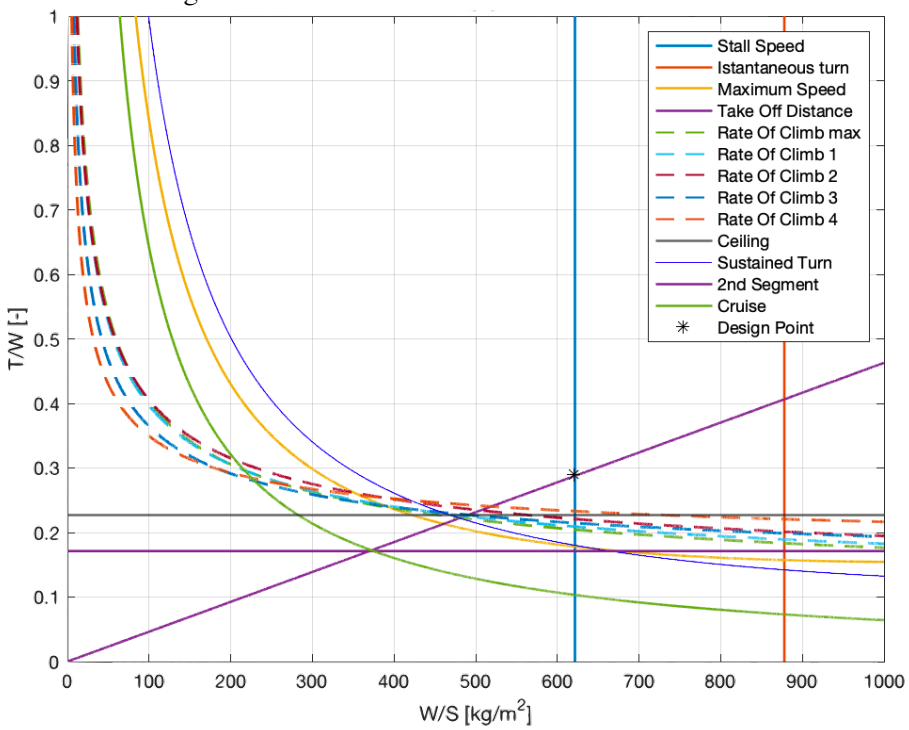

Figure 2.10: Matching chart

The design space can be identified as the part of the graph characterized by T/W greater than the most stringent requirement (in this case: takeoff, the last climbing phase and the sustained turn) and W/S lower than the most stringent requirement (in this case: stall speed). In particular, the point of intersection is located where the maximum wing loading is reached, combined with a thrust-to-weight ratio slightly higher than what is theoretically achievable with a larger wing area. Usually, the maximum wing loading (i.e., the minimum required wing area) is selected. In this case, the optimal design point is characterized by weight-to-power ratio and wing loading equal to:

$$\frac{T}{W} = 0{,}29 \qquad\qquad \frac{W}{S} = 620$$

Now, it is sufficient to correctly multiply these values by the takeoff mass (M_{TO}) to obtain the thrust and wing area. The aircraft that is being designed must have a wing area equal to

$$S = \frac{1}{W/S} \cdot M_{TO} = 99{,}16\ m^2$$

and must be equipped with engines capable of delivering a total thrust of

$$T = \frac{T}{W} \cdot M_{TO} = 175\ kN$$

2.9.10 Workflow and Data Validation

The workflow that led to these results is widely used and has proven to be quite reliable. However it is wise to perform a comparison. From Table 2.1, it can be noted that the Airbus A318 is equipped with a total thrust of 212 kN. This discrepancy seems reasonable when considering that the A318 needs more thrust due to its takeoff mass more than 6500 kg greater than the aircraft under study. Moving on to the wing loading, all aircraft in the A320 family have the same wing area of 122 m². If one considers that this wing area is sufficient to lift an aircraft with a takeoff mass of 93000 kg like the A321 Neo, it is intuitive to think that the obtained wing area is a realistic value. Furthermore, for a more precise comparison, one can observe data related to the now-dated Boeing 737-300, which has a takeoff mass of 63300 kg and a wing area of 105 m², perfectly in line with the calculated values considering the generational differences. As extensively described in the previous sections, wing area and thrust are delicate parameters that cannot be estimated with a simple statistical analysis. However, it is believed that this comparison demonstrates the quality of the work performed and the accuracy of the obtained data.

2.9.11 Coffin Corner

Having estimated the minimum and maximum speeds, the aircraft's ceiling and the wing area, we can digress briefly on the coffin corner. The term “coffin corner" in aviation refers to a critical and dangerous situation that can occur during high-altitude flight. This term primarily applies to aircraft capable of flying at high altitudes and speeds, such as transport airplanes. The coffin corner is a condition in which aircraft operate with a very narrow margin between two critical speed limits.

- Stall Speed Limit: at high altitudes the air is thinner, meaning it has lower density. This affects aircraft performance, especially stall speed: at very high altitudes, the aircraft must fly at higher speeds to avoid aerodynamic stall (stall) of the wings, so the stall speed limit increase.
- Maximum Speed Limit: on the other hand, the aircraft has a maximum speed that cannot be exceeded and this complicates the situation.

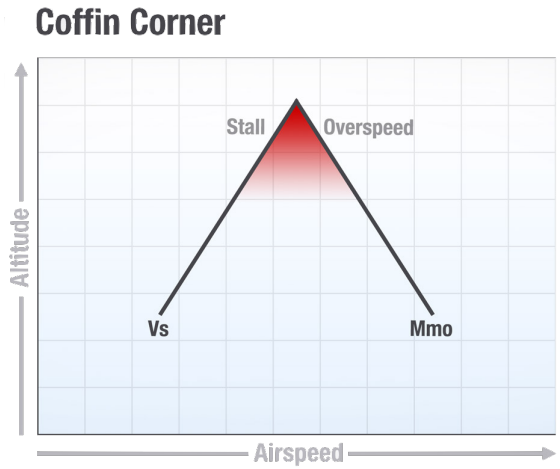

Figure 2.11: coffin corner

The "coffin corner" represents the range of speeds between the increasing stall speed limit and the maximum speed limit. In this zone, the safety margin could be small, and aircraft must be handled with caution. If a pilot attempts to increase speed to avoid a stall, they could dangerously approach the maximum speed limit, while decreasing speed could lead to a stall. Therefore, unable to change the stall speed and needing to ensure the aircraft reaches the service ceiling, the aircraft must be sized in such a way that the maximum speed provides a sufficiently high margin in the coffin corner to ensure high-altitude safe flight. In the case under examination, a stall speed of 205 km/h was imposed at sea level. Translating this value to the maximum altitude, i.e., the service ceiling at 40000 ft, we get:

$$V_{S_{ceiling}} = \sqrt{\frac{2 \cdot M_{TO} \cdot g}{\rho_{ceiling} \cdot S \cdot CL_{MAX}}} = 413 \frac{km}{h}$$

This value is well below the maximum flight speed at that altitude. In fact, starting from the maximum operating Mach number = 0.85, it is possible to calculate the maximum speed at the ceiling:

$$V_{mo_{ceiling}} = 0{,}85 \cdot \sqrt{\gamma R \left(T_o - 6{,}5 \cdot z_{ceiling} \right)} = 930 \frac{km}{h}$$

The difference between the stall speed and the maximum speed at the service ceiling is not only positive but also provides a good margin of adaptability to ensure safe flight.

2.10 Iteration

Aeronautical design is a complex field that requires a deep understanding of a wide range of scientific and engineering disciplines. Creating a safe and efficient aircraft is a challenge that demands an iterative process of development and refinement. Iteration is a key element in this process and plays a fundamental role in ensuring the success of aeronautical projects. Although this thesis project deals with only a small part of an aeronautical project, iteration is crucial in this work too. As mentioned earlier, the results presented in the previous sections are the product of various numerical and geometrical iterations, which have been omitted for brevity. However, at this stage of the project, it is necessary to introduce an iteration that will modify all estimated parameters and the obtained results, which is why it is considered deserving of the right attention.
The matching chart has proven to be a fundamental tool that allowed estimating the required thrust and the necessary wing area to generate the correct lift. Although the results obtained may be assumed valid in the preliminary phase of a conceptual design, there is an important aspect to consider. The matching chart was constructed based on various requirements at the end of a workflow that led to the estimation of take-off mass. To estimate various parameters used in the work, thrust and wing area values were used. Remember that the thrust was taken from the one currently installed on an A320 and the wing area was assumed to be that of this aircraft. However, it has been observed that the results obtained from the matching chart, although not far from them, differ from these values. Therefore, it is now necessary to repeat the entire design process using the thrust and wing area values obtained from the matching chart as references, as these quantities have been used since the early stages.

	Assumptions (A320)	Values obtained (matching chart)
Thrust	241 kN	175 kN
Wing area	122 m²	99 m²

Table 2.6: Thrust and Wing Area before and after matching chart

The procedure described in these paragraphs of the second chapter will be entirely retraced, starting from the new values of thrust and wing area. Obviously, not all explanations and descriptions extensively discussed previously in the dedicated sections will be reported; instead, the numerical values of the various parameters and results that differ from the previous ones will be presented.

2.10.1 Aerodynamic Characteristics

Updating the wing area, many of the estimated aerodynamic parameters are modified. Attention must be paid: it is not sufficient to modify only the wing area. In fact, this could lead to unrealistic and skewed results in terms of aspect ratio and aerodynamic efficiency. For instance, wings characterized by a smaller area are likely to have a smaller wingspan. Following numerical iterations to find plausible values, a wingspan of 32 m has been chosen. Furthermore, based on the sketch obtained in section §2.7, the length of the fuselage has been increased to 42,5 m. Since this is still a preliminary design, these were the only updated parameters

besides the wing area. The fuselage diameter, tailplane and engine nacelle surfaces, as well as the winglets, remained unchanged. Bearing these assumptions in mind, it is possible to recalculate all parameters that involve wing area and wingspan.

$$S_{wet} = S_{ref} \cdot 2 + S_{H_{tail}} \cdot 2 + S_{V_{tail}} \cdot 2 + \pi \cdot D_{iameter_{fuselage}} \cdot L_{ength_{fuselage}} + S_{engine} \cdot 2 = 927{,}4\, m^2$$

$$Wetted\ Area\ Ratio = \frac{S_{wet}}{S_{ref}} = 9{,}27$$

$$Aspect\ Ratio = \left(\frac{Wingspan^2}{S_{ref}} \right) + 1.9 \cdot \frac{h}{Wingspan} = 10{,}38$$

$$E_{Max} = 15.5 \cdot \sqrt{\frac{Aspect\ Ratio}{Wetted\ Area\ Ratio}} = 16{,}4 \qquad E_{cruise} = 14{,}2$$

2.10.2 Mass Fractions Estimation

The changes made also affect the mission profile, particularly the weight fractions that the aircraft loses due to the consumed fuel mass in each phase. Indeed, efficiency values influence the Breguet formula and thus the calculations must be repeated, keeping all other parameters related to mission phases constant. The following table presents the updated mass fraction values.

Phase	$w_i w_{i-1}$
Take-off	0,9999
Total climb	0,9955
Cruise (2400 km)	0,9612
Cruise (3400 km)	0,9455
Descent	0,9988
Holding	0,9936
Approach	0,9992
Attempted landing	0,9999

Diversion	
Phase	$w_i w_{i-1}$
Total climb	0,9968
Diversion	0,9971
Descent	0,9988
Holding	0,9989
Approach	0,9992
Attempted landing	0,9999

Table 2.7: mission segment weight fraction of the mission profile

Following the process described in section §2.3.4, updated mass coefficients which include all mission phases were derived. Subsequently, fuel fractions were calculated for the three reference missions, as previously done. All values are presented:

$$w9w0 = 0{,}9400 \qquad wfw0 = 1.087 \cdot (1 - w9w0) = 0{,}0652$$
$$w9w0_{RangeMax} = 0{,}9247 \qquad wfw0_{RangeMax} = 1.087 \cdot (1 - w9w0_{RangeMax}) = 0{,}0819$$
$$w5w0 = 0{,}9488 \qquad wfw0_{actual} = 1.087 \cdot (1 - w5w0) = 0{,}0557$$

2.10.3 Take-Off Weight Calculation

At this point, all the updated data are available to calculate the new take-off weight value, bearing in mind that this is calculated using the formula:

$$W_{TO} = \frac{W_{crew} + W_{payload}}{1 - \left(\frac{W_f}{W_{TO}}\right) - \left(EMF_{correct}\right)}$$

The masses due to the presence of the crew and payload remain unchanged, $w_f w_0$ has just been calculated with the updated values, while $EMF_{correct}$ has been computed using the same formula as presented in section §2.4. The value that will be used in the iterative calculation for W_{TO} will be different from the previous one, indeed it includes values that have been updated in this iteration such as aspect ratio, thrust, and reference area. Following the process outlined in section §2.5, it is straightforward to calculate the maximum take-off mass, the fuel mass for the three missions under consideration, as well as the values of empty mass fraction and empty weight of the aircraft. The calculated values are reported:

$$M_{TO} = 62282\,kg \qquad Fuel\ Mass = wfw0 \cdot M_{TO} = 4059\,kg$$
$$EMF_{correct} = 0{,}6874 \qquad Fuel\ Mass_{RangeMax} = wfw0_{RangeMax} \cdot M_{TO} = 5099\,kg$$
$$EW = 42813\,kg \qquad Fuel\ Mass_{actual} = wfw0_{actual} \cdot M_{TO} = 3467\,kg$$

2.10.4 Geometry

The payload remains unchanged, so it is intuitive to assume that the dimensions of the passenger cabin and cargo bay also remain the same. For this reason, needing to utilize the remaining space in the lower part of the fuselage, the dimensions of the forward tanks also remain the same. This means that the forward tanks are capable of containing 17 m^3 of fuel in this iteration too. However, in this case the total fuel to be loaded on board is 84 m^3, which means the main tank must carry 67 m^3 of fuel, 7 m^3 more than what was reported in paragraph §2.6. For this reason it must be larger: considering the two hemispheres with a diameter of 3,6 m (the frontal dimensions remain unchanged), the cylindrical section must be 4,2 m long. This way, a tank 7,8 m long is obtained, capable of containing the 67 m^3 of fuel required. At this point, it is immediate to verify that considering the forward tanks (1035 kg) and the rear tank (4065 kg), it is possible to load on board the 5100 kg of fuel required for the longest mission, as calculated in this iteration.

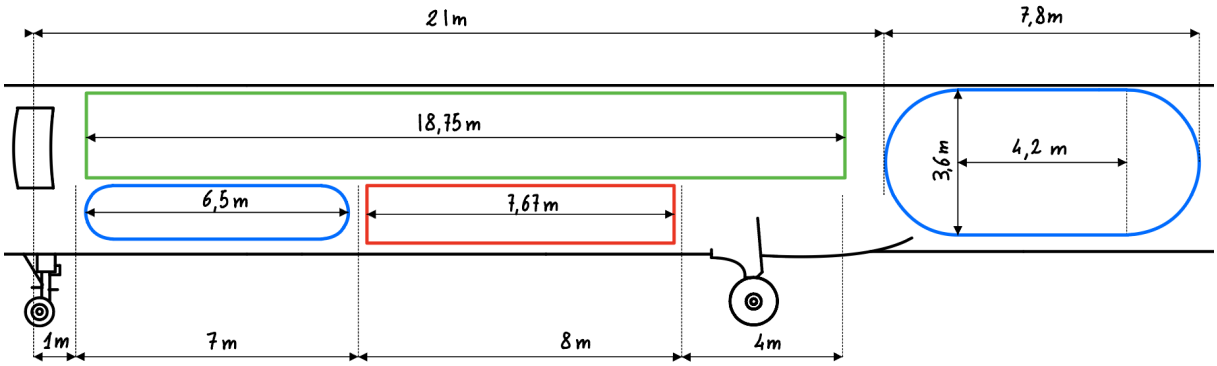

Figure 2.12: Internal arrangments

The external dimensions remain unchanged. In fact, the nose and tail are the same, as well as the landing gear and emergency exits. The only thing that changes from the previous work is the rear tank, which is 0,7 m longer. Fortunately, during the creation of the sketches presented in section §2.7 a good margin was maintained between the rear tank and the tail cone. This allowed the insertion of the longer new tank within the same external geometry. Of course, the rear hemisphere will occupy part of the tail cone, potentially reducing the volume dedicated to the APU. However, considering the preliminary nature of the calculations, this is not a problem to take into consideration at this stage.

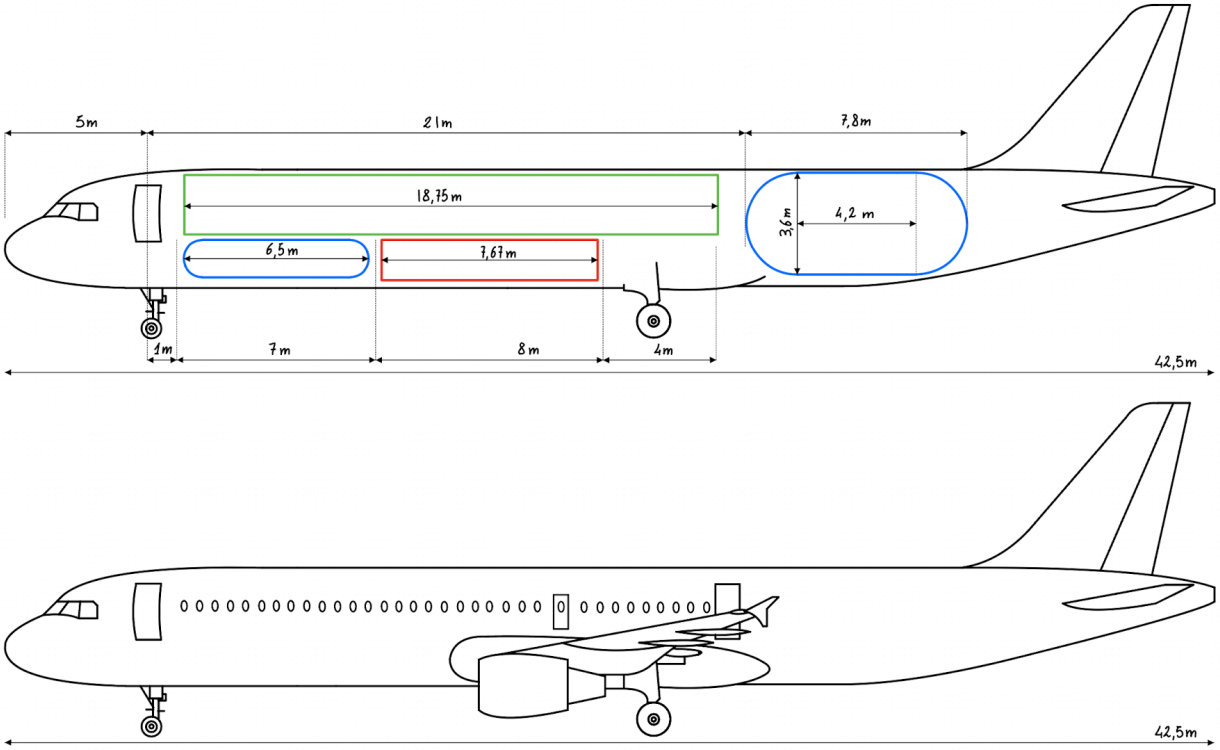

Figure 2.13: External dimensions

2.10.5 Payload-Range Diagram

Having modified the fuel mass consumed and the maximum take-off weight of the aircraft, the payload-range diagram could also undergo variations. Thus, it is appropriate to create one that takes the new parameters into account. The payload is the same as before, so points 1 and 2 remain unchanged. Furthermore, the mission profile remains the same, so the range of point 3 also remains unchanged. However, the increased fuel load requires a reduction in the transportable payload to fully fill the tank, which decreases to 13943 kg. This means that considering the new data, the aircraft will be able to carry one less person than before (139 passengers) over a distance of 4000 km. Finally, to calculate point 4 the same procedure described in paragraph §2.8.2 is repeated. In particular, the range with zero payload is sensitive to the mass fraction consumed in cruise which has now changed. Consequently, the abscissa of point 4 will be slightly different. Using the updated data, the Breguet formula yields a range of 4366 km, net of the diversion distance.

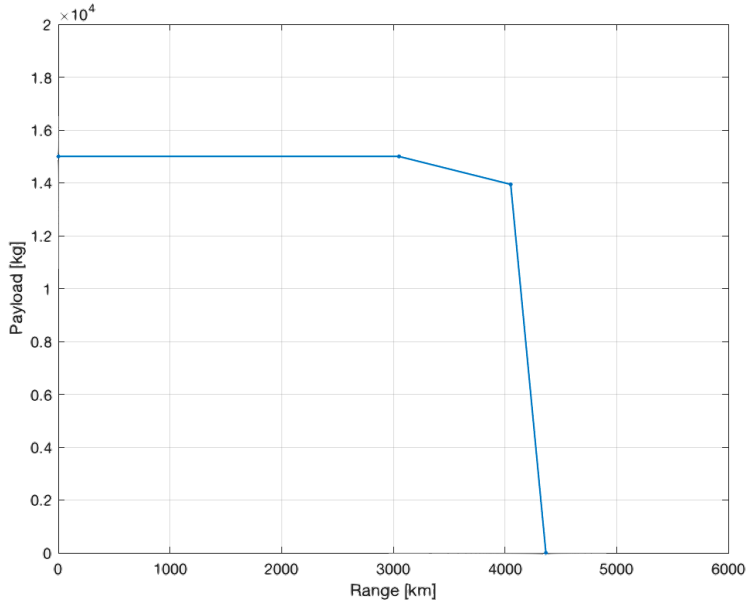

Figure 2.14: Payload-Range diagram

2.10.6 Matching Chart

Building the updated matching chart is easy, as all previously used equations remain valid. Of course, updated parameters must be used within them. In particular, the calculation of the CL_α slope is influenced, and consequently, the CL_{max} that the aircraft can generate without high-lift devices at an angle of incidence of $\alpha = 14°$ is slightly higher:

$$CL_{max} = 1{,}5$$

To calculate the CL_{MAX} generated using flaps and slats the same method is used, doubling the value yields:

$$CL_{MAX} = 3$$

Consequently, the CL_{TO} corresponding to the aerodynamic configuration used during takeoff now equals:

$$CL_{TO} = 1{,}86$$

All the speeds set by the designer remain unchanged, as well as the distances, altitudes, and load factors in turns. Considering the reported lift coefficients and inserting the correct data into the equations, the curves generating the updated matching chart shown in the Figure 2.13 are obtained.

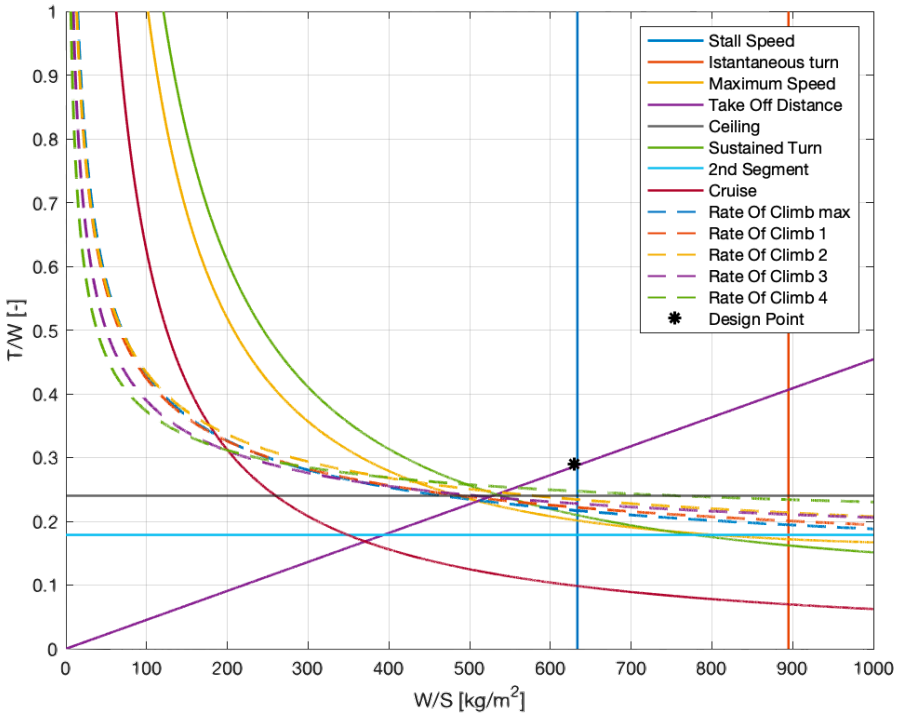

Figure 2.13: Matching chart

The design point has shifted slightly, resulting in the following values for power-to-weight ratio and wing loading:

$$\frac{T}{W} = 0{,}29 \qquad\qquad \frac{W}{S} = 630$$

To find the updated values of thrust and wing area, it is sufficient to consider the updated take-off weight:

$$S = \frac{1}{W/S} \cdot M_{TO} = 99{,}9\, m^2 \qquad\qquad T = \frac{T}{W} \cdot M_{TO} = 177\, kN$$

In contrast to what was obtained previously, this time the values found are very similar to those used throughout the process. It is worth noting that using the data obtained from the first matching chart, a thrust of $175\, kN$ and a wing area of $99{,}17\, m^2$, in the procedure just described were used from the start. These values are extremely similar to the results obtained at the end of this iteration, suggesting that the process has likely converged.

2.10.7 Results Verification

To provide accuracy verification of the values obtained at the end of this iteration, it is advisable to compare them with the initial statistical population reported in Table 2.1. In particular, for a fair comparison, it is not recommended to look at the thrust and wing areas, which may rightfully refer to aircraft different from the one being analyzed. Instead, it is suggested to compare the thrust-to-weight ratios and wing loadings to make a comparison of design points on the just-obtained matching chart. First, it is necessary to calculate T/W and W/S for each of the aircraft listed in Table 2.1. Then, it is possible to insert the obtained points into the matching chart of the aircraft under design. For convenience, the average design point was also calculated, which is a theoretical point obtained by averaging all the thrust-to-weight ratios and wing loadings of all the aircraft in the statistical population (marked red in the Figure 2.14).

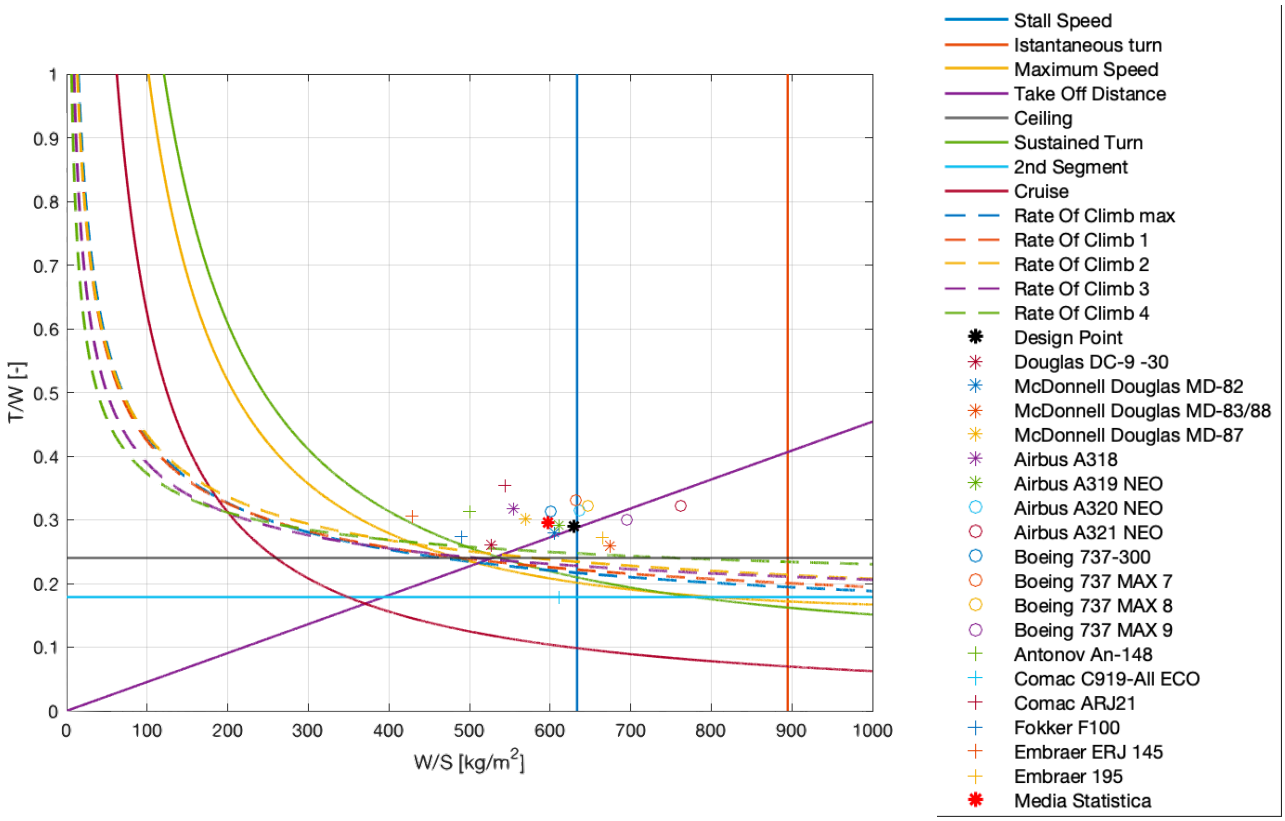

Figure 2.14: matching chart and statistical population

As can be seen in Figure 2.14, the design point obtained for the aircraft under examination is entirely within the area of validity and is also quite close to the statistical average. This result provides further confirmation of the power of Raymer's method and the reliability of the results obtained, especially when considering the different technology used on this aircraft.

2.11 Margin of static stability

The results obtained in paragraphs §2.10.6 and §2.10.7 have shown that the design process has converged, and the obtained results are considered reliable. However, before definitively setting the design point, it is necessary to perform an additional check. As it is well known, all aircraft must have the center of gravity and the aerodynamic center positioned in such a way to ensure static stability (apart from some high-performance military aircraft). Static stability in commercial aircraft is a fundamental concept and plays a crucial role in ensuring the safety and control of the aircraft during flight. This refers to the aircraft's tendency to automatically return to its desired position and attitude after being disturbed by a deviation caused by an external disturbance, such as a gust of wind or a sudden movement of the flight controls. In other words, static stability indicates the aircraft's ability to spontaneously return to a stable flight condition without requiring constant pilot intervention. To achieve static stability in a commercial aircraft, it is necessary to act on the position of the center of gravity relative to its aerodynamic center. The aerodynamic center is the point where the resultant aerodynamic forces (such as lift and drag) act. To achieve static stability, the center of gravity must be positioned ahead of the aerodynamic center. This creates a restoring moment that automatically brings the aircraft back to its stable condition. To assess the stability of the aircraft, a new parameter called the margin of stability (MS) is introduced, representing the percentage rate of the distance between the neutral point and the center of gravity and the position of the neutral point itself.

$$Margin\ of\ stability = \frac{x_{aerodinamic\ center} - x_{center\ of\ mass}}{x_{aerodinamic\ center}} \cdot 100\,\%$$

The margin of stability must not only be positive but must also fall within an acceptable range of values. Indeed, a value that is too low could make the aircraft twitchy and uncomfortable to fly despite being stable, whereas too high a margin of stability would make the aircraft very sluggish in maneuvers and lethargic to control. To check the static stability of the aircraft, it is necessary to calculate the margin of stability. The examined aircraft is characterized by a mass distribution that, in addition to being different from that of traditional aircraft, varies widely throughout the mission. For this reason, it is considered necessary to perform this check not for a single aircraft configuration but at least for the 3 points of use on the matching chart (excluding the first point), considering the different load configurations. The neutral point of the aircraft remains constant in the various configurations as it depends only on the external geometry. Consequently, it is necessary to calculate it only once. To accurately calculate the aerodynamic center would require specific calculations that do not fall within a conceptual project's scope. For this reason, this point is estimated geometrically. It is known that in subsonic conditions, the neutral point is positioned approximately at 25% of the mean aerodynamic chord (MAC). The mean aerodynamic chord is approximated by calculating the mean chord of the trapezoidal wing of the same surface area (indicated in red in Figure 2.15). In fact, although the aircraft's wing has been constructed by scaling the A320 wing, approximating it with a simplified wing allows for easy calculation of the mean aerodynamic chord using the geometric method of diagonals. Once the MAC is determined, the neutral point is fixed at one-quarter forward along the MAC. In

the case under examination, measurements taken from the sketch show that the aerodynamic center is located 21,9 m from the nose.

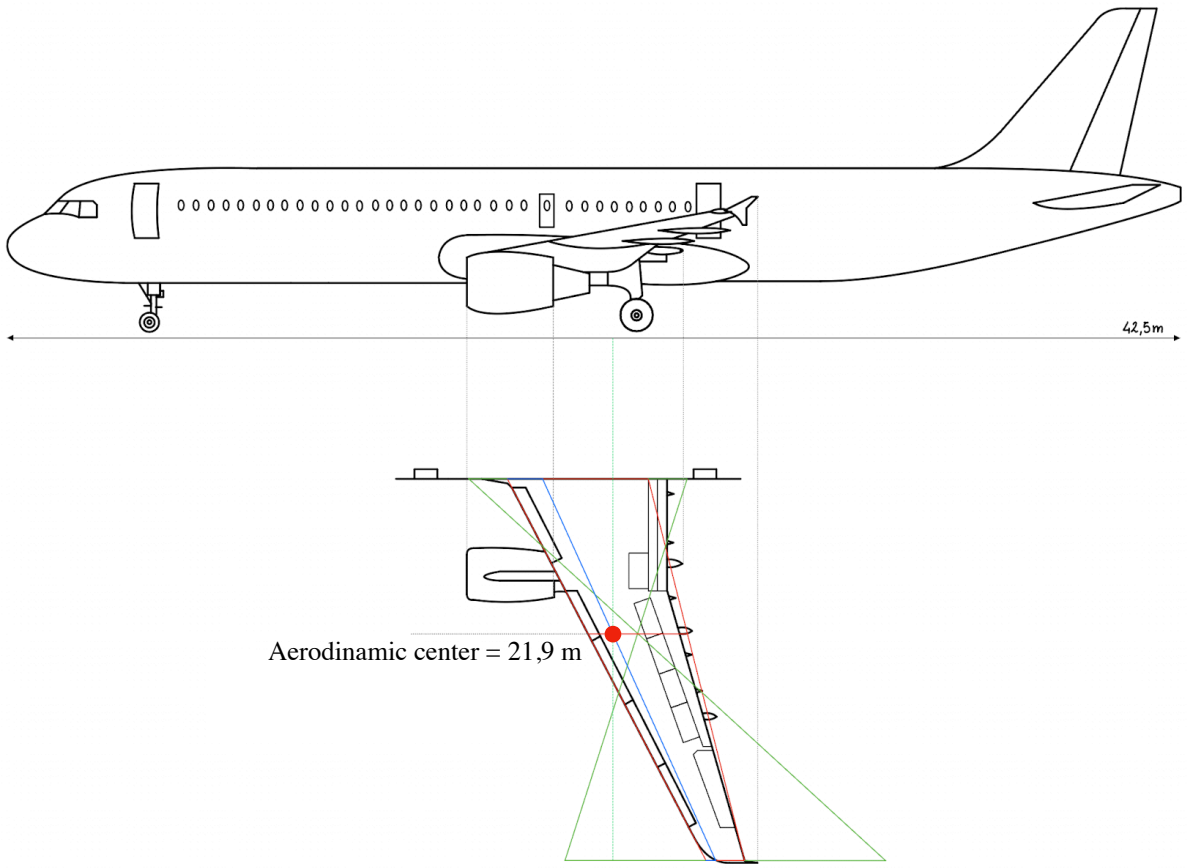

Figure 2.15: Aerodinamica center

To verify static stability, it is now necessary to calculate the aircraft's center of gravity for different load conditions corresponding to the points on the payload-range diagram. Starting from point 2, consider a payload mass of 15000 kg: this payload is divided into passenger mass (12000 kg, positioned in the passenger cabin's center at 15,5 m) and baggage mass (3000 kg, positioned in the cargo bay's center at 17 m). At the same position as the baggage mass, add the 400 kg due to the presence of 5 ULD containers [73], while the crew contributes 425 kg positioned in the cabin at 2,5 m. Moving on to the fuel, consider that at the halfway point of the front tank (9,5 m), there is a fuel mass of 1517 kg and the tank's structural mass is estimated at 506 kg, considering the gravimetric coefficient of the liquid hydrogen tanks estimated in section §1.3.4. Using the same method, consider 5078 kg of hydrogen and 2022 kg of structure for the rear tank positioned at 29,5 m. Subtracting all the known masses listed above from the take-off mass of the aircraft at point 2 (equal to M_{TO}), it is found that there are still 37334 kg. This is the airframe mass and must obviously be considered in the center of mass calculation. This leads to say that the position of this mass is approximated to the center of the aircraft at 21,25 m from the nose without better estimates.

At this point, it is easy to calculate the longitudinal position of the center of mass at the start of the mission:

$$x_{2_{take-off}} = 20{,}17\,m$$

However it is important not to forget that at the end of the mission, the tanks could be nearly empty if an emergency diversion consumes all the fuel. This situation can significantly affect the distribution of masses within the aircraft and should be considered. To evaluate the center of gravity upon landing, calculation is repeated assuming the fuel masses are 0 kg, resulting in the center of mass position at landing:

$$x_{2_{landing}} = 19{,}88\,m$$

The same procedure is followed for the other two points. For point 3, consider the same take-off mass but with different payload and fuel masses. In particular, the payload is divided into a passenger mass of 11200 kg and a baggage mass of 2800 kg, positioned respectively in the passenger cabin and the cargo bay's center. Since the front tanks are already full, the only fuel mass changing is within the rear tank, which in this configuration reaches 4075 kg. All other masses remain unchanged, allowing for the calculation of a center of gravity located at:

$$x_{3_{take-off}} = 20{,}41\,m$$

As before, repeat the calculation assuming fuel masses are zero to obtain the center of mass position at the end of the mission:

$$x_{3_{landing}} = 19{,}97\,m$$

Finally, for point 4, the same airframe mass as in points 2 and 3 is considered, but with a reduced take-off mass equal to 48992 kg. The payload is zero, so neither passenger nor baggage mass is considered. The only remaining masses are those of the crew and cargo hold containers, which maintain their previous values by approximation. Tank masses are identical to those in points 2 and 3, while fuel masses are the same as in point 3. In this configuration, the center of mass is found at:

$$x_{4_{take-off}} = 21{,}71\,m$$

Repeating the calculation without fuel:

$$x_{4_{landing}} = 21{,}27\,m$$

At this point, the neutral point's position and the 6 positions of the center of gravity in the 3 examined cases is obtained. It is easy to calculate the stability margins of the various configurations:

$$MS_{2_{take-off}} = 7{,}9\,\% \qquad MS_{3_{take-off}} = 6{,}8\,\% \qquad MS_{4_{take-off}} = 1\,\%$$

$$MS_{2_{landing}} = 9{,}2\,\% \qquad MS_{3_{landing}} = 8{,}8\,\% \qquad MS_{4_{landing}} = 2{,}8\,\%$$

It can be noted that in all circumstances, the aircraft is statically stable, ensuring a positive margin of stability. This is a very important result as it guarantees the maneuverability of the aircraft under all operating conditions, demonstrating that the obtained results meet the expected requirements.

For the reasons discussed in this and the previous paragraph, it is considered that the conceptual design is now completed and the design point is fixed based on the results obtained in paragraphs §2.10.

3. Costs

The cost of the entire lifecycle of an aircraft by an airline is a fundamental concept in the aviation industry and encompasses a range of financial elements that go well beyond the initial purchase of the aircraft. These costs can vary significantly depending on the type of aircraft, the operating route, company policies, and other factors. The evolution of an aircraft, from design to production, operation, and finally disposal, is defined as airplane lifecycle. A typical aircraft lifecycle involve various aspects, including technical, economic, psychological, and environmental considerations. It can be divided into the following phases:

- Planning and Conceptual Design: initial planning primarily involves mission requirements research, and some very preliminary cost studies are conducted during this phase.
- Preliminary Design and System Integration: design trade-off studies are conducted to find the combination of technology and cost that might result in a viable aircraft program.
- Detail Design and Development: finalization of aircraft and system integration design for certification flight testing and production.
- Manufacturing and Acquisition: aircraft production and delivery to the customer.
- Operation and Support: aircraft acquisition by the user and operation with associated support activities.
- Disposal: this phase marks the end of the operational life of the aircraft. Activities in this phase may include the destruction of the aircraft and the discarding of remaining materials. Disposal becomes necessary when an aircraft has reached the limit of its technological or economic life.

The costs of research, development, test, and evaluation (RDTE) can be considered part of the same category. This cost source includes all costs incurred in the design, from conceptual and preliminary to detailed design, and during development. However, the primary focus of this work is to estimate operating costs. This cost source represents the expenses incurred during management of the aircraft in the operational phase and is paid by the transportation company, although aircraft manufacturer and its suppliers usually incur certain support costs during this phase. The reason why this work primarily focuses on this phase is its economic weight on the total lifecycle cost. It should be noted that the operating cost source is much larger than the acquisition cost source, which is in turn much larger than the RDTE cost source.

$$Cop > Cacq > C_{RDTE}$$

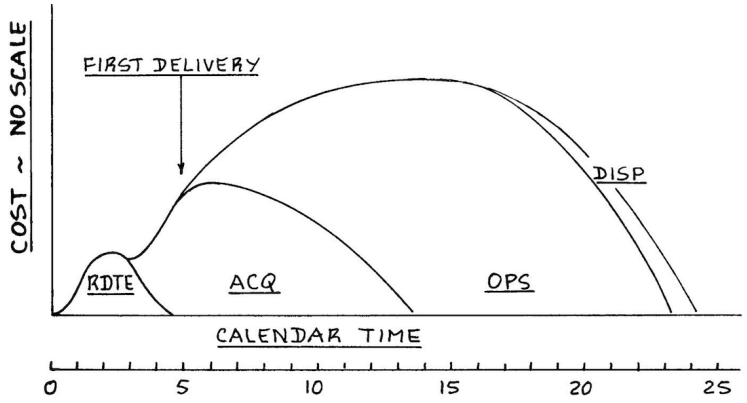

Figure 3.1: Representation of lifecycle cost history of typical airplane [82]

Keeping an aircraft in service is a complicated economic challenge because it costs a lot to support all needs, not just technical ones. The main cost items that an airline must bear are:

- Maintenance: this is one of the most significant expenses for an airline. It includes scheduled maintenance (such as regular checks and inspections), unscheduled maintenance (for repairing failures), and long-term structural maintenance.
- Fuel: the cost of fuel represents a significant portion of the operational expenses for an airline.
- Personnel: this includes the salaries and benefits of pilots, cabin crew members, ground staff, and management. Personnel costs are often large components of operational expenses and cannot be neglected.
- Insurance: airlines must cover various risks, including accidents, aircraft damage, civil liability, and more.
- Depreciation: aircraft depreciate over time, meaning their value decreases. Airlines must account for depreciation in their financial calculations.
- Airport and Navigation Fees: airlines must pay fees and charges for the use of airports, air traffic control systems, and airport infrastructure.

The sum of all these costs is defined as the operating cost of an aircraft and can vary significantly depending on the type of aircraft used, its age, the routes served, and, as will be discussed in this chapter, the technology used. The primary objective of this chapter is to estimate the operational costs of the aircraft designed in Chapter 2. In particular, the focus is on innovative technology to understand how it can impact the aircraft's competitiveness. An increase in operational costs due to hydrogen must be redistributed to passengers, and this can affect the cost of air tickets. A significant increase may provide consumers with a not acceptable cost and consequently the aircraft under consideration, while technically feasible, may be considered economically unviable. The consumer is the one who ends up paying for all the activities required to design, produce, use, and dispose of aircraft. Estimating these costs borne by the airline is challenging, especially for an aircraft using innovative technologies like hydrogen. To accomplish this task, it is essential to refer to an authoritative and reliable model. In this thesis project, the cost analysis is carried out using the Roskam method outlined in the book "Airplane Design Part VIII - Airplane Cost Estimation" by the same author [82].
For an airline, operating costs represent the expenses incurred to operate and maintain the fleet of aircraft in regular service. These costs include a range of factors contributing to the daily operation of the company and are significantly greater than the initial purchase and design costs of aircraft. The cost of fuel represents a significant portion of operating costs. Airlines must purchase large quantities of fuel to power their aircraft. This is a fundamental aspect of this work, as the most significant difference compared to a traditional aircraft is the fuel. As discussed in Chapter 1, hydrogen is a much more expensive fuel compared to kerosene. Furthermore, it should be considered that, at the current state of the art, this fuel is not yet produced for widespread use: nowadays, the high costs of this technology are also due to limited production and technological backwardness in production facilities. However, the aircraft under study is part of a future program, with entry into service around 2035, and therefore the values that will make up the operating costs will be estimated for that date. Although inflation will increase most individual cost items compared with today, fuel costs will follow the opposite trend. In fact, current estimates all agree that in the future, liquid

hydrogen as a fuel will have a lower price. It will remain more expensive than kerosene, but this trend will help make hydrogen a more competitive technology in the future.

Airlines constantly seek to improve operational efficiency: accurate cost management is crucial for the long-term financial success of airlines. Using an analogy from Roskam, the aircraft program manager is like the captain of a ship navigating close to an iceberg. The program manager faces many pressures to reduce research, development, test, and evaluation (RDTE) costs to optimize costs in the short term. However, yielding to these pressures may actually increase the overall lifecycle cost (LCC). In fact, spending more capital on additional RDTE work when directed toward designing to minimize operating costs, can lead to significant savings for the customer in terms of LCC and therefore for company as a whole. During the preliminary aircraft design process many design decisions are made that have a significant effect on the aircraft's lifecycle cost. Designers must be aware of these effects if their designs are to be economically advantageous and this is precisely the aspect addressed in this chapter.

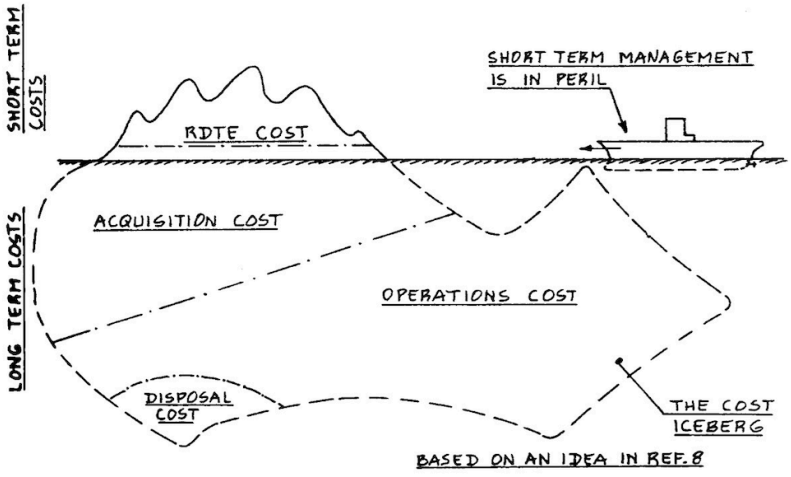

Figure 3.2: The iceberg effect in airplane program management [82]

At this point, it should be noted that all the costs mentioned so far are those that can be directly measured in currency (whether it's euros or dollars). These costs are also referred to as economic costs; there are also other types of costs: social, psychological, and environmental, to name a few.

If a company decides to relocate its activities to another part of the country (or the world), social costs will be incurred due to the loss of jobs, the relocation of families, etc. The burden of bearing the economic costs associated with social costs is usually borne by the taxpayer. The use of hydrogen could play a significant role in this field. In fact, Chapter 1 explains that liquid hydrogen (especially green hydrogen) has a production cost that could vary depending on the place of origin. For instance, countries near the equator or with abundant renewable energy sources could be more competitive. This could induce companies operating in the fuel production sector to relocate jobs. However, this aspect is not directly the responsibility of airline companies and would be difficult to estimate, so it is neglected in this work.

Aircraft tend to generate a significant amount of noise during takeoff and landing. This can cause discomfort for people and can be considered a psychological cost. Psychological discomfort can become severe enough

to lead to noise pollution legislation, as seen in FAR Part 36 [83] and ICAO annex 16 [84]. This aspect should be taken into consideration by the designer. In fact, it is now crucial to build quieter and quieter aircraft. Noise is primarily due to engines, so they must be optimized to be as quiet as possible. However, this technical aspect pertains to a detailed phase beyond the scope of this thesis project.

Pollution caused by air operations represents an environmental cost. Examples include atmospheric pollution due to exhaust gases, fuel discharge in emergencies, and chemical discharges resulting from production and maintenance processes. These types of costs are important but they are difficult to quantify economically. However, there is a straightforward way to consider them: taxes and fees often take into account the pollution produced by an aircraft, charging more for aircraft that pollute more. In this case, it could be hypothesized that the treated aircraft does not pay the percentage of fees due to pollution since it does not emit carbon dioxide. Economically, the advantage of this technology will be considered through fees.

3.1 Estimation Of Operating Cost

The investment programs of commercial operators are often very complex and spread over several years. Additionally, the fleet size plays a significant role in costs, and different companies may have to incur very different costs. Furthermore, this thesis project does not intend to perform the economic analysis of an airline; the focus is on the economic feasibility study of an aircraft, analyzing its competitiveness with traditional kerosene-powered aircraft. For these reasons, the operating costs will be calculated with a single aircraft as a reference and normalized for passengers transported and kilometers traveled. Furthermore, the same method used to estimate the costs of the aircraft under study will be used to estimate the operating costs of a traditional aircraft to enable a comparison. To ensure a fair comparison, the traditional aircraft must have similar capacities to the one in the design phase. Although the A320 was used as a reference aircraft during the conceptual design phase, as can be clearly seen in Table 2.1 it has a range and a payload capacity quite different from what was obtained. A more similar aircraft could be the McDonnell Douglas MD-87. However this aircraft, besides being structured differently, belongs to a very different generation which could distort a potential comparison. The Airbus A318 seems to represent a good compromise. In fact, despite having a slightly higher takeoff mass and maximum range than the aircraft under design, it belongs to the A320 family used as a reference during the design. The cost per passenger/kilometer of the designed aircraft and the traditional ones will be calculated to compare their operating costs and estimate the impact of using liquid hydrogen as fuel.

It must be said that “Airplane Design” [82] is an American textbook, so it uses imperial units of measurement. Given their widespread use in the field of aviation, it was preferred to follow the Roskam method respecting this notation. Only at the end of the calculations the results will be expressed in International System units and in the European currency for clarity. Throughout the process leading to the estimation of operating costs, the economic items will all be expressed in US dollars. Many of the results obtained are also normalized for distance traveled in nautical miles. The choice to consider the nautical mile, as opposed to the statute mile, is entirely arbitrary as stated by the author as well. There are no reliable

methods to predict what cost variations will be among different companies, so reasonable averages will be used for the individual cost items borne by the airline.The operating costs of an airline can be divided into direct operating costs and indirect operating costs, each with different characteristics and purposes. Direct Operating Costs (DOC) are the costs that an airline incurs directly to operate and maintain its aircraft, expenses directly associated with aircraft operation and maintenance. These costs are closely related to flight activities and fleet management. Direct operating costs include aircraft fuel, landing and takeoff fees, flight crew salaries, aircraft maintenance costs, navigation fees, and other costs directly related to aircraft usage. On the other hand, Indirect Operating Costs (IOC) pertain to general and support business expenses that enable the entire operation to function but are not specifically tied to an individual flight or aircraft. They are costs associated with the overall operation of the airline but are not directly related to flight activities or aircraft maintenance. These costs concern support and business management activities. They encompass expenses such as general administrative costs (administrative staff, offices, supplies), marketing and advertising costs, legal expenses, ground facility maintenance costs (such as hangars), and other costs not directly associated with flight.

$$C_{ops} = C_{ops_{dir}} + C_{ops_{ind}}$$

where:

- $C_{ops_{dir}}$ is the program direct operating cost for the airline, expressed in USD.
- $C_{ops_{ind}}$ is the program indirect operating cost for the airline, expressed in USD.

The aircraft program's direct and indirect operating costs can be estimated as follows:

$$C_{ops_{dir}} = DOC \cdot R_{bl_{ann}} \cdot N_y$$

$$C_{ops_{ind}} = IOC \cdot R_{bl_{ann}} \cdot N_y$$

where:

- N_y is the number of years during which the aircraft is operated by the customer. It must be recognized that aircraft are sold and resold during their operational lives. For cost estimating purposes, it is suggested to use 20 years for transport aircraft.
- DOC is the direct operating cost per nautical mile of the aircraft expressed in USD/nm.
- IOC is the indirect operating cost per nautical mile of the aircraft expressed in USD/nm.
- $R_{bl_{ann}}$ is the total annual block miles flown by the customer, expressed in nautical miles (nm) per aircraft.

Given that the total annual block miles have been mentioned, it is useful to insert a small explanation on the block parameters. Flight parameters are fundamental for in-flight control and navigation, while block parameters are crucial for operational planning and overall airline resource management. Block parameters are quantities used to measure and describe the comprehensive operation of an aircraft during a flight from a departure point to a destination point. Block parameters take into account all activities and phases involved in the overall operation of an aircraft, from when it leaves the departure gate to when it reaches the destination gate. This means that ground operations, such as taxiing on the ground, the time elapsed between

pushback and actual takeoff, landing time, and final taxiing at the destination, are all integral parts of block parameters. The concept of block values is visually illustrated in Figure 3.3.

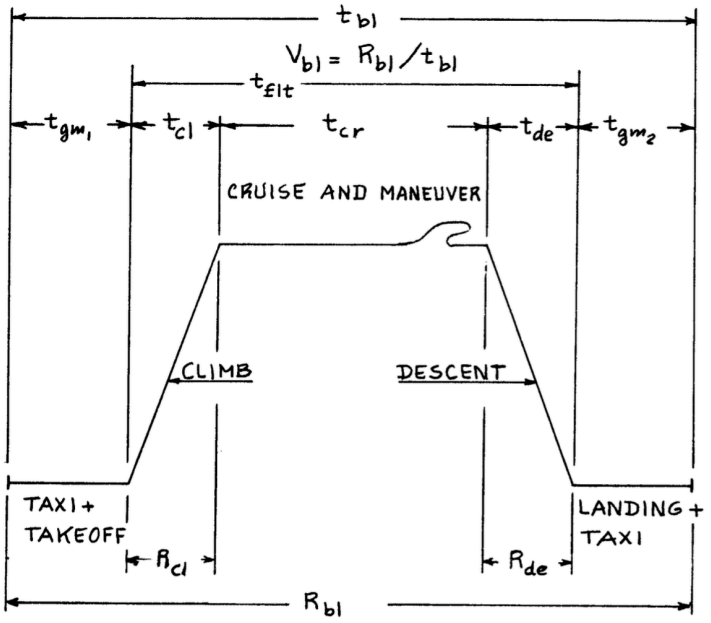

Figure 3.3: Block parameters definition [82]

Block distance is the total distance covered by an aircraft during a flight between two points. This parameter encompasses the distance traveled during ground taxiing, the actual flight distance between the two airports and the distance covered during final taxiing. Block distance is essential for calculating the fuel required for the flight and for route planning. The total annual block miles, represented as $R_{bl_{ann}}$, can be calculated in the following manner.

$$R_{bl_{ann}} = V_{bl} \cdot U_{ann_{bl}}$$

In this equation:

- V_{bl} is the block speed measured in nautical miles per hour (nm/hr).
- $U_{ann_{bl}}$ denotes the annual utilization in block hours, which is contingent on the type of aircraft and the routes flown.

The annual utilization in block hours, $U_{ann_{bl}}$, is contingent on the aircraft type and the routes chosen. In the absence of more detailed information, for passenger transports, Roskam recommends to determine it as follows.

$$U_{ann_{bl}} = 10^3 \left[3.4546 t_{bl} + 2.994 - \left(12.289 t_{bl}^2 - 5.6626 t_{bl} + 8.964\right)^{1/2}\right]$$

On the other hand, block speed represents the average speed that an aircraft would keep during a flight between two points and it's typically expressed in nautical miles per hour (nm/hr). This parameter is very useful because it takes into account all speed variations during the flight, including takeoff, landing, and

cruising. Furthermore, it also considers all ground operations within it. If the wind is not taken into account, block speed can be determined in a simplified way by employing the formula:

$$V_{bl} = \frac{R_{bl}}{t_{bl}}$$

Here:

- R_{bl} represents the block distance measured in nautical miles (nm).
- t_{bl} is the block time in hours.

Block time is the total time spent by an aircraft from the moment it begins moving from the parking position until it comes to a stop at the final destination. It includes ground taxiing time, actual flight time, and final taxiing time. It can be computed as follows:

$$t_{bl} = t_{gm} + t_{cl} + t_{cr} + t_{de}$$

where:

- t_{gm} corresponds to the time spent on ground maneuvers, including activities like departing from the gate, taxiing to the active runway, the takeoff run, landing ground run, and taxiing to the gate at the final destination. This time is expressed in hours. Ground maneuver time can be estimated using the equation provided by Roskam, which also incorporates a one-minute allowance for the takeoff run:

  $$t_{gm} = 0{,}51 \cdot 10^{-6} \cdot M_{TO} + 0{,}125$$

- t_{cl} represents the time required for ascent and acceleration to reach the cruise speed.
- t_{de} is the time required for descent.
- t_{cr} denotes the time spent in cruise and is also expressed in hours. In general, it can be estimated using:

  $$t_{cr} = \frac{1{,}01 \cdot R_{bl} - R_{cl} - R_{de} - R_{man}}{V_{cr}}$$

  - The factor 1,01 is applied to account for the fact that, for various reasons, optimal routes are usually not feasible.
  - R_{cl} corresponds to the distance covered during the climb and acceleration to reach the cruise speed, measured in nautical miles (nm).
  - R_{de} represents the distance traveled during the descent, with this measurement also expressed in nm.
  - R_{man} indicates the distance covered while performing maneuvers due to air traffic control (ATC) constraints, measured in nm.

    $$R_{man} = V_{man} \cdot t_{man}$$

    The speed during these ATC maneuvers is indicated as V_{man} and it is recommended to use 250 knots for altitudes below 10,000 feet; t_{man}, on the other hand, represents the time spent in ATC maneuvers, and it can be determined using the provided equation.

    $$t_{man} = 0{,}25 \cdot 10^{-6} \cdot M_{TO} + 0{,}0625$$

3.2 Method for estimating direct operating costs: DOC

In the previous sections, it's been explained what operational costs are, why it's essential to obtain reliable estimates, and how to calculate them. The next step involves calculating the two categories into which these costs are divided: direct and indirect operational costs. The purpose of this section is to present the method used to estimate the direct operating cost (DOC) in USD/nm incurred during the operation of commercial airplanes. The Roskam method presented here is an adaptation of the so-called ATA - AIR TRANSPORT ASSOCIATION of America method.

The direct operating cost per nautical mile, DOC, is broken down as follows:

$$DOC = DOC_{flt} + DOC_{maint} + DOC_{depr} + DOC_{lnr} + DOC_{fin}$$

where:

DOC_{flt} is the direct operating cost of flying in USD/nm

DOC_{maint} is the direct operating cost of maintenance in USD/nm

DOC_{depr} is the direct operating cost of depreciation in USD/nm

DOC_{lnr} is the direct operating cost of landing fees, navigation fees, and registry taxes in USD/nm

DOC_{fin} is the direct operating cost of financing in USD/nm

3.2.1 Direct Operating Cost of Flying:

The direct operating costs of flying (in USD/nm) represent the expenses associated with operating an aircraft during a specific flight. These costs are crucial for airlines and include various key elements:

$$DOC_{flt} = C_{crew} + C_{pol} + C_{ins}$$

Where:

C_{crew} represents the crew cost in USD/nm.

C_{pol} represents the cost of fuel and oil in USD/nm (pol stands for petroleum, oil, and lubricants).

C_{ins} represents the cost of airframe insurance in USD/nm.

3.2.1.1 Cost per nautical mile for Crew: C_{crew}

These costs encompass the wages and benefits of the flight personnel. Crew costs can vary depending on the type of aircraft, flight duration, and union regulations. They are influenced by the number of crew members on board and their hourly or annual compensation. The crew cost per nautical mile, C_{crew}, can be calculated as follows:

$$C_{crew_i} = \frac{1+K}{V_{bl}} \frac{SAL}{AH} + \frac{TEF}{V_{bl}}$$

Where:

- K is a factor that takes into account items such as paid leave, training cost, crew bonuses, crew insurance, and wage taxes. This factor varies from one operator to another. In the absence of more detailed data on company rules and benefits, it is suggested to use: K = 0,26.

- SAL is the annual salary paid to a crew member. Crew salaries depend on factors such as:
  - Equipment used: Salaries tend to increase with aircraft weight and speed.
  - Seniority
  - Union and company rules
- AH is the number of flight hours per year for a crew member. In the absence of actual data, the quantities suggested as applicable to all flight crew members of jet aircraft are: AH = 800 hours for domestic operations and for international operations AH = 750 hours.
- TEF is the travel expense factor associated with each type of crew member. Since flight crews typically stay at the same hotel, there is no need to vary TEF from one crew member to another. Roskam in 1990 suggested to use:
  - Domestic routes: TEF = 7,0 USD/b1hr
  - International routes: TEF = 11,0 USD/b1hr

The subscript i in the equation indicates that the calculation refers to an individual crew member. To calculate the total crew cost, you need to repeat the calculation for each crew member and sum up each contribution.

$$C_{crew} = \sum C_{crew_i}$$

The number of crew members to be carried depends on government regulations, company rules, and union rules. In general, Roskam suggests considering 1 captain and 1 first officer (for aircraft with 2 people in the cockpit) for planned block times < 10 hours, and for planned block times > 10 hours consider 2 crew members for each command rank.

Note: The cost of flight attendants is considered in indirect operating costs.

3.2.1.2 Cost of Fuel and Oil per nautical mile: C_{pol}

These costs represent the expense of the fuel required to power the aircraft during the flight and the oil needed for proper engine operation. However, lubricating oil costs are negligible when compared to fuel costs. Additionally, for the aircraft under consideration, it is assumed that the engine is a Leap 1-A that has been appropriately converted for hydrogen operation. Detailed information about the engine technology and the quantity of oil required is not known, which could affect the accuracy of estimated costs. For these reasons, lubricating oil costs will be neglected. Fuel costs are influenced by the route, aircraft type, and fuel prices in the market. They can represent a significant portion of the total operating costs for a flight. The cost of fuel per nautical mile, C_{pol}, can be estimated as follows:

$$C_{pol} = \frac{W_{F_{bl}}}{R_{bl}} FP$$

Where:

- $W_{F_{bl}}$ Block fuel used in pounds, which is the same as mission fuel used.
- FP is the fuel price in USD/lb.

3.2.1.3 Cost of Airframe Insurance per Nautical Mile: C_{ins}

Aircraft operators purchase insurance to protect themselves from the risk of damage or loss of the airframe on the ground and during flight. Most aircraft operators will want to obtain insurance for airframe damage in an amount equal to the replacement value of the aircraft. Insurance rates for airframe damage or loss depend on the so-called airframe loss rate. For detailed information on insurance rates, Roskam himself recommends consulting an aviation insurer. In the absence of precise information, an alternative method to consider airframe insurance is to treat this expense as a percentage of the total direct operating cost:

$$C_{ins} = 0{,}02DOC$$

Of course, airlines purchase many other types of insurance, including:

- Liability for passengers in case of injury or death
- Liability to third parties in case of injury or death
- Cargo damage risk

However, these points are considered part of the IOC (Indirect Operating Cost) and therefore they will not be considered in this calculation.

3.2.2 Direct Maintenance Cost: DOC_{maint}

Direct operating costs related to maintenance are associated with the upkeep, repair, and management of the aircraft and its components. Maintenance labor includes the wages and benefits of maintenance technicians, mechanics, and engineers who work to ensure that the aircraft is in a safe operational state and compliant with regulations. Labor is necessary for conducting regular inspections, repairs, and preventive maintenance. On the other hand maintenance materials encompass the purchase of spare parts, components, and materials required for the maintenance and repair of the aircraft. This can include airframe parts, engines, electrical, electronic, and hydraulic systems. Material costs can vary significantly based on the age and type of the aircraft. Given the diversity of the items that make up these expenses, if one were to estimate the direct maintenance cost in a detailed manner, it would be advisable to break it down as follows:

$$DOC_{main} = C_{lab_{ap}} + C_{lab_{eng}} + C_{mat_{ap}} + C_{mat_{eng}} + C_{amb}$$

Where:

$C_{lab_{ap}}$ Maintenance cost for airframe and non-engine systems in USD/nautical mile.

$C_{lab_{eng}}$ Maintenance cost for engines in USD/nautical mile.

$C_{mat_{ap}}$ Material maintenance cost for airframe and non-engine systems in USD/nautical mile.

$C_{mat_{eng}}$ Material maintenance cost for engines in USD/nautical mile.

C_{amb} Maintenance burden applied in USD/nautical mile.

Unfortunately, this method requires a lot of data subject to significant uncertainty. For instance, labor costs can vary greatly between different companies, and spare parts can be very different for different aircraft, making estimating their cost complex. Furthermore, it's impossible to predict the maintenance needs of the new technologies used in the aircraft studied in this work. An alternative method could be to estimate

maintenance costs based on maintenance costs per flight hour that companies currently incur to ensure the efficiency of an aircraft of the same category. These costs are much more reliable as they encompass all the small variations that can occur between different assessment cases. Effective management of direct operating costs related to maintenance is essential to ensure that aircraft are safe, reliable, and efficient.
Airlines must plan and schedule maintenance to minimize aircraft downtime and maximize operational availability. Additionally, preventive maintenance is crucial to avoid costly repairs and extend the aircraft's service life.

3.2.3 Direct Cost of Depreciation: DOC_{depr}

The depreciation cost of an aircraft is a significant component of direct operating costs associated with the operation of a commercial aircraft. Depreciation represents the loss of value over time of the aircraft and its components. Depreciation is an important accounting item for airlines and is used to reflect the decrease in the value of the aircraft and its components over the years. This cost is taken into account in the assessment of direct operating costs because airlines need to consider the depreciation of the aircraft when calculating the cost per nautical mile or per flight hour. It is important to note that depreciation can vary due to various factors, including the type of aircraft, age, usage, and the aviation market. Airlines must carefully manage depreciation to optimize operating costs and assess the feasibility of replacing or upgrading the aircraft when it becomes economically advantageous. Here's how it can be broken down:

$$DOC_{depr} = C_{dap} + C_{deng} + C_{dprp} + C_{dav} + C_{dapsp} + C_{dengsp}$$

Where:

- C_{dap} is the Airframe Depreciation cost without engines and propellers, avionics, and spare parts (structure) in USD/nautical mile. Airframe Depreciation covers the loss of value of the aircraft's airframe itself, which includes the main part of the structure, such as the fuselage, wings, and tail. Airframe depreciation is calculated based on various factors, including the age of the aircraft, total flight hours, and maintenance performed.
- C_{deng} is the Engine Depreciation cost (as installed on the aircraft) in USD/nautical mile and represents a significant component of its overall value. Engine depreciation takes into account the decrease in their value over time and can vary based on engine age and condition.
- C_{dprp} is the Propeller Depreciation cost in USD/nautical mile. If the aircraft is equipped with propellers, their depreciation can be an additional cost. Here again, propeller depreciation is influenced by their age and condition.
- C_{dav} is the Avionics Depreciation cost in USD/nautical mile and refers to the loss of value of avionics systems on board the aircraft, such as navigation, communication, and control systems. Avionics technology evolves rapidly, which can influence the depreciation of these systems.
- C_{dapsp} is the Spare Parts Depreciation cost for the aircraft in USD/nautical mile.
- C_{dengsp} is the Engine Spare Parts Depreciation cost in USD/nautical mile.

The cost of airframe depreciation per nautical mile, C_{dap}, can be estimated as follows:

$$C_{dap} = \frac{F_{dap} \cdot (AEP - N_e \cdot EP - N_p \cdot PP - ASP)}{DP_{ap} \cdot U_{ann_{bl}} \cdot V_{bl}}$$

Where:

- F_{dap} is an Airframe depreciation factor. This factor depends on the perceived resale value of the aircraft.
- AEP is the estimated aircraft price in USD.
- N_e is the number of engines per aircraft.
- EP is the engine price (per engine) in USD.
- N_p is the number of propellers per aircraft.
- PP is the price per propeller in USD.
- ASP is the avionics system price per aircraft in USD.
- DP_{ap} is the depreciation period of the aircraft. This depends on the operator's business strategy.

The cost of engine depreciation per nautical mile, C_{deng}, can be determined as follows:

$$C_{deng} = \frac{F_{deng} \cdot N_e \cdot EP}{DP_{eng} \cdot U_{ann_{bl}} \cdot V_{bl}}$$

Where:

- F_{deng} is an Engine depreciation factor. This factor depends on the perceived resale value of each engine.
- DP_{eng} is the engine depreciation period. This depends on the operator's business strategy.

The cost of avionics system depreciation, C_{dav}, in USD/nautical mile, can be estimated as follows:

$$C_{dav} = \frac{F_{dav} \cdot ASP}{DP_{av} \cdot U_{ann_{bl}} \cdot V_{bl}}$$

Where:

- F_{dav} is an Avionics system depreciation factor. This factor depends on the perceived resale value of avionics systems. Experience has indicated a low or no resale value.
- DP_{av} is the avionics system depreciation period. This depends on the operator's business strategy and federal regulations.

The cost of spare parts depreciation for the aircraft, C_{dapsp}, in USD/nautical mile, can be estimated as follows:

$$C_{dapsp} = \frac{F_{dapsp} \cdot F_{apsp} \cdot (AEP - N_e \cdot EP)}{DP_{apsp} \cdot U_{ann_{bl}} \cdot V_{bl}}$$

Where:

- F_{dapsp} is an Aircraft spare parts depreciation factor. This factor depends on the perceived resale value of aircraft spare parts.

- F_{apsp} is an Aircraft spare parts factor. This is equal to the ratio of the cost of aircraft spare parts to the cost of the aircraft minus engines. This factor depends on operational experience in aircraft repair and maintenance.
- DP_{apsp} is the depreciation period of aircraft spare parts. This depends on the operator's business strategy.

The cost of engine spare parts depreciation can be estimated in the same way as the cost of aircraft spare parts depreciation.

3.2.4 Direct Landing, Navigation, and Registration Fees: DOC_{lnr}

There is no unanimous consensus on whether expenses incurred for landing fees, navigation fees, and registration taxes should be classified as direct or indirect operating costs. Roskam includes them within direct operating expenses and the same decision has been made in this work. Direct operating expenses related to landing fees, navigation fees, and various taxes can be detailed as follows:

$$DOC_{lnr} = C_{lf} + C_{nf} + C_{rt}$$

Where:

- C_{lf} represents direct operating expenses attributed to landing fees in USD/nautical mile.
- C_{nf} represents the cost of navigation fees in USD/nautical mile.
- C_{rt} represents the direct cost of registration taxes expressed in USD/nautical mile.

3.2.4.1 Landing Fees

Landing fees are costs that an airline must pay to the airport or airport authority for using airport facilities during the landing of an aircraft. These fees represent a portion of the direct operating costs associated with the operation of a commercial flight. Landing fees can vary significantly from one airport to another and may be calculated in different ways. Often, they are based on the mass of the aircraft (such as maximum takeoff weight) or the type of aircraft (e.g., jet aircraft vs. turboprop aircraft). The revenue generated from landing fees is used by the airport authority to cover the costs of maintaining and operating the airport itself. These costs may include runway maintenance, control towers, terminal facilities, and airport support services. These can be determined as follows:

$$C_{lf} = \frac{C_{aplf}}{V_{bl} \cdot t_{bl}}$$

Where:

C_{aplf} is the landing fee for a single landing of the aircraft.

3.2.4.2 Navigation Fees

Air navigation fees are costs that airlines must incur for using air navigation services provided by air traffic control authorities and aviation regulatory bodies. Air navigation fees cover air navigation and air traffic control services, which include managing air traffic, radar monitoring, flight route coordination,

communication with flight crews, and more. These services are essential for ensuring the safety and efficiency of flights. Air navigation fee rates can vary based on various factors, including the distance traveled by the aircraft, flight altitude, aircraft weight, and the geographical region crossed. Often, these rates are established by aviation regulatory authorities and may differ from one country to another. Air navigation fee rates and regulations are often set at the national or regional level and must comply with international standards established by the International Civil Aviation Organization (ICAO). An estimate can be obtained as follows:

$$C_{lf} = \frac{C_{apnf}}{V_{bl} \cdot t_{bl}}$$

Where:

C_{apnf} is the navigation fee charged for each flight of an aircraft, expressed in USD/flight. This fee varies based on the flight route and country.

3.2.4.3 Registration Taxes

In commercial aviation, registration taxes refer to fees or charges imposed on airlines or aircraft owners to register and maintain information about their aircraft with the civil aviation authorities of a specific country or jurisdiction. Before an aircraft can be operated commercially, it must be registered with the civil aviation authority of the country where it is based or used. Registration involves documentation and recording detailed information about the aircraft, such as the serial number, model, ownership, technical data, and airworthiness certificates. Registration taxes often include fees or charges associated with registering the aircraft and maintaining its information in the official registry. These costs can vary from country to country and may be calculated based on various factors, including the size and type of the aircraft. To estimate registration tax costs, Roskam recommends using the following formula:

$$C_{rt} = f_{rt} \cdot DOC$$

Where:

f_{rt} is a factor dependent on the aircraft's size. This factor is based on regulations established by state and national governments regarding registration taxes. In the absence of actual data, it is advisable to use:

$$f_{rt} = 0{,}001 + 10^{-8} \cdot M_{TO}$$

3.2.5 Direct Financing Operating Costs: DOC_{fin}

Direct operating costs related to aircraft financing in USD/nautical mile, DOC_{fin}, depend on how an operator chooses to finance its fleet of aircraft. Operators can opt to borrow money for the purchase of aircraft and spare parts and for financing their operations. They often decide to lease some or all of their aircraft equipment. Even when an operator chooses to use its own funds to finance aircraft and related operations, there are interests associated with it. The methods for estimating financing costs are considered beyond the scope of this thesis project. However, given their significant value, it is necessary to consider these costs in

the calculation of direct operating costs. The following recommended proportion from Roskam is chosen for accounting financing costs:

$$DOC_{fin} = 0{,}07DOC$$

This practical rule is based on the observation that financing costs typically amount to about 7 percent of the total DOC.

3.4 Method for Estimating Indirect Operating Costs: IOC

The purpose of this section is to provide a method for estimating indirect operating costs (IOC) in USD per nautical mile incurred during the operation of commercial aircraft. The indirect operating costs of an airline represent expenses that are not directly attributable to individual flight operations or specific aircraft but support the overall operation of the airline. These costs can vary significantly from one airline to another and can constitute a significant part of the total operating expenses. All ground personnel are included within indirect operating costs: this includes the salaries and benefits of employees working on the ground such as maintenance personnel, ground personnel at airports, management personnel, administrative personnel, and more. These employees play crucial roles in aircraft maintenance, ground operations management, and passenger assistance. Additionally, on the ground, airlines must cover the costs of airport facilities, including aircraft maintenance hangars, offices, refueling stations, and other infrastructure necessary for maintenance and operational support. Administrative expenses are also included, encompassing a wide range of costs such as office rents, legal services, corporate insurance, office supplies, consulting services, and more. Airlines also incur a range of advertising and marketing costs to promote their services and attract passengers. These costs include media advertising, promotional campaigns, and customer loyalty programs. The indirect operating cost per nautical mile of a commercial aircraft can then be divided into the following components of IOC cost:

$$IOC = IOC_{pax} + IOC_{sta} + IOC_{ascf} + IOC_{pse} + IOC_{gaa}$$

Where:

- IOC_{pax} represents the indirect operating cost for passenger services, expressed in USD per nautical mile.
- IOC_{sta} represents the indirect cost for maintenance and depreciation of ground equipment and ground facilities, expressed in USD per nautical mile.
- IOC_{ascf} represents the indirect operating cost for aircraft maintenance and traffic control and cargo services, expressed in USD per nautical mile.
- IOC_{pse} represents the indirect operating cost for promotion, sales, and entertainment, expressed in USD per nautical mile.
- IOC_{gaa} represents the indirect operating cost for general administrative expenses, expressed in USD per nautical mile.

It is evident that within the IOC category, there are a multitude of sectors, and these have little to do with individual aircraft; therefore aircraft designers have limited influence over this cost category. As it's been

already said, this work does not intend to detail the financial balance of an airline but rather to assess the competitiveness of the aircraft described in Chapter 2. For this reason this calculation can be simplified and the proposed method for estimating indirect operating costs assumes that the IOC can be expressed as a simple fraction of the DOC:

$$IOC = f_{ioc} \cdot DOC$$

Where:

f_{ioc} is the fraction of the DOC used to estimate the IOC.

Examining data on the relationship between IOC and DOC, it is clear that f_{ioc} depends heavily on the distance traveled and the type of aircraft. In the absence of actual data on IOC, f_{ioc} can be estimated based on Figure 3.4, which provides some data related to this fraction. Although this method may seem overly simplified, the values obtained are in line with those currently available [85]. Furthermore, as it depends only on the mission, f_{ioc} will be the same in the calculation of costs for the innovative aircraft under examination as well as for the traditional comparison aircraft, thus not distorting the comparison in any way.

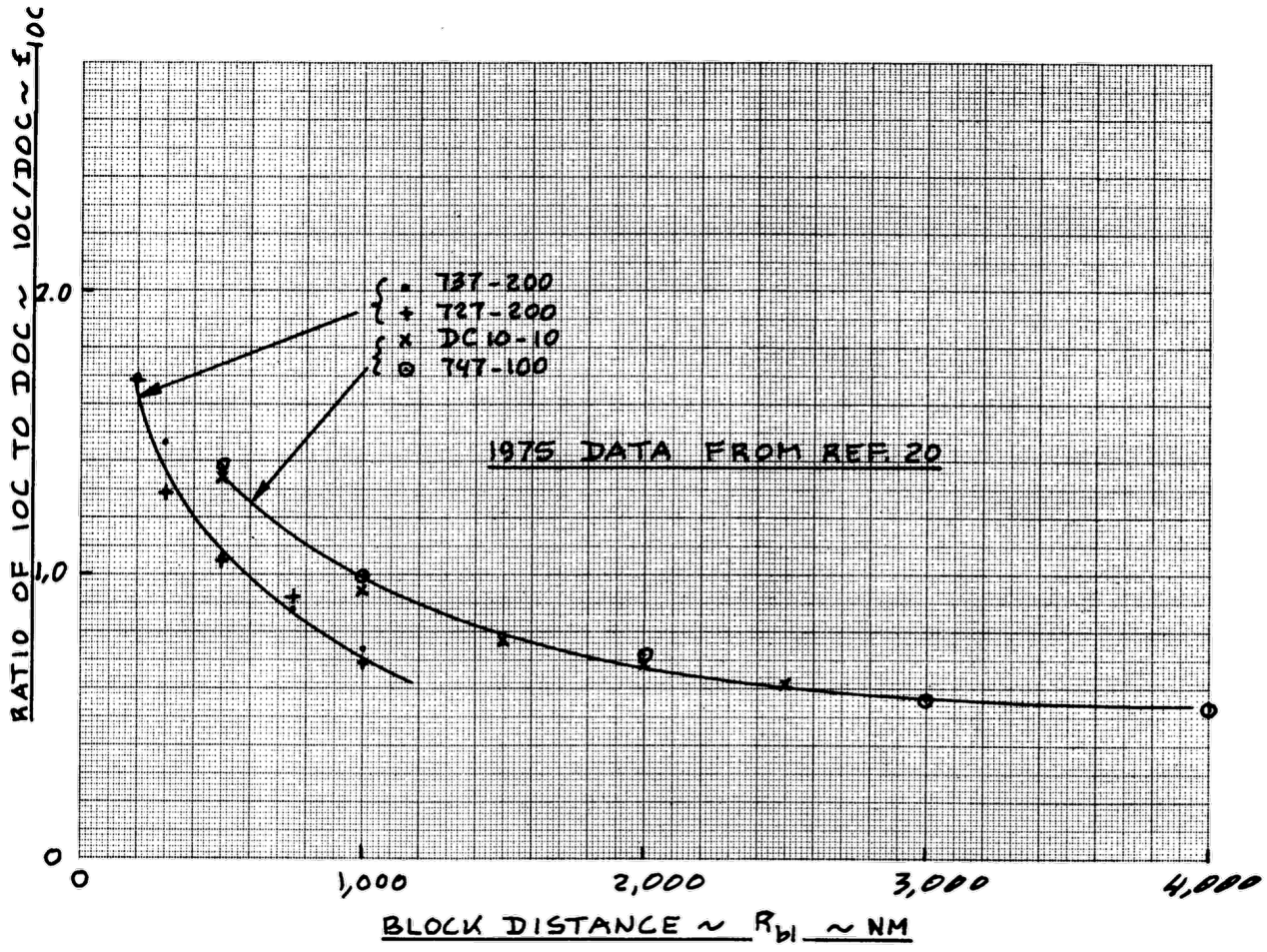

Figure 3.4: Effect of block distance on the ratio of IOC to DOC [82]

4. Costs of LH2 and traditional aircraft

In Chapter 3 the costs related to the lifecycle of an aircraft were described, with a particular focus on operating costs. To compare the aircraft discussed in Chapter 2 with a traditional aircraft in order to assess the economic feasibility of a hydrogen-powered aircraft, it is necessary to calculate the direct and indirect operational costs of both aircraft to have values for comparison.

4.1 Inflation

It is important to note that the hydrogen-powered aircraft has been designed with a potential entry into service in 2035; therefore all calculations in this chapter will refer to that date. Calculating future costs is a crucial activity for financial and operational planning in any company, including an airline. It is essential to account for inflation when projecting future costs, as inflation can increase the value of costs over time. Inflation is the rate at which prices of goods and services tend to rise over time. Historical inflation data or economic forecasts can be used to estimate future inflation. The assistance of the U.S. Bureau of Labor Statistics has proven to be very useful in this regard [86]. In effect the Roskam book is quite old, and many of the recommended cost values are referenced to the publication date. The CPI Inflation Calculator was used to accurately adjust all cost items from past years to 2023 (the year this document is written) [87]. Afterward, all obtained costs were further projected to their values in 2035. To do this, the average inflation rate of the last 20 years was used as a reference which is approximately 3% annually [88,89]. Once the inflation rate was estimated, future costs could be calculated by applying this rate to current costs. The following formula will be used to calculate future costs:

$$Future\ Cost = Current\ Cost \cdot (1 + Inflation\ Rate \cdot years)$$

This process was repeated for all costs projected into the future, both those estimated at the current date and those adjusted from the past. For simplicity, the same inflation rate was chosen for all costs, although inflation may vary slightly depending on the type of goods or services. In the end, the sum of all values was calculated considering the projected future costs in order to obtain a comprehensive picture of the expected costs for the 2035 scenario. It is important to note that inflation forecasts are not always accurate, so a slightly conservative value was chosen in estimating future inflation.

4.2 LH2 aircraft

In this chapter, the focus is on the mission outlined in point 2 of the payload range diagram. The calculations will be based solely on this mission, which involves transporting 150 passengers over a distance of 3000 km. It's useful to begin by referencing some fundamental data calculated in section §2.10.3, specifically the takeoff mass of the aircraft and the amount of fuel required to complete the mission.

$$M_{TO} = 62282\,kg \qquad Fuel\ Mass = 4060\,kg$$

The reported fuel mass would enable a range of 3500 km, but diversion is not considered within the flight plan.

An operational life of 20 years has been estimated for the aircraft in question. This value, in addition to being the reference value recommended by Raymer, represents a good realistic average for current generation aircraft [90,91]. Some aircraft can last longer with proper maintenance and repairs, furthermore modern aircraft entering service in the future could be equipped with technologies capable of extending their operational life. However, as there are no certainties regarding such values, it was decided to use this value as a conservative one.

Now, it is possibile to begin calculating block distances and times, which are essential for direct operating cost calculations. The time spent in Air Traffic Control maneuvering (t_{man}) can be estimated as:

$$t_{man} = 0.25 \cdot 10^{-6} \cdot WTO + 0.0625 = 0{,}0968\, hrs$$

Assuming a maneuvering speed of 250 knots, it is possibile to estimate the distance traveled during the maneuvering phase as:

$$R_{man} = V_{man} \cdot t_{man} = 24{,}2\, nm$$

The distances covered during climb (R_{cl}) and descent (R_{de}) were calculated during the mission profile development. Summing the various sub-phases and converting units, distances are obtained:

$$R_{cl} = 178\, nm \qquad R_{de} = 153\, nm$$

Considering the cruise speed is 484 knots, we can calculate the time spent in the cruise phase (t_{cr}):

$$t_{cr} = \frac{1{,}01 \cdot R_{bl} - R_{cl} - R_{de} + R_{man}}{V_{cr}} = 2{,}74\, hrs$$

The times needed to complete the climb and descent phases were also calculated during the mission profile definition. They were initially in seconds and have been converted to hours for consistency:

$$T_{cl} = 0{,}56\, hrs \qquad T_{de} = 0{,}52\, hrs$$

It's important to note that the block time includes all ground operations, so it is also necessary to estimate the time spent in ground maneuvers (t_{gm}):

$$t_{gm} = 0{,}51 \cdot 10^{-6} \cdot WTO + 0.125 = 0{,}2 hrs$$

At this point, we can simply sum these values to calculate the block time in hours:

$$t_{bl} = t_{gm} + t_{cl} + t_{cr} + t_{de} = 4\, hrs$$

Another crucial temporal parameter for cost calculations is the annual utilization in block hours. Raymer suggests using a formula dependent on the block time of the individual mission just calculated. This method has been found to provide reliable results consistent with typical uses of aircraft in this category [85,92], making it a trustworthy choice:

$$U_{ann_{bl}} = 0{,}66 \cdot \left[10^3 \cdot \left(3{,}4546 \cdot t_{bl} + 2{,}994 - \sqrt{12{,}289 \cdot t_{bl}^2 - 5{,}6626 \cdot t_{bl} + 8{,}964} \right) \right] = 2170\, hrs$$

Having calculated the block time, it's possible to estimate the block speed and the total annual block miles covered:

$$V_{bl} = \frac{R_{bl}}{t_{bl}} = 402{,}9\, \frac{nm}{hr} \qquad R_{bl_{ann}} = V_{bl} \cdot U_{ann_{bl}} = 874230\, nm$$

4.2.1 LH2 aircraft direct operating cost

4.2.1.1 LH2 Direct Operating Cost of Flying: DOC_{flt}

First, let's calculate the crew cost. Given a short mission, let's assume a simple crew consisting of a captain and a first officer. Regarding annual salaries (SAL), Roskam suggests a specific range of values for each rank. Using the average value for each rank and adjusting it to 2023 through the CPI Inflation Calculator yields reliable values, similar to those obtained through a quick economic analysis of the industry [93]. Finally, the calculated values have been projected to 2035, assuming an annual inflation coefficient of 3%. The same procedure has been applied to calculate the travel expense factor (TEF) associated with each type of crew member.

$$Captain\ SAL_{1990} = 90000\,USD \qquad First\ officer\ SAL_{1990} = 45000\,USD$$
$$Captain\ SAL_{2023} = 222339\,USD \qquad First\ officer\ SAL_{2023} = 111170\,USD$$
$$Captain\ SAL_{2035} = 302380\,USD \qquad First\ officer\ SAL_{2035} = 151190\,USD$$
$$TEF_{2035} = 22{,}36\,USD/block\ hour$$

As mentioned in paragraph §3.3.1, Roskam suggests using an annual flight hours value of 800 for jet aircraft. However, current FAA guidelines impose a maximum limit of 1000 hours per year. For this reason an AH value of 900 hours is used. Now it's possible to calculate the cost of the captain and first officer in USD/nm:

$$C_{crew_{Captain}} = \frac{1+K}{V_{bl}} \frac{Captain\ SAL_{2035}}{AH} + \frac{TEF}{V_{bl}} = 1{,}11\,USD/nm$$

$$C_{crew_{First\ officer}} = \frac{1+K}{V_{bl}} \frac{First\ officer\ SAL_{2035}}{AH} + \frac{TEF}{V_{bl}} = 0{,}58\,USD/nm$$

Where k = 0,26 is a factor that accounts for items such as vacation pay. It's easy to calculate the crew cost:

$$C_{crew} = C_{crew_{Captain}} + C_{crew_{First\ officer}} = 1{,}69\,USD/nm$$

The cost of fuel also fits within flight operating costs. The mass of hydrogen required to complete the mission is set at 4060 kg = 8952 lb, as defined by the mission itself. As for the cost, we rely on the values found in paragraph §1.3.2, choosing a plausible value:

$$FP = 2{,}5\ €/\text{kg} = 1{,}25\ \text{USD/lb}$$

Now, it's possible to calculate the cost of fuel per nautical mile:

$$C_{pol} = \frac{W_{F_{bl}}}{R_{bl}} FP = 6{,}90\,USD/nm$$

Finally, to take in consideration insurance, let's assume it accounts for 2% of direct operating costs. By iterating to convergence and inserting the DOC value calculated in the following sections, it's obtained:

$$C_{ins} = 0{,}02DOC = 0{,}53\,USD/nm$$

With insurance costs, crew costs, and fuel costs at hand, it's possible to calculate the direct operating costs of the flight:

$$DOC_{flt} = C_{crew} + C_{pol} + C_{ins} = 9{,}11\,USD/nm$$

4.2.1.2 LH2 Direct Operating Costs of Maintenance: DOC_{maint}

As previously mentioned in section §3.3.2, estimating maintenance costs can be quite complex if we aim to account for every single item. However, it's possible to overcome this obstacle by referencing the maintenance cost per flight hour. For an A320 family aircraft, this cost is typically around $500 per block hour [94]; in some cases estimates can go as high as $700/bh [95]. The aircraft under consideration incorporates innovative technologies, and it's unclear whether these will require more or less intensive maintenance. For this reason, it's assumed a value of $700/hr, which has then been projected to 2035:

$$M_{bh_{2017}} = 700\,USD/bh \qquad M_{bh_{2035}} = 1172\,USD/bh$$

To obtain the cost per nautical mile, simply consider the velocity:

$$DOC_{maint} = \frac{M_{bh_{2035}}}{V_{bl}} = 2{,}91\,USD/nm$$

4.2.1.3 LH2 Direct Operating Cost of Depreciation: DOC_{depr}

Calculating depreciation costs first requires estimating some parameters. Specifically, it's necessary to estimate the Airplane Estimated Price (AEP), which is complicated because it not only incorporates technologies not yet in use but is also challenging to compare with an aircraft currently in use with similar dimensions, payload, and range. Attempting to obtain a reliable estimate, the prices of A320 family aircraft are used, taking into account their maximum takeoff weight:

$$AEP_{A318} = 73\,mln\,USD \qquad M_{TO_{A318}} = 68\,ton$$
$$AEP_{A319} = 79\,mln\,USD \qquad M_{TO_{A319}} = 75\,ton$$
$$AEP_{A320} = 110\,mln\,USD \qquad M_{TO_{A320}} = 78\,ton$$
$$AEP_{A321} = 130\,mln\,USD \qquad M_{TO_{A321}} = 93\,ton$$

Next, the prices were normalized based on weight, and an average was calculated. Then, it was sufficient to multiply this value by the takeoff weight of the aircraft under study to obtain the estimated market value. To account for the complexity of the technology used, a 20% markup was assumed.

$$AEP = 1{,}2 \cdot \frac{\frac{73}{68} \cdot \frac{79}{75} \cdot \frac{110}{78} \cdot \frac{130}{93}}{4} \cdot 63 = 93{,}27\,mln\,USD$$

Regarding the engines, the assumptions presented in the previous chapters were used, referencing the Leap 1-A engines installed on A320 aircraft with a cost of $EP = 14{,}5\,mln\,USD$. Finally, the cost of avionics (ASP) was estimated at $3\,mln\,USD$. Depreciation factors were set at 0,85 as suggested by Roskam, with the exception of avionics, which is assumed to have no value at the end of its useful life and thus has a depreciation factor of 1.

Finally, the last parameter to consider is the depreciation time. This varies for each subsystem and also depends on the company's policy. For the airframe, a depreciation time equal to the aircraft's operational life of 20 years was assumed; while for avionics, a generational replacement was assumed at about half of the aircraft's operational life resulting in a depreciation time of 10 years. Engines deserve in-depth study:

Roskam suggested a value of 7 years, however this no longer appears to be adequate for the current market. In fact, years of service are not the only method to estimate the operational life of an engine; it can also be considered based on flight hours or the number of takeoff/landing cycles the engine will perform (takeoff is the phase that stresses the engine the most). For this reason, an operational life composed of 12000 cycles was assumed [96], which correspond to the depreciation time:

$$DP_{eng} = 12000 \frac{t_{bl}}{U_{ann_{bl}}} = 22{,}2\, years$$

which is greater than the operational life of the aircraft. For this reason the depreciation time of the engines could be set equal to that of the aircraft:

$$DP_{eng} = 20\, years$$

However, it is not uncommon for commercial airliners to go through engines substitution during their lifetime, even 3-4 sets of engines. For this reason it's been chose to hypothesize an engine change in the aircraft lifetime as done with the avionic, using:

$$DP_{eng} = 10\, years$$

At this point, all the necessary data is available to calculate individual depreciation costs and finally DOC_{depr}. The result obtained refers to the year of the creation of this work, so the cost fraction obtained must be projected to 2035 using the method outlined earlier.

	Depreciation period	Depreciation factor	Estimated Price
Airframe	20 years	0,85	93,27 mln USD
Engine	10 years	0,85	14,5 mln USD
Avionic	10 years	1	3 mln USD

Table 4.1: depreciation data

$$C_{dap} = F_{dap} \frac{AEP - 2 \cdot EP - ASP}{DP_{ap} \cdot \frac{U_{ann_{bl}}}{cdotV_{bl}}} = 2{,}98\, USD/nm$$

$$C_{deng} = F_{deng} \frac{2 \cdot EP}{DP_{eng} \cdot \frac{U_{ann_{bl}}}{cdotV_{bl}}} = 2{,}82\, USD/nm$$

$$C_{dav} = F_{dav} \frac{ASP}{DP_{av} \cdot \frac{U_{ann_{bl}}}{cdotV_{bl}}} = 0{,}34\, USD/nm$$

$$DOC_{depr_{2023}} = C_{dap} + C_{deng} + C_{dav} = 4{,}73\, USD/nm$$

$$DOC_{depr_{2035}} = 6{,}44\, USD/nm$$

4.2.1.4 LH2 Direct Operating Cost of Fees and Taxes: DOC_{lnr}

The method described in Chapter 3 takes into account three different types of taxes: landing fees, navigation fees, and registry taxes. An airline must pay a fee each time an aircraft of its fleet lands at an airport. Each airport has its own taxation rules for landing charges. This makes it difficult to calculate taxes that represent realistic usage at different airports. To overcome this issue, landing fees were calculated at the busiest airport in major European countries considering an aircraft with $M_{TO} = 62\,ton$ and $150\,PAX$. In fact the common cost driver for all airports is the aircraft's weight; however passenger count also significantly affects the taxes. All calculations are based on airport laws in 2023 and should be considered in € per takeoff/landing.

$C_{lf_{Istanbul}} = 3578$ € [97] $C_{lf_{Charles\,de\,Gaulle}} = 2069$ € [98] $C_{lf_{Shiphol}} = 3235$ € [99]

$C_{lf_{Fiumicino}} = 2746$ € [100] $C_{lf_{Lisbon\,Airport}} = 2154$ € [101] $C_{lf_{Fraport}} = 3050$ € [102]

$C_{lf_{Adolfo\,Suarez\,Madrid-Barajas}} = 3149$ € [103] $C_{lf_{Athens\,International\,Airport}} = 1835$ € [104]

Now it's wise to average the values obtained since it's impossible to know in advance which airports the aircraft will use over its operational life.

$$C_{aplf} = \frac{C_{lf_{Athens}} + C_{lf_{Lisbon}} + C_{lf_{Frankfurt}} + C_{lf_{Madrid}} + C_{lf_{Amsterdam}} + C_{lf_{Paris}} + C_{lf_{Istanbul}}}{7} = 2725\,€$$

$$C_{aplf_{2035}} = 4076\,USD$$

The direct operating cost due to landing fees in USD/nm is:

$$C_{lf} = \frac{C_{aplf_{2035}}}{V_{bl} \cdot t_{bl}} = 2{,}52\,USD/nm$$

European air navigation charges are managed by EUROCONTROL, a European organization dedicated to the cooperation and coordination of air traffic in the Central European region [105]. EUROCONTROL provides air navigation charge coordination and pricing services covering a broad geographic area that extends beyond individual European nations. This pan-European approach helps ensure consistency and efficiency in air navigation services throughout Central Europe. European charge rates vary based on flight routes, distance traveled, and other factors for fair pricing based on the actual use of air navigation services. Air navigation charge rates vary from one country to another; these charges depend on the distance traveled, the weight of the aircraft, and a factor called Unit Rate of Charge, different for each nation. Its cost, C_{apnf}, is given by:

$$C_{apnf} = Distance\,factor \cdot Weight\,factor \cdot Unit\,Rate\,of\,Charge$$

As defined by Eurocontrol in [106], the distance factor is obtained by dividing the number of kilometers traveled by one hundred. This operation is repeated for each charging zone overflown. The weight factor is a function of the aircraft's Maximum Take-Off Weight (MTOW) expressed in metric tonnes, as shown:

$$Weight\,factor = \sqrt{\frac{M_{TO}}{50}}$$

Finally, the Unit Rate of Charge is defined as the charge in euros applied by a charging zone to a flight operated by an aircraft of 50 metric tonnes (weight factor of 1) and for a distance factor of 1. Unit rates are

adjusted each month in line with the exchange rate of the euro against the national currencies concerned. In this work, data from [106] were used dated September 2023. Calculating navigation charges poses a problem similar to that encountered in calculating landing charges and this was resolved in a similar way too: it was decided to calculate C_{apnf} by averaging the unit rate of charge for each of the European countries.

Portugal Santa Maria	10.03
Belg.-Luxembourg	113.21
Allemagne / Germany	73.04
Estonie/ Estonia	36.04
Finlande / Finland	43.92
Royaume-Uni / United Kingdom	87.88
Pays-Bas / Netherlands	92.00
Irlande/ Ireland	26.46
Danemark / Denmark	61.04
Norvège / Norway	47.66
Pologne / Poland	47.22
Suède / Sweden	73.05
Lettonie / Latvia	43.39
Lituanie / Lithuania	70.82
Espagne / Spain - Canarias	45.97
Albanie / Albania	55.71
Bulgarie / Bulgaria	36.78
Chypre / Cyprus	28.51
Croatie / Croatia	45.83
Espagne / Spain - Continent.	54.71
France	73.69

France	73.69
Grèce / Greece	25.54
Hongrie / Hungary	35.49
Italie / Italy	72.37
Slovénie / Slovenia	65.32
République Tchèque / Czech Republic	69.48
Malte / Malta	24.50
Autriche /Austria	66.91
Portugal Lisboa	47.39
Bosnie Herz. / Bosnia Herzegovina	30.78
Roumanie / Romania	46.24
Suisse / Switzerland	120.92
République de Türkiye / Republic of Türkiye	22.68
Moldavie / Moldova	226.37
Macédoine du Nord /North Macedonia	49.70
Serbia/Montenegro/ KFOR	39.50
République Slovaque / Slovak Republic	72.32
Ukraine Sud / Ukraine South	18.45
Arménie / Armenia	47.66
Géorgie / Georgia	31.94
Ukraine	46.91

Figure 4.2: EUROCONTROL Unit rate of charge for different European countries

$$Unit\ Rate\ of\ Charge = \frac{\sum Unit\ Rate\ of\ Charge_i}{41} = 56{,}76$$

In this way the unit rate of charge to insert into the equation for calculating C_{apnf} is obtained, and by calculating the weight factor and the distance factor the value of the navigation fee charged per flight is calculated and and projected:

$$C_{apnf} = 1912\ € \qquad C_{apnf_{2035}} = 2600\ USD$$

The cost of navigation fees in USD/nm is:

$$C_{nf} = \frac{C_{apnf_{2035}}}{V_{bl} \cdot t_{bl}} = 1{,}77\ USD/nm$$

Finally, direct costs of registry taxes expressed in USD/nm are calculated. Regarding the purely administrative and bureaucratic aspect, Roskam suggests using a fraction of direct operating costs for these taxes, with a factor dependent on takeoff weight:

$$f_{rt} = 0{,}001 + 10^{-8} \cdot M_{TO} = 0{,}0024$$

The European Union also imposes a pollution tax on every company operating in European territory through the "EU emissions trading system." However the aircraft under consideration, emitting no carbon dioxide, is exempt from this tax which will be adequately explored when estimating the costs of a traditional aircraft. For this reason the direct cost of registry taxes expressed in USD/nm is:

$$C_{rt} = f_{rt} \cdot DOC = 0{,}063\ USD/nm$$

At this point, all the necessary data is available for calculating the operating costs related to taxes:

$$DOC_{lnr} = C_{lf} + C_{nf} + C_{rt} = 4{,}35\ USD/nm$$

4.2.1.5 Direct Operating Cost of Financing: DOC_{fin}

To complete the calculation of direct operating costs, it's necessary to estimate the financing costs (regardless of their type). As mentioned in Section §3.3.5, these amount to approximately 7% of the direct operating costs. Therefore, it's easy to calculate:

$$DOC_{fin} = 0{,}07 DOC = 1{,}86\ USD/nm$$

4.2.2 LH2 Aircraft Operating Cost

Summing all the components contained within DOC, the direct operating costs are obtained:

$$DOC = DOC_{flt} + DOC_{maint} + DOC_{depr} + DOC_{lnr} + DOC_{fin} = 26{,}58\ USD/nm$$

To calculate the aircraft's operating costs, indirect operating costs must also be estimated. However, these costs not only vary from one airline to another but are also independent of the aircraft. Since this work is aimed at a comparison and remembering what described in Section §3.4, the calculation of direct operating costs is approximated as a simple percentage of direct operating costs. By observing Figure 4.1 obtained from Roskam, it can be noted that this percentage changes with the mission distance. In particular, for the mission under consideration, an estimated factor of approximately 0,4 is observed, meaning indirect

operating costs amount to 40% of direct operating costs. Although this is an approximate percentage, it reasonably reflects the real values characterizing today's airlines as mentioned in §3.4 so it was deemed valid and used to calculate IOC:

$$IOC = 0{,}4DOC = 10{,}63\ USD/nm$$

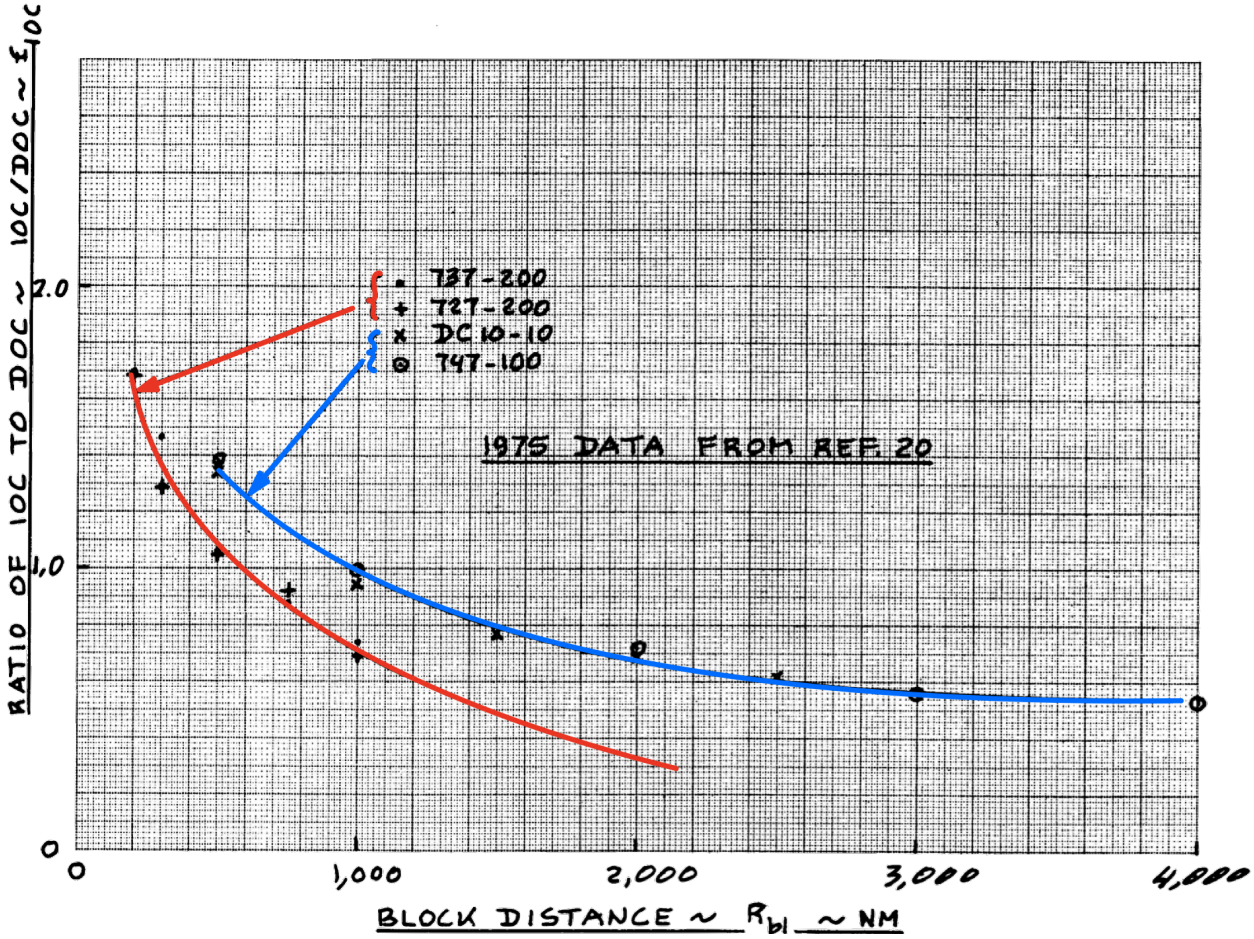

Figure 3.5: Estimation of IOC to DOC ratio [82]

At this point, the two main components are available, and it's possible to calculate the total operating costs of the aircraft under study.

$$C_{op} = DOC + IOC = 37{,}22\ USD/nm$$

For clarity, the results are also provided in other measurement units:

Direct operating costs DOC

$$DOC = 26{,}58\ USD/nm$$
$$DOC = 13{,}05\ €/km$$
$$DOC = 0{,}087\ €/km/pax$$

Total operating costs C_{op}

$$C_{op} = 37{,}22\ USD/nm$$
$$C_{op} = 18{,}27\ €/km$$
$$C_{op} = 0{,}122\ €/km/pax$$

4.3 Traditional Aircraft

To obtain the necessary comparison to evaluate the competitiveness of the studied aircraft, it's necessary to analyze the costs of a traditional aircraft too. To perform the calculations wisely, it's prudent to fix the mission. Even though the traditional aircraft could carry a different number of passengers and/or fly farther, calculations should assume the same mission characterized by 150 passengers and 3000 km. It has been previously seen that the most similar aircraft in terms of range and maximum takeoff weight is the Airbus A318, making it a good candidate for analysis. However even in full economy configuration this aircraft is unable to carry 150 passengers, which could alter the comparison especially if a comparison with the same number of passengers is desired. For this reason, attention has shifted to the Airbus A319. It belongs to the same family and is capable of carrying slightly more passengers, making it the chosen reference aircraft. The Airbus A319 is characterized by a maximum takeoff weight of:

$$M_{TO_{A319}} = 75\,ton$$

Furthermore, the chosen aircraft can carry a maximum of 160 passengers and has a maximum operational range of 6900 km, so it is fully capable of performing the predefined mission. The goal is to evaluate the cost differences that hydrogen technology could entail, so everything that could potentially remain constant will be kept fixed and the corresponding cost items will be the same as calculated in the previous sections. Of course, all calculated costs will be reported for clarity, providing more detail for costs that undergo variations. It should also be noted that a fair comparison must be made assuming the same year, so in this case, costs will also be calculated in 2035 using methods similar to those seen previously.

4.3.1 Traditional Aircraft Direct Operating Cost

Even though the mission remains the same, dealing with a different aircraft can bring various changes. The number of years during which the airplane is operated is held constant at 20 years. Another parameter estimated in the same way is the speed maintained during Air Traffic Control (ATC) maneuvering, which is set at 250 knots. However, the time spent in ATC maneuvering, as estimated in Section §4.2.1, depends on the takeoff mass and will therefore assume a slightly different value, which will also influence the distance covered while maneuvering due to ATC:

$$t_{man} = 0.25 \cdot 10^{-6} \cdot WTO + 0.0625 = 0{,}10\,hrs$$

$$R_{man} = V_{man} \cdot t_{man} = 25{,}96\,nm$$

The distance covered and the time spent during climb and descent are assumed to be constant, just like in the previous case. However, the time required to complete the cruise is slightly different due to the distance covered during maneuvering and the cruise speed, which for an Airbus A319 is typically 840 km/h [107,108].

$$t_{cr} = \frac{1{,}01 \cdot R_{bl} - R_{cl} - R_{de} + R_{man}}{V_{cr}} = 2{,}93\,hrs$$

Just like the time spent in ATC maneuvering, the time spent in ground maneuvers is approximated as a function of the maximum takeoff mass. This, together with the differences just mentioned, results in a slight increase in block time (minimal variations of a few minutes).

$$t_{gm} = 0{,}51 \cdot 10^{-6} \cdot WTO + 0.125 = 0{,}21\, hrs$$

$$t_{bl} = t_{gm} + t_{cl} + t_{cr} + t_{de} = 4{,}22\, hrs$$

At this point, the values of annual utilization in block hours, block speed, and total annual block miles can also be reported.

$$U_{ann_{bl}} = 0{,}66 \cdot \left[10^3 \cdot \left(3{,}4546 \cdot t_{bl} + 2{,}994 - \sqrt{12{,}289 \cdot t_{bl}^2 - 5{,}6626 \cdot t_{bl} + 8{,}964}\right)\right] = 2173\, hrs$$

$$V_{bl} = \frac{R_{bl}}{t_{bl}} = 383{,}5\, \frac{nm}{hr} \qquad R_{bl_{ann}} = V_{bl} \cdot U_{ann_{bl}} = 833320\, nm$$

4.3.1.1 Traditional Aircraft Flight Operational Costs

In this section, some costs will remain unchanged between the two aircraft while others will undergo significant variations, so it is necessary to investigate the individual items.

Regarding crew costs, the situation remains the same and therefore the costs are identical to the previous case. However, due to the values calculated in Section §4.3.1, the normalized cost value per nautical mile traveled undergoes some slight variations.

$$Captain\ SAL_{2035} = 302380\,\$ \qquad First\ officer\ SAL_{2035} = 151190\,\$$$

$$TEF_{2035} = 22{,}36\,\$/block\ hour$$

$$C_{crew_{Captain}} = \frac{1+K}{V_{bl}} \frac{Captain\ SAL_{2035}}{AH} + \frac{TEF}{V_{bl}} = 1{,}16\, USD/nm$$

$$C_{crew_{First\ officer}} = \frac{1+K}{V_{bl}} \frac{First\ officer\ SAL_{2035}}{AH} + \frac{TEF}{V_{bl}} = 0{,}61\, USD/nm$$

$$C_{crew} = C_{crew_{Captain}} + C_{crew_{First\ officer}} = 1{,}77\, USD/nm$$

When it comes to fuel costs, there are more significant changes. Jet A1 in fact has a much lower specific cost compared to hydrogen, but kerosene engines consume much more fuel. To estimate the amount of fuel consumed in the treated mission, a simple consumption per kilometer of a CFM International LEAP 1A engine installed on the A319 aircraft was used. According to various estimates, Airbus A319 Neo consume an average of 3 kg of fuel per kilometer traveled [109,110,111]. Basing on this estimate, it is easy to calculate the total fuel consumption. Kerosene prices, on the other hand, are much easier to find, although these can fluctuate based on market fluctuations, the most recent data suggest a value of 0,7 USD/kg [112,113,114]. The cost of Jet fuel is the only item that will not be projected to 2035 considering inflation. In fact, this value varies significantly over the years and does not follow a linear trend, making it almost impossible to predict its future trajectory. Furthermore, over the last 20 years, the average cost of Jet fuel remained stable at

around 2,5 USD per gallon, despite significant fluctuations [115]. Therefore, it has been decided to keep this value constant even in future perspective.

Having available the quantity of fuel necessary to complete the entire mission and its unit cost, it is easy to calculate the fuel cost in USD/nautical mile:

$$M_{fuel} = 2{,}8 \cdot R_{bl} = 8400\,kg \qquad FP = 0{,}6976\,USD/kg$$

$$Cpol = \frac{M_{fuel}}{R_{bl}} \cdot FP = 3{,}8\,USD/nm$$

The cost of insurance is estimated in the same way as done before, assuming 2% of the direct operating costs. After the various iterations leading to the calculation of DOC, the result obtained is:

$$C_{ins} = 0{,}02DOC = 0{,}46\,USD/nm$$

The direct operating costs inherent to the flight phase are:

$$DOC_{flt} = C_{crew} + C_{pol} + C_{ins} = 6{,}30\,USD/nm$$

4.3.1.2 Traditional Aircraft Maintenance Operational Costs

The calculation of maintenance costs follows the same procedure as done before. However, for the hydrogen aircraft, consideration was given to the possible difficulty introduced by the new technology using a limit value for the maintenance cost per flight hour of a similar A320 aircraft. In this case, a value that better falls within the average of the found values has been chosen, which is 600 USD/hr. Once appropriately adjusted to fit the 2035 scenario, it can be used to calculate the costs in USD/nautical mile:

$$M_{bh_{2035}} = 924\,USD/blh$$

$$DOC_{maint} = \frac{M_{bh_{2035}}}{V_{bl}} = 2{,}41\,USD/nm$$

4.3.1.3 Traditional Aircraft Depreciation Operational Costs

As mentioned earlier, depreciation costs vary from company to company as different corporate policies come into play. Not having more precise data available, most of the assumptions made for the hydrogen aircraft have been maintained. The engine is the same, so price, time, and depreciation factor are exactly the same. The same goes for avionics: the category is the same and, assuming a comparison in the same year, it is assumed that both aircraft will have the same technologies available. The only thing that changes in depreciation costs is the market value of the aircraft, which has been estimated at 79 million dollars for the A319.

	Depreciation period	Depreciation factor	Estimated Price
Airframe	20 years	0,85	79 mln USD
Engine	10 years	0,85	14,5 mln USD
Avionic	10 years	1	3 mln USD

Table 4.3: depreciation data

Once all the necessary data have been fixed, it is possible to make the necessary calculations to obtain the depreciation costs:

$$C_{dap} = F_{dap}\frac{AEP - 2 \cdot EP - ASP}{DP_{ap} \cdot \frac{U_{ann_{bl}}}{cdotV_{bl}}} = 2{,}40\ USD/nm$$

$$C_{deng} = F_{deng}\frac{2 \cdot EP}{DP_{eng} \cdot \frac{U_{ann_{bl}}}{cdotV_{bl}}} = 2{,}96\ USD/nm$$

$$C_{dav} = F_{dav}\frac{ASP}{DP_{av} \cdot \frac{U_{ann_{bl}}}{cdotV_{bl}}} = 0{,}36\ USD/nm$$

$$DOC_{depr_{2023}} = C_{dap} + C_{deng} + C_{dav} = 5{,}71\ USD/nm$$

$$DOC_{depr_{2035}} = 7{,}77\ USD/nm$$

4.3.1.4 Traditional Aircraft Operational Tax Costs

The taxes section is interesting because some items remain the same as for the hydrogen aircraft while others change significantly, resulting in higher costs for the traditional aircraft. Among the taxes that remain unchanged, airport landing fees can certainly be mentioned. These fees undergo a small variation due to the higher take-off weight of the A319 but are calculated exactly the same way, starting from the average of the busiest airports in the major European countries.

$C_{lf_{Istanbul}} = 3696\ €$ [97] $C_{lf_{Charles\ de\ Gaulle}} = 2123\ €$ [98] $C_{lf_{Shiphol}} = 3300\ €$ [99]

$C_{lf_{Fiumicino}} = 2799\ €$ [100] $C_{lf_{Lisbon\ Airport}} = 2255\ €$ [101] $C_{lf_{Fraport}} = 3051\ €$ [102]

$C_{lf_{Adolfo\ Suarez\ Madrid-Barajas}} = 3243\ €$ [103] $C_{lf_{Athens\ International\ Airport}} = 1914\ €$ [104]

$$C_{aplf} = \frac{C_{lf_{Athens}} + C_{lf_{Lisbon}} + C_{lf_{Frankfurt}} + C_{lf_{Madrid}} + C_{lf_{Amsterdam}} + C_{lf_{Paris}} + C_{lf_{Istanbul}}}{7} = 2797\ €$$

$$C_{aplf_{2035}} = 4185\ USD$$

The direct operating cost due to landing fees in USD/nm is:

$$C_{lf} = \frac{C_{aplf_{2035}}}{V_{bl} \cdot t_{bl}} = 2{,}58\ USD/nm$$

The same considerations apply to navigation fees. Navigation fees depend on the distance traveled, the countries crossed, and the maximum take-off weight. Since it's the same mission, the distance is the same and the Unit Rate of Charge for different countries is taken into account through their average value, as calculated in Section §4.2.1.4. The only term in the equation that changes is the weight factor, which is a

function of the aircraft's Maximum Take-Off Weight (MTOW). At this point, it is possible to calculate the costs related to navigation fees, project them to 2035, and normalize them per nautical mile.

$$Weight\,factor = \sqrt{\frac{M_{TO}}{50}} \qquad Unit\,Rate\,of\,Charge = 56{,}76$$

$$C_{apnf} = Distance\,factor \cdot Weight\,factor \cdot Unit\,Rate\,of\,Charge = 1911\,€$$

$$C_{apnf_{2035}} = 2600\,USD$$

$$C_{nf} = \frac{C_{apnf}}{V_{bl} \cdot t_{bl}} = 1{,}77\,USD/nm$$

Finally, the direct costs of registry taxes. Just as was done for the hydrogen aircraft, in this case administrative costs are estimated as suggested in Roskam:

$$f_{rt} = 0{,}001 + 10^{-8} \cdot M_{TO} = 0{,}0027 \qquad C_{rt} = f_{rt} \cdot DOC = 0{,}061\,USD/nm$$

It should be noted that the European Union imposes a tax on carbon dioxide emissions on every airline operating within the European Union. This tax increases based on the pollution produced and is calculated through the EU Emissions Trading System (EU ETS) [116]. The European Union's Emissions Trading System, also known as the EU Carbon Market, is one of the European Union's key environmental policy tools for addressing climate change. It was established to help economically efficiently reduce greenhouse gas emissions in the European Union. The primary goal of EU ETS is to reduce greenhouse gas emissions, particularly carbon dioxide (CO_2), from industries and energy sectors covered by the system. These sectors represent a significant portion of the EU's total greenhouse gas emissions. The system allocates a limited number of CO2 emission allowances to companies operating in high-energy-consuming sectors, which they can buy, sell, or trade among themselves. Companies exceeding their allowances must purchase additional allowances or face hefty financial penalties. This creates an economic incentive to reduce emissions. EU ETS covers various industrial sectors, including electricity generation, steel production, cement, oil refining, and commercial aviation. Starting in 2013, an increasing number of emission allowances have been auctioned rather than given away for free to companies. This has generated revenue for EU member states and further incentivized emissions reductions. The environmental measures adopted became effective for the aeronautical sector in 2012 when aircraft operators in Europe began paying for their CO_2 emissions. The primary objective of this action is to reduce aircraft CO_2 emissions in the coming years. To achieve this goal, the EU started distributing emission permits (also known as Emissions Certificates or EC) to airlines from 2012 onwards. Each certificate allows an aircraft operator to emit 1 tonne of CO_2 within the current year. If an airline's emissions exceed the allocated ECs, the operator must pay a fine. Over time, these fines have become more expensive. Additionally, generic aircraft operators can purchase emissions permits from other participants in the Emissions Trading System (ETS). Each year, the EU allocates a fixed number of certificates for free, with the remainder being auctioned or held in reserve. The percentage of free certificates

will decrease in the coming years. In [117], a method can be found to calculate the impact of CO_2 emission costs on aircraft's direct operating costs, as outlined in the ETS described above. These emissions-related costs are referred to as CETS i.e. the costs due to the EU ETS per flight. It is assumed that aircraft operators can cover their emissions with ECs, avoiding the need to pay fines.

Firstly, it is necessary to calculate the CO_2 emissions per flight. According to ETS estimations, the CO_2 emission per kilogram of Jet A-1 fuel burned amounts to 3,15 kg. Once the mass of fuel burned during one trip (M_{fuel}) is known, the CO_2 emissions can be calculated. Remembering that a certain amount of ECs is free, this quantity is not subject to charges: the free percentage of EC is named $p_{CO_2,\,free}$. The resulting formula for the calculation of CETS (cost per flight) is quite complex:

$$CETS = \frac{3{,}15 \cdot 10^{-3} \cdot M_{fuel} \cdot ct_{CO_2} \cdot \left[17{,}6 + 0{,}7 \cdot (n_y - 2010)\right] \left[1 - \frac{p_{CO_2,\,free}}{100 + 2{,}5 \cdot (n_y - 2005)}\right]}{64{,}4 + 3{,}1 \cdot (n_y - 2010)}$$

Here:

- ct_{CO_2} represents the average costs per EC traded on the market. Every year, the costs of Emissions Certificates that are not provided for free increase more and more. Their price follows market trends, undergoing many fluctuations. As of today, the highest price is around €105 per EC [118]. The price will certainly rise in the future, but as it's impossible to estimate their future cost, this maximum value will also be used for the 2035 scenario;
- n_y is the year for which the cost is calculated;
- the two terms containing (n_y –2010) take into account the future number of aircraft movements with 2010 as the reference year. This assumes an average worldwide Revenue Passenger Kilometer (RPK) growth of 4,8% and an average RPK growth of 4,0% in Europe from 2011 to 2030;
- $p_{CO_2,\,free}$ is the predefined percentage of free ECs for a specific year (for example, it represents 85% of the emission target in 2012 and 82% of the emission target from 2013). In this case the reference year is 2005, which serves as the baseline year for defining emission targets. The quantity of ECs distributed for free by the European Union decreases each year, with the goal of continually reducing CO2 emissions. In 2035, it is estimated that the European Union will distribute only 50% of Emissions Certificates for free.

Calculating the costs per flight in the 2035 scenario yields:

$$CETS = 699{,}25\,€$$

These costs are related solely to polluting emissions and do not include bureaucratic registry costs: the two calculated items must be added together to calculate the total cost of registry tax-related operating costs:

$$C_{rt} = f_{rt} \cdot DOC + \frac{CETS}{R_{bl}} = 0{,}49\,USD/nm$$

At this point, the tax operating costs can be calculated:

$$DOC_{lnr} = C_{lf} + C_{nf} + C_{rt} = 4{,}84\,USD/nm$$

4.3.1.5 Traditional Aircraft Financing Operating Costs

To complete the calculation of direct operating costs, the costs related to financing are also estimated as 7% of the direct operating costs:

$$DOC_{fin} = 0{,}07DOC = 1{,}61\ USD/nm$$

4.3.2 Traditional Aircraft Operating Costs

Summing all the components contained within DOC, the direct operating costs are obtained:

$$DOC = DOC_{flt} + DOC_{maint} + DOC_{depr} + DOC_{lnr} + DOC_{fin} = 22{,}93\ USD/nm$$

Finally, indirect operating costs need to be calculated. In this case too, they are calculated as a percentage of direct operating costs. The ratio between DOC and IOC in the Roskam model depends solely on the distance traveled. Having considered the same mission for both aircraft, the parameter f_{ioc} remains the same. By setting the parameter to 0,4 it's obtained:

$$IOC = 0{,}4DOC = 9{,}17\ USD/nm$$

Direct and indirect operating costs allow us to estimate the total operating costs of an Airbus A319 Neo, which are also presented in other measurement units for clarity:

$$C_{op} = DOC + IOC = 32{,}11\ USD/nm$$

Direct operating costs DOC	Total operating costs C_{op}
$DOC = 22{,}93\ USD/nm$	$C_{op} = 32{,}11\ USD/nm$
$DOC = 11{,}26\ €/km$	$C_{op} = 15{,}76\ €/km$
$DOC = 0{,}075\ €/km/pax$	$C_{op} = 0{,}11\ €/km/pax$

The operating costs required to keep an aircraft in service are not always easy to calculate because airlines typically have large and diverse fleets consisting of many different types of aircraft. Moreover, these costs can be values that major airlines are reluctant to share with their competitors. For this reason, it is difficult to find a wealth of data on this topic in the literature. However, some data can be obtained from the Airline Cost Management Group (ACMG). Although the names of the companies providing the data are not available, the data found falls within the same order of magnitude as the results obtained considering the increase due to the different years [92,119]. This suggests that, while the method used is a significant simplification of reality, the calculated costs can be considered reliable. What is important for the purposes of this work is not the absolute values of the costs required to keep an airliner in service, but the comparison between the operating costs of a traditional aircraft and a potential hydrogen aircraft. In this way, even if some simplifications may provide data that is not entirely reliable, these modifications equally affect the costs of both aircraft, canceling each other out when making a direct comparison.

5. Conclusions

The objective of this thesis is to analyze the realization of a hydrogen-powered aircraft from both an engineering and economic perspective. After conducting a brief but necessary investigation into the technology to be implemented, both aspects have been explored.

In Chapter 2, the conceptual design of the aircraft was discussed. To achieve this endeavor, an Airbus A320 Neo was used as a reference aircraft from which some fundamental parameters were derived to proceed with the work. The Raymer method, as described in the book "Aircraft Design: A Conceptual Approach", was employed to estimate a crucial parameter of the aircraft: take-off mass. Subsequently, the internal volumes of the fuselage were studied to optimize the spaces. Following this, a graphical sketch was provided. It should be noted that the proposed arrangement should not be considered in any way definitive, as it is based on strong simplifications. Designing a commercial aircraft is a long process that spans several years, and certainly more in-depth analyses are required. The payload-range diagram was used to assess the aircraft's operational capabilities based on the previous steps. Furthermore, it proved to be a tool capable of easily demonstrating the aircraft's ability to meet high-level requirements. Finally, through the matching chart, the technical capabilities of the aircraft in terms of thrust and wing area were verified to ensure that it is fully capable of performing the mission.

Subsequently, costs were analyzed with a focus on operating costs. These costs were estimated using the workflow described in Roskam's book "Airplane Design Part VIII: Airplane Cost Estimation". Although this text is now dated, the Roskam method remains valid and widely used in the aerospace industry. The primary cost item was the operating costs, which were properly divided into costs related to flight, maintenance, depreciation, taxes, and financing. Indirect operating costs, on the other hand, were approximated as a percentage of the operating costs, yielding results characterized by good reliability.

5.1 Conceptual Design

The conceptual design completed in Chapter 2 can be considered the embryonic phase of a hydrogen-powered commercial aircraft project. What emerges from this work is that it seems possible to build a passenger transport aircraft fueled by hydrogen and this idea represents one of the most intriguing prospects for the future of sustainable aviation. In recent years, interest in hydrogen as an energy carrier for aviation has grown significantly, as airlines and the aerospace industry seek solutions to reduce greenhouse gas emissions and combat climate change. The physical characteristics of hydrogen that most influence such a project are its mass and energy density. Hydrogen, even in cryogenic liquid form, has an extremely low mass density. This means that a large volume is required to transport a certain amount of hydrogen. However on the other hand its energy density is very high, so producing a certain amount of energy from combustion requires a smaller quantity of hydrogen compared to conventional fuels. The designed aircraft is influenced by these characteristics. It requires a limited amount of fuel to cover a certain operating range (4060 kg for 3500 km) compared to traditional aircraft. Nevertheless it was necessary to completely revolutionize the

volume management to transport the fuel, as the required tanks are so voluminous that they cannot be accommodated in the wings. Additionally they occupy a considerable volume even in the fuselage: the sketches presented in Chapter 2 clearly show how these conditions make the realization of the aircraft challenging necessitating a total paradigm shift from current aircraft. However, despite the necessary safety factors, dead spaces, and volumetric efficiencies, a configuration has been achieved that could potentially be realized and meet all high-level requirements. Nevertheless, some simplifications made in this thesis would warrant more detailed work. For example, hydrogen engines require significant technological developments compared to traditional fossil fuel engines. Highly efficient and reliable engines are needed to handle hydrogen's different behavior compared to fossil fuel. Additionally, the presence of high-pressure tanks located in the fuselage near passengers certainly requires advanced safety analyses. Despite these and other challenges, the realization of a hydrogen-powered aircraft seems to be possible, especially considering the technological advancements that will arrive in the coming years. Proof of this result is provided by the fact that many airlines and aerospace companies are investing in research and development of hydrogen-powered aircraft in spite of the large amount of work. Some projects are already underway, with prototypes in the testing phase [120,121].

5.2 Costs

As mentioned in the previous section, it is evident that a hydrogen-powered aircraft is technically feasible from an engineering standpoint (at least following a preliminary analysis). However, this information alone is insufficient to ensure the feasibility of a project. The birth of a new aircraft, especially if it revolutionizes many technical aspects, comes with a very high cost so there must be certainty that such an investment can be repaid during its use. For this reason, the economic feasibility of this project was analyzed by studying its competitiveness compared to a traditional aircraft operating in the same market sector such as the Airbus A319. By comparing the data calculated in Chapter 4, some interesting considerations can be made. As expected, the hydrogen-powered aircraft is characterized by higher but economically sustainable operating costs. As shown in Figure 5.1, the operating costs related to the hydrogen-powered aircraft incur greater expenses primarily due to the fuel cost, which accounts for 28% of the direct operating costs. This phenomenon is mainly attributed to the cost of hydrogen which, according to the estimates provided in chapter 1, will remain more expensive than kerosene even in the 2035 scenario. Nevertheless, part of the cost increase due to hydrogen is offset by taxes: traditional aircraft operating in Europe impose costs on airlines due to carbon dioxide emissions through the mechanism of the European Union Emissions Trading System. These costs account only for 2% of the direct operating costs of the examined A319 aircraft but are entirely absent in the costs of the hydrogen-powered aircraft.

Considering these factors and other minor differences, it is possible to estimate the percentage increase in direct and total operating costs that a hydrogen-powered aircraft would incur compared to a traditional aircraft. Following the notation proposed by Roskam, calculations were performed using the operating costs in USD/nm, however the results are also presented in €/km and €/flight hour for clarity. Although all

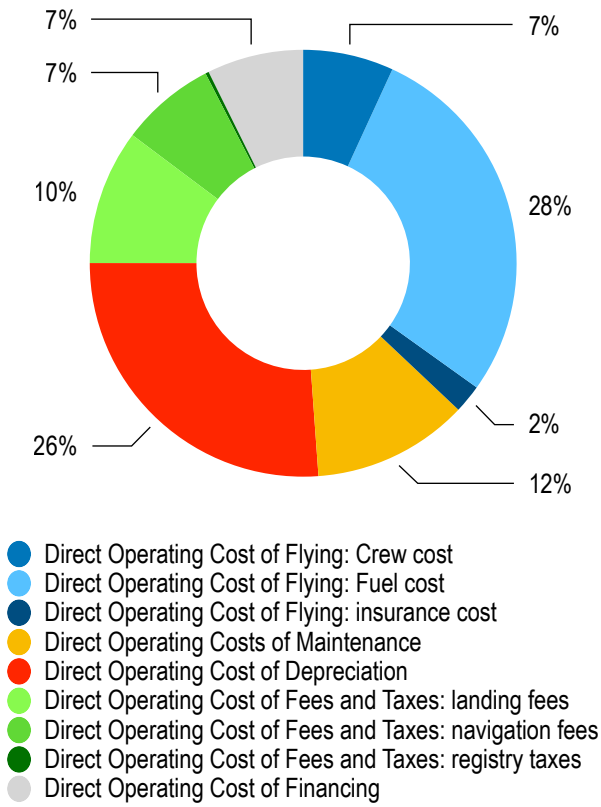

Figure 5.1: LH2 aircraft Direct Operating Cost

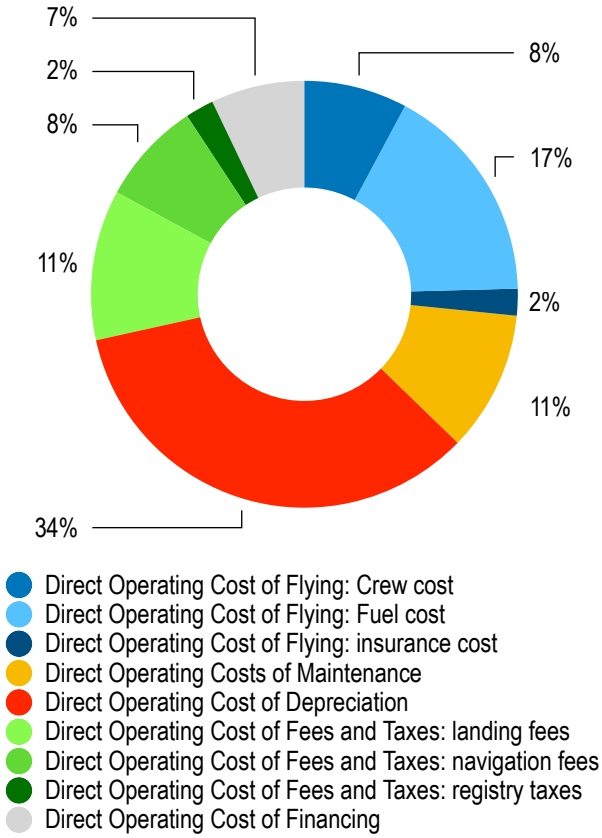

Figure 5.2: Traditional aircraft Direct Operating Cost

calculations were projected to 2035, as it is not possible to predict its future trends, the current exchange rate between the US dollar and the euro was used, which as of September 2023 is equal to: 1 EUR = 1,1 USD [122].

$DOC_{LH_2} = 26{,}58\ USD/nm$ → $+15{,}9\,\%$ → $DOC_{A319Neo} = 22{,}93\ USD/nm$

$DOC_{LH_2} = 13{,}05\ €/\text{km}$ → $DOC_{A319Neo} = 11{,}26\ €/\text{km}$

$DOC_{LH_2} = 9738\ €/\text{hr}$ → $+21{,}8\,\%$ → $DOC_{A319Neo} = 7995\ €/\text{hr}$

$C_{opLH_2} = 37{,}22\ USD/nm$ → $+15{,}9\,\%$ → $C_{opA319} = 32{,}11\ USD/nm$

$C_{opLH_2} = 18{,}27\ €/\text{km}$ → $C_{opA319} = 15{,}76\ €/\text{km}$

$C_{opLH_2} = 13633\ €/\text{hr}$ → $+21{,}8\,\%$ → $C_{opA319} = 11193\ €/\text{hr}$

Another interesting data point to show is the cost per passenger-kilometer. This is very useful because by multiplying it by the distance covered by the assumed mission, it is possible to calculate the cost per passenger and make a comparison between the two aircraft. The cost increases due to the hydrogen-powered aircraft must be borne by someone, and certainly cannot be passed on to the airlines (otherwise there would

be no advantage in using this new technology). The cost increase will inevitably be borne by the passengers, and this increase will demonstrate the actual economic competitiveness of the technology over time.

$$DOC = 0{,}087\,€/\text{km/pax} \quad C_{op} = 0{,}1218\,€/\text{km/pax} \xrightarrow{+16\,\%} DOC = 0{,}075\,€/\text{km/pax} \quad C_{op} = 0{,}1051\,€/\text{km/pax}$$

Assuming the typical mission of 3000 km and 150 passengers for both aircraft, an increase of 50€ per individual passenger on the purchase of an airline ticket is calculated. The growing pressure to reduce carbon emissions and address climate change is driving the aviation industry towards cleaner solutions. A hydrogen-powered aircraft would offer a competitive advantage in terms of sustainability, which could translate into greater appeal for passengers who might potentially be willing to accept higher fares. However, the objective of this thesis project has been achieved by showing the economic comparison and calculating the increase that a passenger would need to bear to fly emission-free. It is not the task of the proposed work to assert whether the calculated data represent an economically feasible and/or advantageous scenario; these are aspects that need to be evaluated by economic experts. What can be added to support these results is that the magnitude of the data shown align with the comparison made by the International Civil Aviation Organization (ICAO) in the "ICAO Special Supplement: Long-Term Aspirational Goal", although a little greater [123]. In this document, the International Civil Aviation Organization estimates an increase of 14$ per passenger for a 2900 km mission aboard a sustainably powered aircraft in 2035. This parallelism demonstrates the reliability of the Roskam method.

In conclusion, a hydrogen-powered aircraft is an exciting innovation in the field of sustainable aviation and represents a promising solution for reducing carbon emissions in the aviation industry. However, it is important to consider that the operating costs of a hydrogen-powered aircraft will be slightly higher than those of a traditional fossil fuel-powered aircraft that use kerosene, at least initially. With the increasing production of green hydrogen obtained from renewable sources and the improvement of production technologies, hydrogen costs will decrease over time making its use as an aircraft fuel more cost-effective. Although operating costs may be slightly higher, a hydrogen-powered aircraft could offer long-term benefits in terms of carbon emission reduction and adaptation to increasingly stringent environmental regulations. This could result in economy savings and greater resilience of the airline compared to fossil fuel-based fleets, especially looking over a long period time in the future.

6. Bibliography

1. Klöwer, M., Allen, M. R., Lee, D. S., Proud, S. R., Gallagher, L., & Skowron, A. (2021). Quantifying aviation's contribution to global warming. *Environmental Research Letters*, *16*(10). https://doi.org/10.1088/1748-9326/ac286e
2. Fichter, C. (n.d.). Forschungsbericht 2009-22 Climate Impact of Air Traffic Emissions in Dependency of the Emission Location and Altitude.
3. https://www.iea.org/energy-system/transport/aviation
4. Quadros, F. D. A., Snellen, M., Sun, J., & Dedoussi, I. C. (2022). Global Civil Aviation Emissions Estimates for 2017–2020 Using ADS-B Data. *Journal of Aircraft*, *59*(6), 1394–1405. https://doi.org/10.2514/1.C036763
5. https://www.transportenvironment.org/discover/aviation-2-3-times-more-damaging-climate-industry-claims/
6. Penner, J. E., Lister, D. H., Griggs, D. J., Dokken, D. J., & Mcfarland, M. (1999). Summary for Policymakers Aviation and the Global Atmosphere A Special Report of IPCC Working Groups I and III in collaboration with the Scientific Assessment Panel to the Montreal Protocol on Substances that Deplete the Ozone Layer Published for the Intergovernmental Panel on Climate Change.
7. IATA (2019) FACT SHEET 7: Liquid hydrogen as a potential low- carbon fuel for aviation
8. Ajanovic, A., Sayer, M., & Haas, R. (2022). The economics and the environmental benignity of different colors of hydrogen. *International Journal of Hydrogen Energy*, *47*(57), 24136–24154. https://doi.org/10.1016/j.ijhydene.2022.02.094
9. Panić, I., Cuculić, A., & Ćelić, J. (2022). Color-Coded Hydrogen: Production and Storage in Maritime Sector. In *Journal of Marine Science and Engineering* (Vol. 10, Issue 12). MDPI. https://doi.org/10.3390/jmse10121995
10. https://www.europarl.europa.eu/news/it/press-room/20220701IPR34365/tassonomia-si-all-inclusione-di-attivita-dei-settori-del-gas-e-del-nucleare
11. Clean Sky 2. (2020). *Hydrogen-powered aviation*. A fact-based study of hydrogen technology, economics, and climate impact by 2050. https://doi.org/10.2843/766989
12. Burke, A., & Fulton, L. (2022). Use Of Liquid Hydrogen in Heavy-Duty Vehicle Applications: Station And Vehicle Technology and Cost Considerations.
13. Connelly, E., Penev, M., Elgowainy, A., Hunter Peer Reviewed By, C., Burgunder, A., Martinez, A., Tamhankar, S., By, A., Rustagi, N., Joseck, F., & Satyapal, S. (2019). *DOE Hydrogen and Fuel Cells Program Record: Current Status of Hydrogen Liquefaction Costs*.
14. Path to hydrogen competitiveness A cost perspective. (2020). www.hydrogencouncil.com.
15. Carvalho, F., Osipova, L., & Zhou, Y. (2023). Life-cycle greenhouse gas emissions of hydrogen as a marine fuel and cost of producing green hydrogen in Brazil. www.theicct.org
16. Hydrogen Insights A perspective on hydrogen investment, market development and cost competitiveness. (2021). www.hydrogencouncil.com.

17. Steer. European Climate Foundation. (2023). Analysing the costs of hydrogen aircraft | Final Report
18. Fusaro, R., Vercella, V., Ferretto, D., Viola, N., & Steelant, J. (2020). Economic and environmental sustainability of liquid hydrogen fuel for hypersonic transportation systems. *CEAS Space Journal*, *12*(3), 441–462. https://doi.org/10.1007/s12567-020-00311-x
19. Franzmann, D., Heinrichs, H., Lippkau, F., Addanki, T., Winkler, C., Buchenberg, P., Hamacher, T., Blesl, M., Linßen, J., & Stolten, D. (2023). Green hydrogen cost-potentials for global trade. *International Journal of Hydrogen Energy*. https://doi.org/10.1016/j.ijhydene.2023.05.012
20. Choi, Y., & Lee, J. (2022). Estimation of Liquid Hydrogen Fuels in Aviation. *Aerospace*, *9*(10). https://doi.org/10.3390/aerospace9100564
21. https://www.airbus.com/en/innovation/low-carbon-aviation/hydrogen/zeroe#:~:text=Airbus' ambition is to bring,produce and supply the hydrogen.
22. Khandelwal, B., Karakurt, A., Sekaran, P. R., Sethi, V., & Singh, R. (2013). Hydrogen powered aircraft: The future of air transport. *Progress in Aerospace Sciences*, *60*, 45–59. https://doi.org/10.1016/J.PAEROSCI.2012.12.002
23. Schmidtchen, U., Behrend, E., Pohl, H. W., & Rostek, N. (1997). Hydrogen aircraft and airport safety. *Renewable and Sustainable Energy Reviews*, *1*(4), 239–269. https://doi.org/10.1016/S1364-0321(97)00007-5
24. Alvaro Pena Lopez, Dr Theoklis Nikolaidis, Dr Soheil Jafari. Cranfield University (2021). Gas Turbine Performance Studies For Lh2-Fuelled Engines
25. Fleming, W. A., Kaufman, H. R., Harp, J. L., & Chelko, L. J. (1962). Naca Research Memorandum, Turbojet Performance And Operation At High Altitudes With Hydrogen And Jp -4 Fuels, Committee For Aeronautics Washington.
26. Bjorn's Corner: The challenges of Hydrogen. Part 6. Tank placement. leehamnews.com/2020/08/28/bjorns-corner-the-challenges-of-hydrogen-part-6-tank-placement. (2020).
27. Hua, T. Q., Ahluwalia, R. K., Peng, J. K., Kromer, M., Lasher, S., McKenney, K., Law, K., & Sinha, J. (2011). Technical assessment of compressed hydrogen storage tank systems for automotive applications. *International Journal of Hydrogen Energy*, *36*(4), 3037–3049. https://doi.org/10.1016/j.ijhydene.2010.11.090
28. Burke, A., & Gardiner, A. (n.d.). UC Davis Research Reports Title Hydrogen Storage Options: Technologies and Comparisons for Light-Duty Vehicle Applications Permalink Publication Date. https://escholarship.org/uc/item/7425173j
29. Daniel Brewer, G., & Morris, R. E. (1975). Tank and Fuel Systems Considerations for Hydrogen Fueled Aircraft. In *Source: SAE Transactions* (Vol. 84).
30. Thesis, P. D. (n.d.). Dries Verstraete The Potential of Liquid Hydrogen for long range aircraft propulsion SCHOOL OF ENGINEERING.
31. Thesis, P. D. (n.d.). Steven S. Pietrobon Analysis of Propellant Tank Masses

32. Saias, C. A., Roumeliotis, I., Goulos, I., Pachidis, V., & Bacic, M. (2022). Assessment of hydrogen fuel for rotorcraft applications. *International Journal of Hydrogen Energy*, *47*(76), 32655–32668. https://doi.org/10.1016/j.ijhydene.2022.06.316
33. Brewer, G. Daniel. (1991). Hydrogen aircraft technology. CRC Press.
34. FlyZero. Cryogenic Hydrogen Fuel System And Storage. (2022).
35. Huete, J., & Pilidis, P. (2021). Parametric study on tank integration for hydrogen civil aviation propulsion. *International Journal of Hydrogen Energy*, *46*(74), 37049–37062. https://doi.org/10.1016/J.IJHYDENE.2021.08.194
36. Verstraete, D., Hendrick, P., Pilidis, P., & Ramsden, K. (2010). Hydrogen fuel tanks for subsonic transport aircraft. *International Journal of Hydrogen Energy*, *35*(20), 11085–11098. https://doi.org/10.1016/J.IJHYDENE.2010.06.060
37. Daniel P. Raymer. Aircraft Design: A Conceptual Approach Sixth Edition.
38. https://www.modernairliners.com/douglas-dc9
39. https://www.airlines-inform.com/commercial-aircraft/md-80.html
40. https://www.airbus.com/en/who-we-are/our-history/commercial-aircraft-history/previous-generation-aircraft/a318
41. https://aircraft.airbus.com/en/aircraft/a320-the-most-successful-aircraft-family-ever/a319neo
42. https://aircraft.airbus.com/en/aircraft/a320-the-most-successful-aircraft-family-ever/a320neo
43. https://aircraft.airbus.com/en/aircraft/a320-the-most-successful-aircraft-family-ever/a321neo
44. https://www.airlines-inform.com/commercial-aircraft/boeing-737-300.html
45. https://www.airlines-inform.com/commercial-aircraft/boeing-737-max-7.html
46. https://www.airlines-inform.com/commercial-aircraft/boeing-737-max-8.html
47. https://www.airlines-inform.com/commercial-aircraft/boeing-737-max-9.html
48. https://simpleflying.com/boeing-737-family-variants-weight-differences/
49. https://www.rocketroute.com/aircraft/boeing-737-800
50. https://www.boeing.com/commercial/737max/
51. https://en.wikipedia.org/wiki/Boeing_737_MAX
52. https://antonov.com/en/aircraft/an-148-201
53. https://www.modernairliners.com/comac-c919
54. https://www.airlines-inform.com/commercial-aircraft/comac-c919.html
55. https://www.airlines-inform.com/commercial-aircraft/arj-21.html
56. https://www.flugzeuginfo.net/acdata_php/acdata_fokker100_en.php
57. https://www.skybrary.aero/aircraft/f100
58. https://www.embraercommercialaviation.com/commercial-jets/erj145/
59. https://www.embraercommercialaviation.com/commercial-jets/e195/

60. Rao, A. G., Yin, F., & van Buijtenen, J. P. (2014). A hybrid engine concept for multi-fuel blended wing body. *Aircraft Engineering and Aerospace Technology*, *86*(6), 483–493. https://doi.org/10.1108/AEAT-04-2014-0054
61. https://www.grc.nasa.gov/www/k-12/airplane/sfc.html
62. Manager, P., Alford, W. J., Coordinator, T., & Pride, J. D. (1972). A Fuel Conservation Study For Transport Aircraft Utilizing Advanced Technology And Hydrogen Fuel. Prepared For National Aeronautics And Space Administration Nasa Langley Research Center Contract Nas1-10900
63. Corchero, G., & Montañés, J. L. (n.d.). An approach to the use of hydrogen for commercial aircraft engines.
64. Brewer G. D., Morris R. E., Davis G. W., Versaw E. F., Cunnington Jr. G. R., Riple J. C., Bearst C. F., Garmong G. (1978). *FINAL REPORT-Volume II STUDY OF FUEL SYSTEMS FOR LH2-FUELED SUBSONIC TRANSPORT AIRCRAFT*. Prepared under Contract NAS 1-14614 for NASA Langley Research Center by Lockheed
65. Brewer G. D., Morris R. E., Davis G. W., Versaw E. F., Cunnington Jr. G. R., Riple J. C., Bearst C. F., Garmong G. (1978). FINAL REPORT-Volume I STUDY OF FUEL SYSTEMS FOR LH2-FUELED SUBSONIC TRANSPORT AIRCRAFT. Prepared under Contract NAS 1-14614 for NASA Langley Research Center by Lockheed
66. Carter, Richard, "Development Of A Liquid Hydrogen Combustion High Bypass Turbofan Model In NPSS" (2021). Mechanical Engineering and Materials Science Independent Study. 156. https://openscholarship.wustl.edu/mems500/156
67. FINAL TECHNICAL REPORT (PUBLISHABLE VERSION) CRYOPLANE. Liquid Hydrogen Fuelled Aircraft-System Analysis. (2003).
68. AIRBUS A320 AIRCRAFT CHARACTERISTICS AIRPORT AND MAINTENANCE PLANNING AC. (2020). Issue: Sep 30/85
69. EASA TYPE-CERTIFICATE DATA SHEET No. EASA.E.110 for Engine LEAP-1A & LEAP-1C series engines (2022) TCDS No.: EASA.E.110 Issue: 11
70. Rodrigo Martinez-Val, Emilio Perez and Jose Palacin. (2012). Historical Perspective of Air Transport Productivity and Efficiency. Session: HIS-1: Early Years of Flight. https://doi.org/10.2514/6.2005-121
71. https://contentzone.eurocontrol.int/aircraftperformance/details.aspx?ICAO=A20N
72. Goraj, Z., Zakrzewski P. Aircraft Fuel Systems And Their Influence On Stability Margin.
73. https://www.nordisk-aviation.com/en/ld-containers/akh-ld3-45/nordisk-akh-/
74. Federal Aviation Administration, DOT. EMERGENCY PROVISIONS
75. Linke, F., Radhakrishnan, K., Grewe, V., Vos, R., Niklaß, M., Lührs, B., Feijia, Y., & Dedoussi, I. (2020). *GLOWOPT-A new approach towards global-warming-optimized aircraft design*. https://www.researchgate.net/publication/343306431
76. Scholz D. (n.d.). *Drag Estimation*. http://OPerA.ProfScholz.de
77. Roskam J. Airplane Design Part I Preliminary Sizing of Airplanes. DARcorporation, 1997.

78. ICAO Doc 8168. Aircraft Operations, PROCEDURES FOR AIR NAVIGATION SERVICES Volume I – Flight Procedures. Sixth Edition 2018
79. Sadraey, Mohammad H. Aircraft design: A systems engineering approach. John Wiley & Sons, 2012.
80. https://contentzone.eurocontrol.int/aircraftperformance/details.aspx?ICAO=A318&NameFilter=a318
81. European Aviation Safety Agency. Certification Specifications for Large Aeroplanes CS-25 Amendment 3. 2007
82. Roskam J. Airplane Design Part VIII Airplane Cost Estimation: Design, Development, Manufacturing And Operating. Darcorporation, 1997.
83. https://www.acquisition.gov/far/part-36
84. ICAO Annex 16 - Environmental Protection - Volume I - Aircraft Noise. 8th Edition, July 2017
85. ICAO Economic Development. Airline Operating Costs and Productivity. Tehran, 2017
86. https://www.bls.gov/
87. https://www.bls.gov/data/inflation_calculator.htm
88. https://www.bls.gov/cpi/
89. https://www.usinflationcalculator.com/
90. https://www.airbus.com/en/products-services/commercial-aircraft/the-life-cycle-of-an-aircraft/operating-life
91. https://www.aviationfile.com/how-long-does-a-commercial-aircraft-last/
92. Airline Cost Management Group (ACMG) Enhanced Report-Airline Cost Management Group (ACMG) Report FY 2013 , Enhanced Version. (2014).
93. https://www.bls.gov/oes/current/oes532011.htm#(2)
94. A320 maintenance cost analysis. AIRCRAFT COMMERCE Issue No. 5 • May/June 1999
95. Saxon S., Weber M. A better approach to airline costs. McKinsey&Company Travel, Transport & Logistics July 2017
96. https://simpleflying.com/how-many-engines-do-airliners-go-through/
97. 2022 TARIFF FOR INTERNATIONAL LANDING, STOPOVER, LIGHTING AND APPROACHING General Directorate of State Airports Authority (DHMI)
98. AEROPORTS DE PARIS FEE SCHEDULE FOR SERVICES RENDERED AS SPECIFIED IN ARTICLES R. 224-1 AND R. 224-2 OF THE FRENCH CIVIL AVIATION CODE FOR THE PARIS – CHARLES-DE-GAULLE, PARIS – ORLY and PARIS – LE BOURGET AIRPORTS
99. Final setting Schiphol Airport Charges and Conditions. October 2022
100. AEROPORTI DI ROMA, FIUMICINO - Airport Fees
101. ANA AEROPORTOS DE PORTUGAL. CHARGES GUIDE, ANA NETWORK
102. Frankfurt Airport – Airport Charges according to Art. 19b Air Traffic Act (LuftVG) Charges for Central Ground Handling Infrastructure
103. aena Price Guide 2023
104. Athens International Airport Eleftherios Venizelos, Aeronautical Charges

105. https://www.eurocontrol.int/
106. https://www.eurocontrol.int/crco#key-documents
107. https://www.lufthansagroup.com/en/company/fleet/brussels-airlines/airbus-a319.html
108. https://contentzone.eurocontrol.int/aircraftperformance/details.aspx?ICAO=A19N&NameFilter=319
109. Embraer continues and refines its strategy at the low-end of 100-149 seat sector (2014) leehamnews.com/2014/01/13/embraer-continues-and-refines-its-strategy-at-the-low-end-of-100-149-seat-sector
110. https://alliknowaviation.com/2019/12/14/fuel-consumption-aircraft/
111. Bhaskara V., ANALYSIS: A320neo vs. 737 MAX: Airbus is Leading (Slightly) – Part II (2016) https://web.archive.org/web/20160206082857/http://airwaysnews.com/blog/2016/02/05/a320neo-vs-737-max-pt-ii/
112. https://jet-a1-fuel.com/
113. https://jet-a1-fuel.com/price/italy
114. https://www.iata.org/en/publications/economics/fuel-monitor/
115. https://www.eia.gov/dnav/pet/hist/eer_epjk_pf4_rgc_dpgD.htm
116. https://climate.ec.europa.eu/eu-action/eu-emissions-trading-system-eu-ets_en
117. Johanning, A., & Scholz, D. (2012). Evaluation of Worldwide Noise and Pollutant Emission Costs for Integration into Direct Operating Cost Methods.
118. https://tradingeconomics.com/commodity/carbon
119. Montreal-2013 Maintenance Cost Task Force (MCTF) Airline Cost Management Group (ACMG). (2015).
120. https://www.edie.net/zeroavia-welcomes-successful-zero-emission-hydrogen-aircraft-testing/
121. Klug, H. G., & Faass, R. (2001). CRYOPLANE: hydrogen fuelled aircraft — status and challenges. *Air & Space Europe*, *3*(3–4), 252–254. https://doi.org/10.1016/S1290-0958(01)90110-8
122. https://www.xe.com/currencycharts/
123. Bonnefoy P. A., Schaufele R. Placing Costs Associated with LTAG Integrated Scenarios in Context. ICAO SPECIAL SUPPLEMENT Long-Term Aspirational Goal.